CLUSTER SECONDARY ION MASS SPECTROMETRY OF POLYMERS AND RELATED MATERIALS

Christine M. Mahoney*

Chemical Science and Technology Laboratory, Surface and Microanalysis Science Division, National Institute of Standards and Technology, 100 Bureau Drive, Mail Stop 8371, Gaithersburg, MD 20899-8371

Received 10 September 2008; received (revised) 22 January 2009; accepted 22 January 2009

Published online in Wiley InterScience (www.interscience.wiley.com) DOI 10.1002/mas.20233

Cluster secondary ion mass spectrometry (cluster SIMS) has played a critical role in the characterization of polymeric materials over the last decade, allowing for the ability to obtain spatially resolved surface and in-depth molecular information from many polymer systems. With the advent of new molecular sources such as C_{60}^{+}, Au_3^{+}, SF_5^{+}, and Bi_3^{+}, there are considerable increases in secondary ion signal as compared to more conventional atomic beams (Ar^{+}, Cs^{+}, or Ga^{+}). In addition, compositional depth profiling in organic and polymeric systems is now feasible, without the rapid signal decay that is typically observed under atomic bombardment. The premise behind the success of cluster SIMS is that compared to atomic beams, polyatomic beams tend to cause surface-localized damage with rapid sputter removal rates, resulting in a system at equilibrium, where the damage created is rapidly removed before it can accumulate. Though this may be partly true, there are actually much more complex chemistries occurring under polyatomic bombardment of organic and polymeric materials, which need to be considered and discussed to better understand and define the important parameters for successful depth profiling. The following presents a review of the current literature on polymer analysis using cluster beams. This review will focus on the surface and in-depth characterization of polymer samples with cluster sources, but will also discuss the characterization of other relevant organic materials, and basic polymer radiation chemistry. © 2009 Wiley Periodicals, Inc.,[†] Mass Spec Rev

Keywords: *SIMS; polymers; mass spectrometry; cluster; depth profiling; C_{60}; Bi; SF_5*

I. INTRODUCTION

Secondary ion mass spectrometry (SIMS) is a mass spectrometric-based analytical technique, which is used to obtain information about the molecular, elemental and isotopic composition of a surface. In a conventional SIMS experiment, an energetic primary ion beam, such as Ga^{+}, Cs^{+}, or Ar^{+} is focused onto a solid sample surface under ultra-high vacuum conditions. The interaction of the primary ion beam with the sample results in the desorption of secondary ions from the surface of the material, which are subsequently extracted into a mass spectrometer. Though this technique has been widely employed for the characterization of inorganic materials, widespread use of SIMS for analysis of organic systems has been historically limited by low secondary ion yields and beam-induced damage effects that result from the use of atomic primary ion beams. Organic materials typically require the use of "static SIMS" analysis conditions where the primary ion fluence is maintained below a critical dose to retain the surface in an undamaged state, resulting in decreased sensitivity and precluding compositional depth profiling. This critical dose is defined as the "static limit," and is often reported to be at or below 1×10^{13} ions/cm^2, depending on the sample and the ion beam employed. One potential solution to this limitation is to use cluster or polyatomic primary ion bombardment.

When a cluster ion impacts a surface, the cluster breaks apart and each atom in the cluster retains only a fraction of the initial energy of the ion, thus resulting in a significant reduction in penetration depth of the ion (since penetration depth is proportional to impact energy) (Gillen & Roberson, 1998). This causes surface-localized damage and consequently, preserves the chemical structure in the subsurface region (see Fig. 1). Atomic beams however, will penetrate deeply, resulting in the breaking of molecular bonds deep into the sample and thus precluding the ability to depth profile in molecular samples. Furthermore, because there are more atoms bombarding the sample simultaneously with cluster ions, the sputtering yield can be significantly enhanced. This is in part because of the increased number of atoms per ion, but is also a result of the formation of a high energy density "collisional spike" regime which is formed with cluster ion bombardment (Sigmund & Claussen, 1981), causing non-linear sputtering yield enhancements (i.e., sputtering yield of $C_n^{+} \gg nC^{+}$).

The benefits of utilizing cluster sources was shown as early as 1960, with the observation of non-linear enhancements in sputtering yields when using cluster beams (Gronlund & Moore, 1960; Andersen & Bay, 1974, 1975; Thompson & Johar, 1979). However, cluster sources were not employed for SIMS applications until the mid to late 1980s. One of the earliest works was published in 1982, in which the authors compared the performance of siloxane molecular ions to Hg^{+} ions for characterization of oligosaccharides in a glycerol matrix (Wong,

*Correspondence to: Christine M. Mahoney, Chemical Science and Technology Laboratory, Surface and Microanalysis Science Division, National Institute of Standards and Technology, 100 Bureau Drive, Mail Stop 8371, Gaithersburg, MD 20899-8371.
E-mail: christine.mahoney@nist.gov

© Wiley Periodicals, Inc. [†]This article is a US Government work and, as such, is in the public domain in the United States of America.

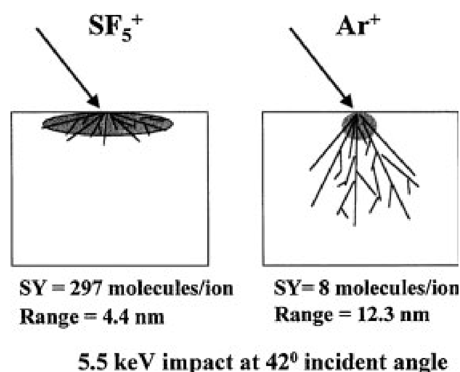

FIGURE 1. Graphic illustration suggesting how high sputter yields and low penetration depths observed with polyatomic bombardment reduces the accumulation of beam-induced damage in an organic thin film. (SY, sputter yield; and Range, penetration depth of ion(s).) Figure from Gillen and Roberson (1998) reprinted with permission from John Wiley & Sons, Ltd, copyright 1998.

Stoll, & Röllgen, 1982). The results showed a large increase in the ionization of the organic molecules when employing the siloxane cluster source as compared to the atomic Hg^{+} ion source.

Later, Appelhans and Delmore (1987) used SF_6 neutral beams to characterize electrically insulating polymer samples such as poly(tetrafluoroethylene) (PTFE), poly(ethyleneterephthalate) (PET), poly(methylmethacrylate) (PMMA) and polyphosphazene, where the authors found that the SF_6 cluster beam yielded three to four orders of magnitude more intense secondary ion yields from these polymer samples than equivalent energy atomic beams. Similar findings were found in the mass spectra of pharmaceutical compounds (Appelhans & Delmore, 1989).

Cornett and co-workers (Cornett, Lee, & Mahoney, 1994) demonstrated that continued bombardment of protein samples with massive glycerol cluster ions yielded constant molecular secondary ion signals with increasing fluence, while the same samples irradiated with Xe^{+} ions yielded the characteristic rapid signal decay that is commonly associated with atomic beams. This indicated that depth profiling (analysis of composition with increasing depth into the sample, *via* sputter removal) in organic materials was feasible.

The first demonstration of a polymer depth profile was published a few years later by Gillen and co-workers (Gillen & Roberson, 1998), who used a polyatomic SF_5^{+} source to profile through a thin layer of PMMA on Si. Since then, there has been an abundance of work on depth profiling and surface characterization in polymeric materials with cluster beams. Cluster primary ion sources such as C_{60}^{+}, C_8^{-}, Au_3^{+}, SF_5^{+}, and Bi_3^{+}, have already generated considerable interest for organic and polymeric SIMS applications, where they have resulted in significant improvements (typically >1,000-fold) in characteristic molecular secondary ion yields and decreased beam-induced, subsurface damage. The surface-localized damage characteristic of cluster sources, coupled with increased sputter removal rates, has led to the ability to depth profile through many organic and polymeric materials without the rapid signal decay typically observed with atomic primary ion sources. With the increased sensitivity, nanoscale depth resolution (~10 nm) and submicrometer lateral resolution, cluster SIMS is a promising new characterization tool enabling high-resolution three-dimensional imaging capabilities for organic and polymeric-based materials.

This review will focus on the characterization of polymeric samples with cluster sources, but will discuss characterization of other relevant organic materials as well as the basic chemistry of polymer irradiation. For more information regarding cluster SIMS fundamentals, molecular dynamics simulations and molecular and biological materials characterization with cluster beams, see the following review articles (Le Beyec, 1998; Brunelle, Touboul, & Laprevote, 2005; Winograd, 2005; Wucher, 2006; Garrison & Postawa, 2008).

II. THEORY

A. Molecular Dynamics Simulations

Comprehensive studies of molecular dynamics (MD) simulations have been performed to better understand the bombardment of surfaces by atomic versus polyatomic primary ion bombardment. Figure 2 compares molecular dynamics simulations of both 15 keV C_{60} and 15 keV Ga projectiles impinging onto a Ag surface (Postawa et al., 2003, 2004). Note the large amount of interlayer mixing that occurs with the Ga^{+} probe. Also note that there is very little material removed from the surface resulting from the Ga^{+} impact. The MD simulations of the C_{60}^{+} impact however, show a much greater amount of material being removed from the surface, with very little damage to the underlying layers. In other words, the damaged area created by the C_{60}^{+} is almost completely removed and does not accumulate.

Molecular dynamics simulations of organic and polymeric samples have yielded similar results. Delcorte and co-workers, have been active in the modeling of both atomic and polyatomic bombardment of polymer samples such as polystyrene (PS) (Delcorte & Garrison, 2000, 2007; Delcorte, 2005; Delcorte, Poleunis, & Bertrand, 2006a; Delcorte et al., 2007) and PET (Delcorte et al., 1999). An interesting example is shown in Figure 3, which shows the simulation of projectile damage created in PS tetramer samples with 5 keV C_{60} as compared to 5 keV Ar. Similar to what was observed with ion bombardment on Ag substrates, the Ar ion was found to penetrate much farther into the PS matrix than the C_{60} ion (Delcorte & Garrison, 2007; Delcorte et al., 2007). The Ar ion therefore caused several bond-scissions and a cascade of collisions extending into the depth of the sample, causing extensive subsurface damage. Furthermore, it was determined that very few branches of the cascade were upward directed, resulting in very low molecular yields with Ar projetiles. In comparison, the damage created by the C_{60} projectile remained in the top 2 nm of the PS target. The damage was therefore confined to a much smaller volume, closer to the surface, and with a very high energy density. This ultimately resulted in significant enhancements in the calculated molecular yield with corresponding decreases in subsurface damage.

Czerwiński et al. (2006) and Postawa et al. (2005) compared Ga and C_{60} ion bombardment on thin organic overlayers of PS tetramers (monolayer) and benzene (three layers) deposited onto

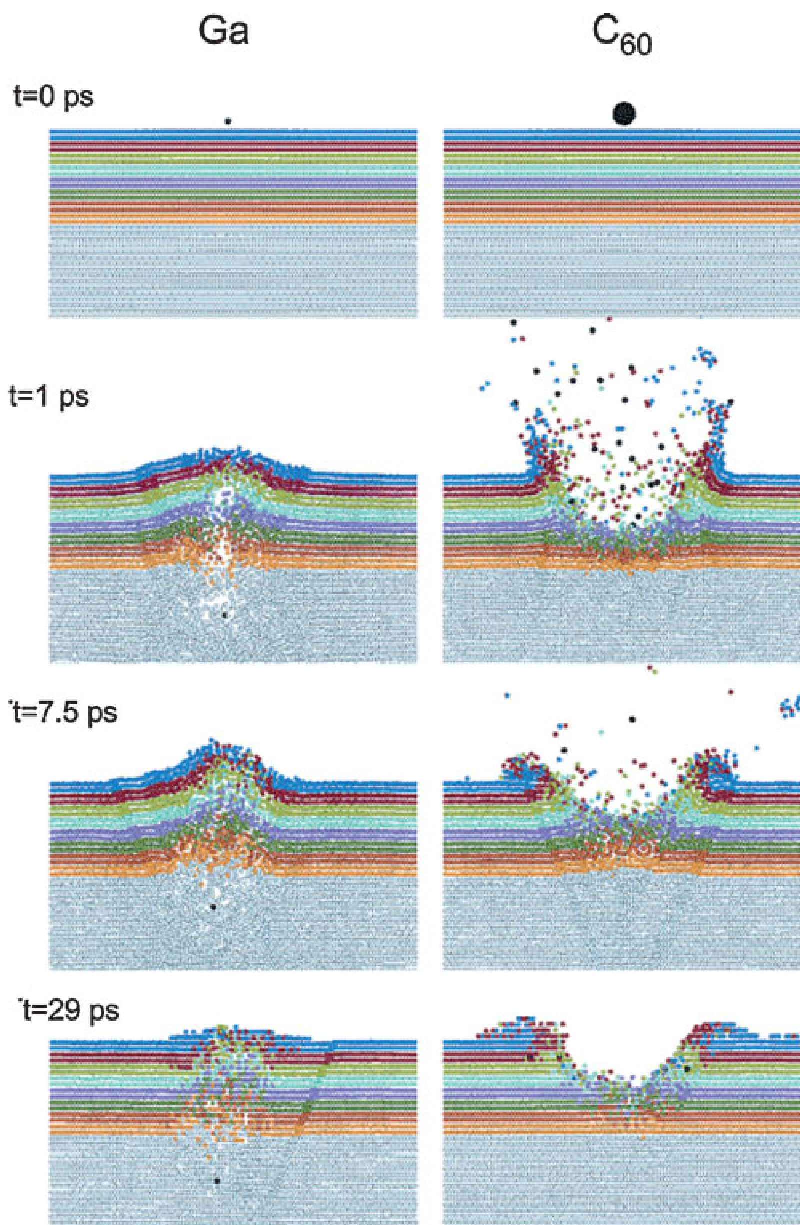

FIGURE 2. Cross-sectional view of the temporal evolution of a typical collision event leading to ejection of atoms due to 15 keV Ga and C_{60} bombardment of a Ag{1 1 1} surface at normal incidence. The atoms are colored by original layers in the substrate. The projectile atoms are black. Figure reprinted from Postawa et al. (2004) with permission from American Chemical Society, copyright 2004. [Color figure can be viewed in the online issue, which is available at www.interscience.wiley.com.]

Ag substrates. The results outlined major differences in the sputter mechanisms between the two ion beams. As opposed to Ga, which induces the typical collision cascade regime when bombarding the surface, eventually resulting in the ejection of organic molecules uplifted by departing substrate atoms, the C_{60} invoked a more collective large-scale process where the individual atoms in the C_{60} work cooperatively to move the Ag atoms rather than behaving as individual atoms initiating their own collision cascades. The result is a shockwave in the Ag, whereby intact molecules are ejected by a concerted action of substrate atoms involved in the unfolding of the crater (described as a ‘‘catapulting mechanism’’). The conclusion from this work was that for thin organic overlayers, approaching monolayer coverage, there is very little gain in the application of the polyatomic projectiles because although emission of the substrate particles is significantly enhanced with the C_{60}, there was little or no enhancement of the ejection of intact molecules. Furthermore, there was significant fragmentation of the ejected species when employing C_{60}. This is consistent with experimental evidence indicating that there is a greater benefit when

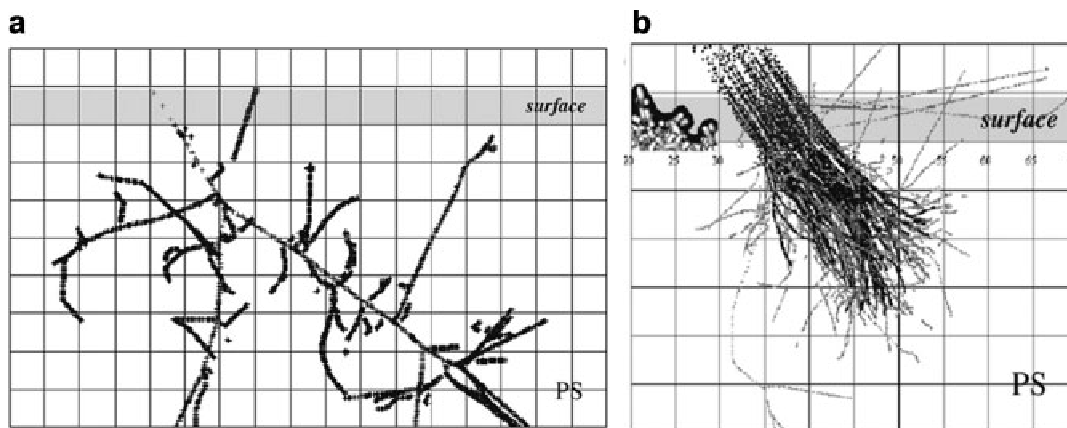

FIGURE 3. Tracks of the atoms forming the collision cascade in a polystyrene tetramer. The successive positions of the projectile and recoil atoms with more than 10 eV of kinetic energy are represented as a function of time up to 200 fsec. Each square of the grid is 5×5 Å^2. The sample-vacuum interface is indicated by the gray area. (**a**) Ar bombardment at 5 keV, and (**b**) C_{60} bombardment at 5 keV. Figure from Delcorte and Garrison (2007a) and Delcorte et al. (2007), reprinted with permission from Elsevier, copyright 2007.

using cluster primary ions for the analysis of thick films as compared to thin molecular overlayers (Gillen & Roberson, 1998; Harris et al., 1999; Stapel, Brox, & Benninghoven, 1999; Stapel, Thiemann, & Benninghoven, 2000; Diehnelt, Van Stipdonk, & Schweikert, 2001; Stapel & Benninghoven, 2001).

MD simulations of organic samples with other ions such as Au atoms and dimers (Harper & Krantzman, 2004) and SF_5 (Townes et al., 1999) have also been reported. In the latter study, the authors compared the molecular yields obtained with atomic Xe and polyatomic SF_5 bombardment of a monolayer of biphenyl molecules on two different substrates, Si (1 0 0) and Cu (0 0 1). In both cases, the molecular yield was greater by a factor of 2 to 4 for the SF_5 than for the Xe, despite the fact that the projectiles are of comparable mass. Most importantly, Si (1 0 0) substrates had much higher calculated molecular yields than Cu (0 0 1), when comparing SF_5 with Xe. This was attributed to differences in the interactions of the polyatomic projectile versus the atomic projectile with the crystalline structures of the substrates. In the close packed Cu lattice, the SF_5 was determined to break apart and reflect toward the vacuum. However, with the Si substrate, the SF_5 projectile was able to penetrate the surface and break apart within the substrate, initiating multiple collision cascades and hence increasing the overall molecular yield.

It should be noted that although these MD simulations are extremely useful for visualization of damage processes in organic materials, they typically only illustrate single impact events, whereas most SIMS experiments involve multiple, simultaneous impacts. For a more complete review of MD simulations, see Garrison and Postawa (2008).

B. Erosion Model for Molecular Depth Profiling

The premise behind the success of cluster SIMS for molecular depth profiling is that these beams tend to cause surface-localized damage with rapid sputter removal rates, resulting in a system at equilibrium, where any damage created is rapidly removed before it can accumulate. A very important model describing this equilibrium was originally presented in a publication by Gillen, Simons, and Williams (1990), and later refined by Cheng, Wucher, and Winograd (2006) and Wucher (2008). This model, referred to as the erosion model, describes the process by which the damage becomes saturated in an organic film with increasing fluence.

To achieve favorable conditions for molecular depth profiling, subsurface molecules must avoid being fragmented by the previous ion collisions necessary to expose them. *This requirement will be favored when the sputtering yield is high and the ion penetration depth is low, such that a fresh supply of undamaged subsurface molecules are available every time an ion strikes the surface*. Figure 4 shows a schematic diagram of the erosion model, where F represents the flux of intact molecules into (F_{supply}) and out of ($F_{sputter}$) an altered layer of thickness (d), as well as damage formation in the form of bond breaking and crosslinking (F_{damage}). For such systems, a steady state is reached, where the disappearance rate ($F_{sputter}$) induced by the removal of intact analyte molecules and the supply rate (F_{supply})

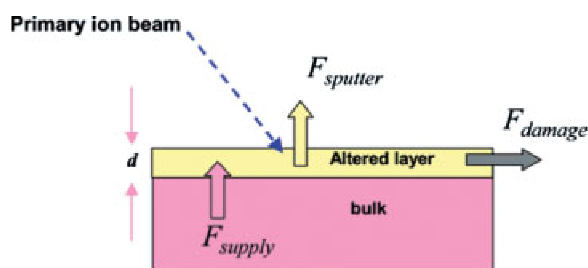

FIGURE 4. Schematic diagram of the erosion model. The variable F represents the indicated flux of intact molecules into and out of the altered layer of thickness d. Figure reprinted from Cheng and Winograd (2006) with permission from American Chemical Society, copyright 2006. [Color figure can be viewed in the online issue, which is available at www.interscience.wiley.com.]

or recovery of undamaged molecules through surface erosion, reach an equilibrium, and no further damage is accumulated.

This damage saturation was predicted by Gillen, Simons, and Williams (1990) to occur at a fluence inversely proportional to the sputtering yield as follows in Equation (1): where d is the depth into the sample that is altered by ion beam interactions, R_d is the mean depth of the damage distribution curve, $Q =$ fluence required for removal of depth d, and n/Y is the density of molecules divided by the molecular yield of the compound.

$$Q = d\frac{n}{Y} = 2R_d\frac{n}{Y} \quad (1)$$

This model was able to predict both the location and the measured signal intensity drop in the surface transient region in a sample of methylene chloride (within a factor of 2) (Gillen, Simons, & Williams, 1990).

The model was further modified by Cheng and co-workers (Cheng & Winograd, 2006) to describe the molecular signal intensity as a function of C_{60}^{+} fluence in trehalose systems, and it was found that the model provided a good fit to the experimental data (see Eq. 2):

$$S(f) = S_{ss} + (S_0 - S_{ss})\exp\left[\left(-\left(\frac{Y}{nd}\right) + \sigma_d\right)f\right] \quad (2)$$

where S_0 is the signal intensity at zero fluence, S_{ss} is the signal intensity at steady state (damage saturation region), f is the ion fluence, and σ_d is the damage cross section associated with the organic material of interest.

The term $[-(Y/nd) + \sigma_d]$ in Equation (2) is defined as the disappearance cross section (see Appendix) where Y/nd is termed, the "clean-up efficiency". Hence if the sputter rate is high, it is expected that the cleanup efficiency will contribute most to the signal decay, while if sputter rate is low and damage is high, the damage cross section will contribute most to the signal decay.

Equation (2) describes the initial exponential decay observed SIMS depth profiles, later referred to as region I, but does not describe any further decline in signal in the steady state region (region II). This region is discussed in greater detail in more recent work by Wucher (2008). Unlike the case described in Equation (2), which assumes a constant erosion rate with increasing fluence in the steady steady state region, this modification describes the case where the erosion rate, or sputter yield (Y), changes with fluence. For the case of a slowly varying sputter yield, a quasi-steady state approximation can be used to describe the signal variation after the initial exponential decay. The fluence-dependent erosion rate model provided a good fit to the experimental data as illustrated in Figure 5.

It should be noted, that the erosion dynamics model described here was developed for molecular depth profiling in organic films, and does not apply strictly to polymer depth profiling. This is because in the case of polymeric depth profiling, one measures the intensities of characteristic fragments of the molecule, not the molecular ion itself, and therefore it is likely to exhibit very different disappearance cross sections. However, this model is still very relevant in terms of the general underlying damage processes occurring during sputtering of polymers and the resulting polymer depth profile shapes that are typically observed.

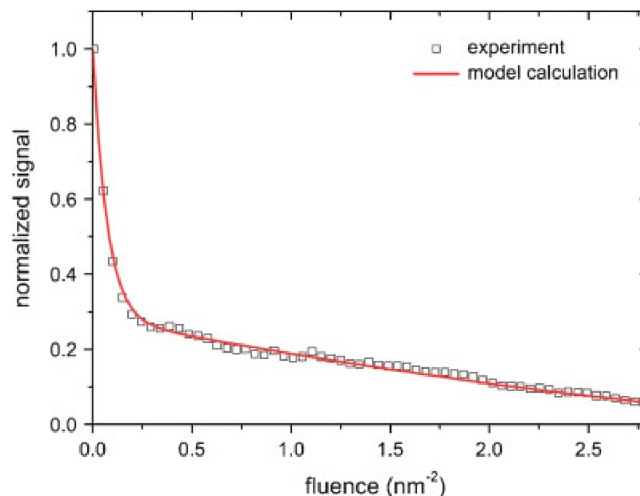

FIGURE 5. Measured $(M-OH)^{+}$ molecular ion signal as a function of projectile fluence for a 350-nm cholesterol film on Si, analyzed by 40-keV C_{60}^{+} projectile ions. The solid line denotes the signal variation as predicted by the erosion model, assuming a linear erosion rate variation in the steady state region. See reference for detailed fitting parameters. Figure reprinted from Wucher (2008) with permission from Wiley-Blackwell, copyright 2008. [Color figure can be viewed in the online issue, which is available at www.interscience.wiley.com.]

III. AVAILABLE CLUSTER SOURCES[1]

A. SF_5^{+}

The SF_5^{+} source is an electron impact design, where SF_6 gas is leaked into an ionization chamber and bombarded with electrons such that SF_n^{+} ions are created, where $n = 1$–5, and $n = 5$ is the most abundant. Prior to the development of SF_5^{+}, Appelhans and Delmore developed a neutral SF_6 ion beam system, in one of the earliest works of organic analysis with a cluster source (Appelhans & Delmore, 1987; 1989), illustrating significant signal enhancements and decreased charging when employing these beams as opposed to atomic beams for organic characterization. Since neutral beams are extremely difficult to focus, Hand et al. utilized charged SF_5^{+} ions and compared the mass spectra of several organic salts to those obtained with other polyatomic ions including N_2^{+} CO_2^{+} and CF_3^{+} (Hand, Majumdar, & Cooks, 1990). The authors noted that the highest efficiencies were obtained for SF_5^{+}, though at the cost of increased fragmentation as compared to the other beams.

These sources were developed commercially for time-of-flight (TOF)-based static SIMS instruments (Kötter & Benninghoven, 1998; Stapel, Brox, & Benninghoven, 1999; Stapel, Thiemann, & Benninghoven, 2000; Stapel & Benninghoven,

[1]Commercial equipment and materials are identified in order to adequately specify certain procedures. In no case does such identification imply recommendation or endorsement by the National Institute of Standards and Technology, nor does it imply that the materials or equipment identified are necessarily the best available for the purpose.

2001). Gillen and co-workers also developed an SF_5^+ source for magnetic sector SIMS instruments (Gillen & Roberson, 1998; Gillen, King, & Chmara, 1999).

B. C_{60}^+ and Other C-Based Sources

Since the introduction of cluster SIMS, there have been many carbon-based sources, including massive glycerol clusters (Mahoney et al., 1991), coronene and coronene dimers ($C_{24}H_{12}$ and $(C_{24}H_{12})_2$) (Blain et al., 1989; Boussofiane-Baudin et al., 1994; Biddulph et al., 2007), phenylalanine ($C_9H_{11}NO_2$) probes (Blain et al., 1989), C_n^+ (Salehpour, Fishel, & Hunt, 1988a), C_n^- (Gillen et al., 2001), $C_xH_y^+$, and $C_xF_y^+$ (Salehpour, Fishel, & Hunt, 1988a,b; Stapel, Brox, & Benninghoven, 1999). C_{60} was introduced as a source for SIMS applications in 1994 (Boussofiane-Baudin et al., 1994), where the authors compared molecular projectiles of Au_n^+, coronene and coronene dimers, C_{37}, C_{60}, and C_{70} in the characterization of various Langmuir–Blodgett (LB) films and phenylalanine films. For all cases studied in this work, the organic cluster ions containing C as opposed to gold had much larger molecular ion yields and increasing beam energies resulted in linear increases in these ion yields. The first commercially available C_{60} source was introduced in 2003 (Wong et al., 2003; Weibel et al., 2003; Hill et al., 2006). It is described as a thermal effusive source, where C_{60} powder is heated and evaporated at $>400°C$, and then is subsequently ionized by electron bombardment. This source is currently one of the most highly utilized cluster sources for organic depth profiling applications.

C. Au_n^+ Clusters

The Au cluster source is a liquid metal ion gun (LMIG) design, similar to a Ga source, but is able to generate Au clusters (Au_n^+, where $n = 1–3$). Benguerba et al. (1991) were among the first scientists to employ a liquid metal ion source for the production of Au_n^+ clusters. The authors used this source for characterization of phenylalanine samples and saw a significant increase in signal intensity characteristic of the molecular ion yield, albeit with corresponding increases in fragmentation. Later (1998), Andersen studied non-linear effects with Au_1^+ to Au_5^+ clusters (Andersen et al., 1998). The first commercially available Au cluster source was finally introduced in 2003 (Davies et al., 2003). Because of the LMIG design, Au (and Bi) sources have extremely high spatial resolutions ($\leq$100 nm), with Au trimers having much improved useful lateral resolutions (Δl) as compared to the atomic beams (Kollmer, 2004). The useful lateral resolution is defined below as:

$$\Delta l = \left(\frac{N}{E}\right)^{1/2} = \left(N\frac{\sigma}{Y}\right)^{1/2} \quad (3)$$

where N is the number of secondary ions detected from the area Δl^2 (Kollmer, 2004), σ is the disappearance cross section of the material, Y is the secondary ion yield and E is the secondary ion formation efficiency (see Appendix). Kollmer (2004) has reported useful lateral resolutions of 1,300 nm for Ga^+, 400 nm for Au^+ and Bi^+ and 150 nm for Au_3^+ and Bi_3^+ for a sample of organic pigments on a color filter array.

D. Bi_n^+ Clusters

Bi has been explored as a potential ion source for sputtering as early as 1979, when Thompson and Johar worked with Bi_n^+ clusters and other sources to study non-linear effects (Thompson & Johar, 1979). However, Bi was not used for SIMS applications until after the development of the Au cluster source. The Bi source, whose design is similar to that of the Au source, was introduced as a commercially available source in 2004 (Kollmer, 2004). The Bi source was found to be beneficial because as compared to Au, Bi emitted larger clusters (Bi_n^+, where $n = 1–7$) and produced higher currents of those clusters. Moreover, bismuth was found to emit a variety of doubly charged clusters. As compared to Au imaging, Bi was found to result in more intense molecular ion images with comparable lateral resolutions (Kollmer, 2004).

E. Massive Au Clusters

Au_{400}^{4+} cluster ions were first introduced by Tempez et al. (2004) where the authors used both small and large gold clusters to characterize peptide samples. It was demonstrated in this work that there were significant signal enhancements as well as decreased damage cross sections when using the Au_{400}^{4+} as compared to Au_5^+ and Au_9^+ ions, making it potentially useful for depth profiling applications. In addition, Au_{400}^{4+} ions are known to further enhance the signal by creating Au-analyte adducts, which are not observed with smaller gold clusters such as Au_5^+ (Hager et al., 2006).

This source was further developed by Schweikert et al. for single impact events, where instead of a focused beam of ions, a single Au_{400}^{4+} primary ion projectile impacts the surface and the resulting secondary ions are recognized as singular events (Guillermier et al., 2006a; Verkjoturov et al., 2006). Though this source is not yet designed for imaging experiments, (currently it can not be determined where the beam is actually sampling) this type of source may have major implications for imaging in the future, as the spatial resolution will only be limited by the lateral extent of the surface area influenced by the single impact event, and not the focusing elements of the source.

It should be noted that the basic design of this source was actually developed earlier (Van Stipdonk, Harris, & Schweikert, 1996) for C_{60}^+, $(CsI)_nCs^+$, and Ga^+ beams, in the event-by-event bombardment and detection mode to investigate the secondary ion yields of CsI and phenylalanine molecules. The single impact C_{60}^+ source was further used by Locklear et al. (2006) to characterize matrices in cluster SIMS, and also by Verkhoturov, who used both C_{60}^+ and Au_{400}^{4+} to characterize glycine samples (Verkjoturov et al., 2006). It was found that the Au_{400}^{4+} projectile induced abundant multi-ion emission (e.g., the average number of detected ions emitted per event from glycine was 12.5, much larger than was observed with C_{60}^+) (Verkjoturov et al., 2006).

F. Gas Cluster Beams

Gas cluster ion beams consist of hundreds to thousands of atoms or molecules of gaseous materials. The individual gas atoms are first condensed into neutral clusters, generated through cooling in

a supersonic expansion. These neutral clusters of varying size are subsequently ionized by electron bombardment, and accelerated. The chemistry of these beams is variable and can be comprised of Ar, O_2, CO_2, or SF_6 gases, to name a few. These large gas clusters are used mainly for modification of surfaces (growth of well-controlled oxide layers, cluster ion implantation, smoothing of surfaces, cleaning of surfaces, etc.). Not surprisingly, the sputtering yields were found to be much higher for the gas clusters as opposed to the corresponding monomers, and reactive gas clusters, such as O_2 and SF_6 clusters, result in the largest sputtering yields. A very good review of the work done on gas cluster beams was written by Yamada et al. (2001). More recently, a SIMS system employing these gas cluster sources was developed, employing an Ar_{2000} ion beam source (Matsuo et al., 2004, 2008; Ninomiya et al., 2006; Ichiki et al., 2008; Nakata et al., 2008). These sources have a lot of promise in the field of polymer depth profiling in particular.

G. Other Beams

Ionic projectiles such as CsI^+, Cs_2I^+, and $Cs_3I_2^+$ have been used extensively in the past (Blain et al., 1989). Diehnelt also utilized and compared the performance of several of these ionic cluster sources including $(CsI)Cs^+$, $(CsI_2)Cs^+$, $(NaF)Na^+$, $(NaF)_2Na^+$, $(NaF)_4Na^+$, and SiF_5^- (Harris et al., 1999; Diehnelt, Van Stipdonk, & Schweikert, 2001) for characterization of organic overlayers. Other examples of cluster sources that have been discussed in the literature include CF_3^+ (Reuter, 1987; Reuter & Clabes, 1988; Reuter & Scilla, 1988), O_3^+ (Yamazaki & Mitani, 1997), ReO_4^- (Delmore et al., 1995; Groenewold et al., 1997, 1999, 2000; Gresham et al., 2001), $Ir_4(CO)_7^+$ (Mizota et al., 2007; Fujiwara et al., 2006), and $(Bi_2O_3)_nBiO^+$ (Harris et al., 1999).

IV. POLYMER SURFACE ANALYSIS BY CLUSTER BEAMS

A. Static SIMS of Polymers

Cluster ion sources have repeatedly been reported to be superior to atomic sources for mass spectral analysis and imaging of organic and polymeric materials. In most cases, significant enhancements in molecular secondary ion yields, and reductions in beam-induced damage accumulation are observed. This decreased beam-induced damage accumulation allows for longer signal averaging times ''beyond the static limit'' that is required for atomic beams, thus enhancing the signal-to-noise ratio even further.

In 1987, Appelhans and co-workers first demonstrated the potential for using cluster ion beams for polymer characterization, when they used a neutral SF_6 beam to characterize PTFE, PET, PMMA and polyphosphazene without charging, and with three to four orders of magnitude more intense secondary ion yields than equivalent-energy atomic beams (Appelhans & Delmore, 1987). Later, Kötter and Benninghoven (1998) studied characteristic molecular secondary ion emission from polymer surfaces under 10 keV Ar^+, Xe^+ and SF_5^+ bombardment (where Xe^+ and SF_5^+ have similar masses: *m/z* 131 and *m/z* 127 respectively). In this study, secondary ion yields of PET, polyisoprene (PI), polypropylene (PP), PTFE, PS, polycarbonate (PC), PMMA, and PEG were determined under static SIMS conditions. For all investigated bulk polymer surfaces there was an increase in the secondary ion yields in the order of $Ar^+ < Xe^+ < SF_5^+$ primary ion bombardment up to a factor of 1,000. The ion yield enhancement when using SF_5^+ was more prominent in the high mass region.

Since then, countless examples of signal enhancements found in polymers using cluster sources have been reported. Some examples include work by Davies et al. (2003), who found enhancement in signals characteristic of PET and polypeptides when employing Au_3^+ clusters, Nagy and Walker who observed similar enhancements using Au (Nagy, Gelb, & Walker, 2005) and Bi (Nagy & Walker, 2007) clusters for bombardment of polystyrene and other organic materials, and several others [Au clusters (Bryan et al., 2004; Aimoto et al., 2006; Zhu & Kelley, 2006), C_{60} (Weibel et al., 2003; Hill & Blenkinsopp, 2004), SF_5^+ (Gillen & Roberson, 1998; Stapel, Thiemann, & Benninghoven, 2000; Stapel & Benninghoven, 2001; Boschmans, Van Royan, & Van Vaeck, 2005; Van Royen, Taranu, & Van Vaeck, 2005)].

A good example of the benefits of cluster beams in the characterization of polymeric materials is illustrated in Figure 6 (Aimoto et al., 2006). This figure displays the mass spectra obtained from thin films of poly(ethyleneglycol) (PEG) deposited onto Si wafers, where Figure 6a–c depicts the mass spectra acquired with Ga^+, Au^+ and Au_3^+ ions from a low molecular weight PEG sample ($m/z = 400$), and Figure 6d–f depicts the same acquired from a higher molecular weight PEG sample ($m/z = 1{,}000$). There is a clear enhancement in molecular secondary ion signals when using Au^+ as compared to Ga^+, and an even greater enhancement when utilizing Au_3^+ clusters. Also, while the PEG molecular weight distribution is very well defined in the mass spectra acquired with Au_3^+, the corresponding fragment ion distributions are much less intense, indicating decreased fragmentation in polymers with the cluster source. Au_3^+ was reported to have a signal enhancement of up to 100–2,600 times as compared to Ga^+.

Similar examples of molecular weight distribution enhancements can be found for PS, PET, and PTFE with C_{60}^+ (Weibel et al., 2003). In the case of PS 2000 characterized with C_{60}^+, the molecular weight distribution was not even detectable in the mass spectra acquired with the Ga^+ probe, and was only observed in the mass spectra acquired with the C_{60}^+ cluster source. Similar to that observed in Aimoto's work (Fig. 5), the signal enhancement for C_{60}^+ was much greater in the higher mass region, relative to the low mass region indicating decreased fragmentation.

It should be noted that these results are contradictory to other studies involving organic samples where it has been observed that there are actually increases in fragmentation of some organic compounds with cluster beams as compared to atomic beams (Hand, Majumdar, & Cooks, 1990; Benguerba et al., 1991). While for many *organic* materials there are indeed increases in fragmentation with cluster beams, it appears that this is not the case for most *polymer* films, and overall the extent of fragmentation is dependent on the sample as well as the beam.

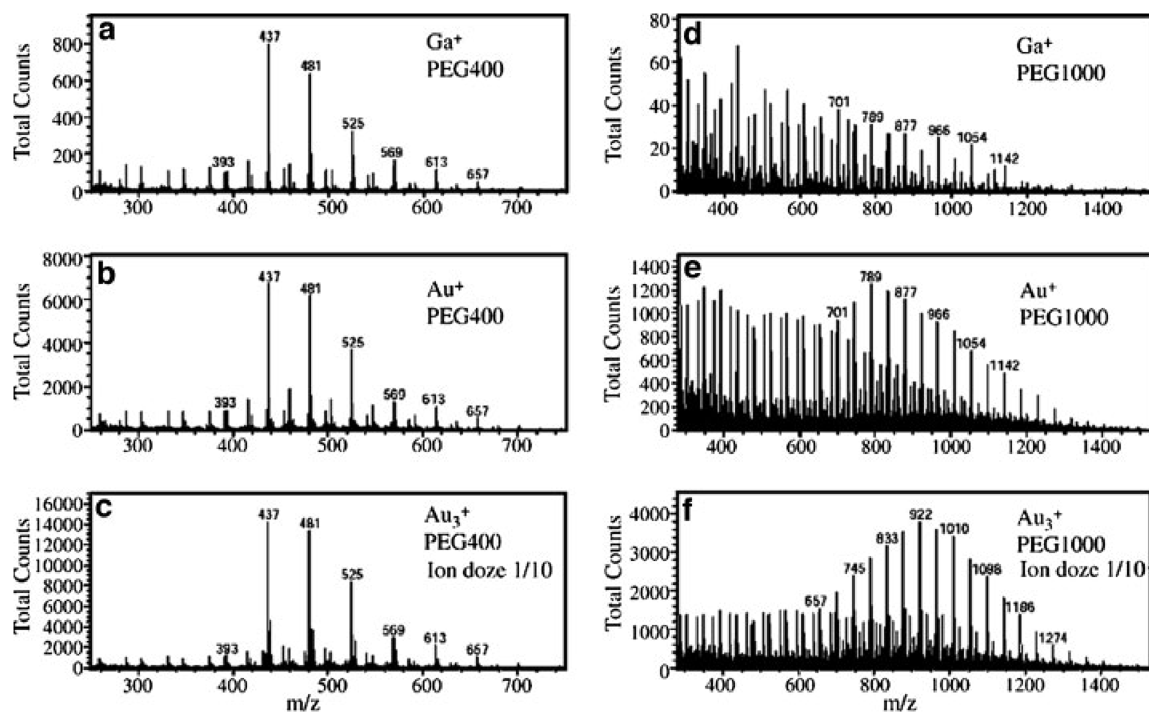

FIGURE 6. TOF–SIMS spectra from PEG 400 (**a**–**c**) and PEG 1,000 (**b**–**f**). Quasi-molecular ion peaks were detected (such as $[M+H]^+$, $[M+Na]^+$; M being the entire molecule, $m/z = 437$, 481, 525, 569, 613, 657, 701, 745, 789, 833, 877, 922, 966, 1,010, 1,054, 1,098, 1,141, and 1,186 are identified as $[M+Na]^+$ peaks with the number of monomer units varying from 9 to 26). Figure reprinted from Aimoto et al. (2006) with permission from Elsevier, copyright 2006.

Diehnelt, Van Stipdonk, and Schweikert (2001), studied this effect with several atomic and polyatomic sources, including Cs^+, $(CsI)Cs^+$, $(CsI)_2Cs^+$, $(NaF)Na^+$, $(NaF)_2Na^+$, $(NaF)_4Na^+$, SiF_5^- and C_{60}^+ for analysis of several organic surfaces. These authors noted that even though C_{60}^+ had very high molecular ion yields, this beam also produced much more fragmentation than Cs^+ and more of the ions underwent metastable fragmentation in the time scale of the experiment. The authors point out that depending upon the chemical composition of the analyzed sample, the most efficient projectile changes. For example, for a multilayer sample of α-cyano-4-hydroxycinnamic acid (ACHA), the most effective primary ion was $(CsI)Cs^+$, whereas for a multilayer sample of octylsulfate (OS), which is roughly the same molecular weight as ACHA, $(CsI)_2Cs^+$ projectiles were most effective. Also, while cluster beams were ideal for thick films, monolayer films still yielded optimal results (decreased fragmentation) with atomic beams (in this case, Cs^+).

In most cases, where polymer ion yield enhancements are studied, the enhancement for PTFE when employing polyatomic sources is much less as compared to other polymeric materials (Kötter & Benninghoven, 1998; Weibel et al., 2003). This is consistent with the fact that PTFE is extremely sensitive to radiation of any sort and suffers marked damage (in the form of depolymerization) even after low irradiation (Chapiro, 1962). Therefore, even atomic beams will yield high signals.

B. Decreased Charging

It has been repeatedly shown that employing cluster sources can eliminate charging (Appelhans & Delmore, 1987; Hirata et al., 2002, 2003; Xu et al., 2004; Cheng & Winograd, 2005). This was discovered early on by Appelhans and Delmore (1987) and has been confirmed several times since in both organic and polymeric samples (Hirata et al., 2002, 2003). With C_{60}^+, charge compensation is often not required, even in the dynamic SIMS mode (Xu et al., 2004; Cheng & Winograd, 2005). This effect has been attributed to an increase in secondary ion sputtering yields when employing cluster sources as compared to atomic beams (Xu et al., 2004). Sample charging typically occurs when there is a net imbalance of primary and secondary ions (i.e., the number of primary ion charges entering the sample, is greater than the number of secondary ion charges being removed from the sample *via* sputtering). An increased flux of secondary ions is therefore expected to offset the charge carried by the primary ion beam.

C. Secondary Ion Formation Efficiencies

While signal intensities tend to increase with cluster beams as compared to atomic beams, the disappearance cross section, defined as the exponential decay in signal as a function of fluence (see Appendix), is often times similar to or greater than that measured for atomic beams. For example, in Kötter's work with SF_5^+ (Kötter & Benninghoven, 1998), disappearance cross

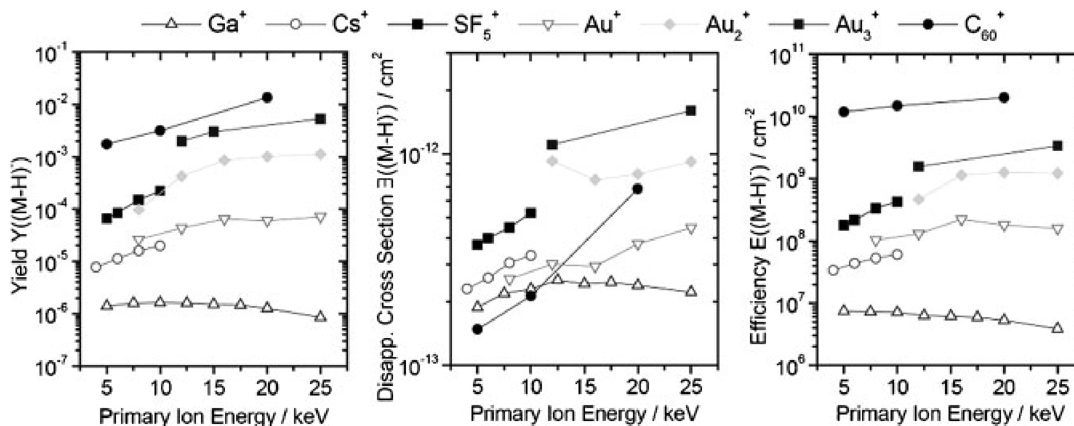

FIGURE 7. Secondary ion yield (Y), disappearance cross section (σ), and efficiency (E), of the quasi-molecular ion $(M-H)^-$ from a submonolayer sample of Irganox 1010 on low density polyethylene (LDPE), plotted as a function of the primary ion energy and species. Figure taken from Kollmer (2004) reprinted with permission from Elsevier, 2004.

sections were calculated from spin-cast films of PC and PS, where it was found that SF_5^+ bombardment yielded the highest disappearance cross sections when compared to Xe^+ and Ga^+.

In the past, with atomic beams, increased disappearance cross sections were considered to be an indication of increased chemical damage to the sample. However, consistent with the erosion model described earlier, the disappearance cross section is actually found to be dependent upon *both* the sputter removal of molecules as well as the accumulation of chemical damage (see Eq. 5, Appendix). With cluster sources, there is a lot more material being removed and therefore this also generally results in an increase in the disappearance cross section. Therefore it is often more useful in such cases to consider the secondary ion formation efficiencies, E (Kötter & Benninghoven, 1998) or the secondary ion yield divided by the disappearance cross section (see Appendix for definitions). In Kötter's work, SF_5^+ was calculated to have the greatest efficiency out of all primary ions studied, despite it having the greatest disappearance cross section.

The relative secondary ion yields, disappearance cross sections and efficiencies acquired from a submonolayer film of Irganox 1010 on a low density polyethylene (LDPE) substrate is shown in Figure 7 (Kollmer, 2004). In this case, C_{60}^+ was found to have the highest efficiency as compared to the other cluster ions, and at low energies, it even appears to have lower disappearance cross sections than atomic sources. More recent work has indicated that Bi clusters with a nuclearity greater than 3, perform similarly to C_{60}^+ in terms of efficiency (Seah, 2007).

Weibel et al. (2003) also studied the disappearance cross sections and efficiencies of PS (MW = 2,000) with both Ga^+ and C_{60}^+ ions. In all cases, C_{60}^+ was found to have considerable increases in the efficiencies, with particularly large increases for the thick samples (>10^3 times that of Ga).

It should be noted here, that other large cluster ions such as Au_{400}^+ and other massive clusters, which may have potential for even greater efficiencies, are not included in Kollmers study (Kollmer, 2004). However, it has been demonstrated that there can be significant signal enhancements and decreases in disappearance cross sections when using the Au_{400}^{4+} as compared to Au_5^+ and Au_9^+ (Tempez et al., 2004).

D. Additives in Polymers

For most applications, some form of additive is doped into the material, and the polymer serves as a binder (e.g., drug delivery, coatings and films, adhesives, etc). There have been several examples demonstrating that when employing cluster beams for analysis in polymer-based systems, a significant enhancement in the molecular signal of these additives is typically observed. For example Braun et al. (2006) published a article on depth profiling in drug-loaded cardiac stents.[2] The stents that were characterized in Braun's work were comprised of poly(styrene-co-isobutylene) (often referred to as SIBS) doped with paclitaxel. SIMS was unable to detect the paclitaxel molecular ion, when employing Ga^+ ions. However, the mass spectra acquired with C_{60}^+ showed strong signal associated with the protonated molecular ion at $m/z = 855$ (see Fig. 8). This molecule has also been detected with SF_5^+ (Mahoney et al., 2006b).

Another study involving additives was published by Bryan et al. (2004). In this study, several organic samples were characterized using a Au cluster source, including several additive-doped polymers. The Au clusters were found to provide a drastic improvement in additive signals with the greatest enhancements occurring from Au^+ to Au_2^+ (Bryan et al., 2004).

[2]A stent is a small, coiled, wire-mesh tube that is inserted permanently into an artery during an angioplasty procedure. The stent acts as a scaffold, helping to keep the artery open and decrease the probability of restenosis of the artery (build up of smooth muscle cells at the site of the stent). To further prevent restenosis, some stents have incorporated a drug delivery system into the structure of the stent, where a drug (e.g., paclitaxel or sirolimus) is released at a controlled rate from a polymer film or multiple polymeric layers. This drug serves to prevent cell regrowth from blocking the artery again at the angioplasty site.

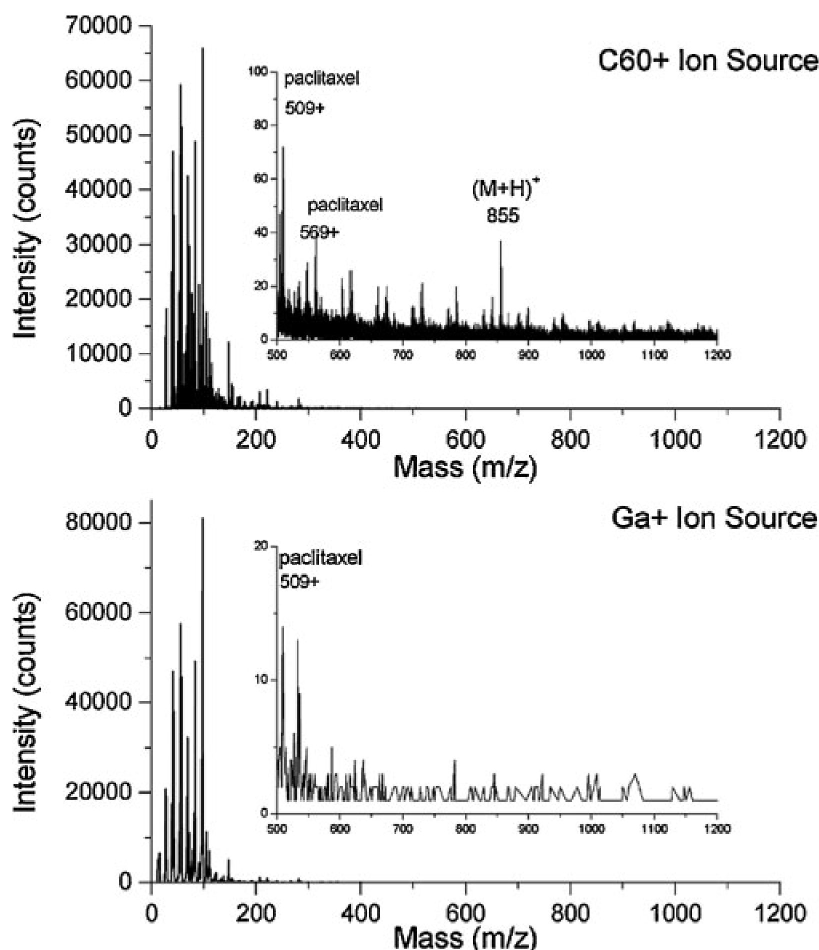

FIGURE 8. Secondary ion mass spectra of a paclitaxel-loaded SIBS [poly(styrene-co-isobutylene)] copolymer. The data were generated utilizing Ga^+ ions (lower spectrum) and C_{60}^+ ions (upper spectrum) with primary ion fluences $\leq 1 \times 10^{12}$ ions/cm^2. The spectra clearly show detection of higher mass species using C_{60}^+ primary ions. Figure taken from Braun et al. (2006) reprinted with permission from American Chemical Society, copyright 2006.

E. Efficacy of Cluster Beams for Thin Films

Consistent with the MD calculations described earlier (Postawa et al., 2005; Czerwiński et al., 2006), secondary ion yield enhancements for organic thin films tend to be much lower than for bulk organics (Gillen & Roberson, 1998; Harris et al., 1999; Stapel, Brox, & Benninghoven, 1999; Stapel, Thiemann, & Benninghoven, 2000; Diehnelt, Van Stipdonk, & Schweikert, 2001; Stapel & Benninghoven, 2001). A good example of the effect of overlayer thickness was demonstrated by Stapel et al., who performed several studies on characterization of thin organic overlayers of varying thickness (Stapel, Thiemann, & Benninghoven, 2000; Stapel & Benninghoven, 2001). The authors found that when characterizing PMA LB layers ranging from $n = 1$ to $n = 9$, the secondary ion yield enhancement was much more pronounced for multilayer coverage (Stapel, Thiemann, & Benninghoven, 2000). The disappearance cross sections for the multilayer films were also much smaller than for the monolayer films when employing cluster sources.

Weibel et al. similarly studied the disappearance cross sections of both thin monolayer and thick films of PS (MW = 2,000) bombarded with both Ga^+ and C_{60}^+ ions (Weibel et al., 2003). For the thin films, the resulting disappearance cross sections for the two primary ions were very similar. However, the signal decay from the multilayer film was much slower with C_{60}^+ as compared to Ga^+, indicating decreased chemical damage in the PS by C_{60}^+.

F. Importance of Cluster Size and Chemistry

The relationship of cluster size to signal enhancement and damage characteristics were also determined by Stapel and co-workers (Stapel, Thiemann, & Benninghoven, 2000; Stapel & Benninghoven, 2001), where the secondary ion yields, disappearance cross sections and efficiencies were plotted as a function of primary ion size and nuclearity for samples of Irganox, polyethylene (PE) (Stapel & Benninghoven, 2001) and

polymethylacrylate (PMA) LB-layers on Si substrates (Stapel, Thiemann, & Benninghoven, 2000). The ions employed were created from an electron impact source and included Ne^+, Ar^+, Xe^+, O_2^+, CO_2^+, SF_5^+, $C_7H_7^+$, $C_{10}H_8^+$, $C_6F_6^+$, and $C_{10}F_8^+$. The resulting yields from these various ions are shown in Figure 9, which displays the yields and normalized yields of characteristic PMA fragment ions as a function of primary ion nuclearity (top) and mass (bottom) (Stapel, Thiemann, & Benninghoven, 2000). As can be seen, a major increase in secondary ion yields occurs from 1 to about 6 atoms (SF_5^+).

Any additional yield increases from 6 to 18 atoms are minimal. In other words, there is some sort of "saturation effect" occurring. This "saturation" effect was also observed when plotting the disappearance cross sections and efficiencies (Stapel, Thiemann, & Benninghoven, 2000), and has been observed in several other works as well (Benguerba et al., 1991; Boussofiane-Baudin et al., 1994; Bryan et al., 2004; Nagy, Gelb, & Walker, 2005; Nagy & Walker, 2007). MD simulations of impacts of C_{60}, C_{70}, C_{76}, C_{78}, and C_{84} on graphite (Webb et al., 1997) are consistent with these results, where authors found that

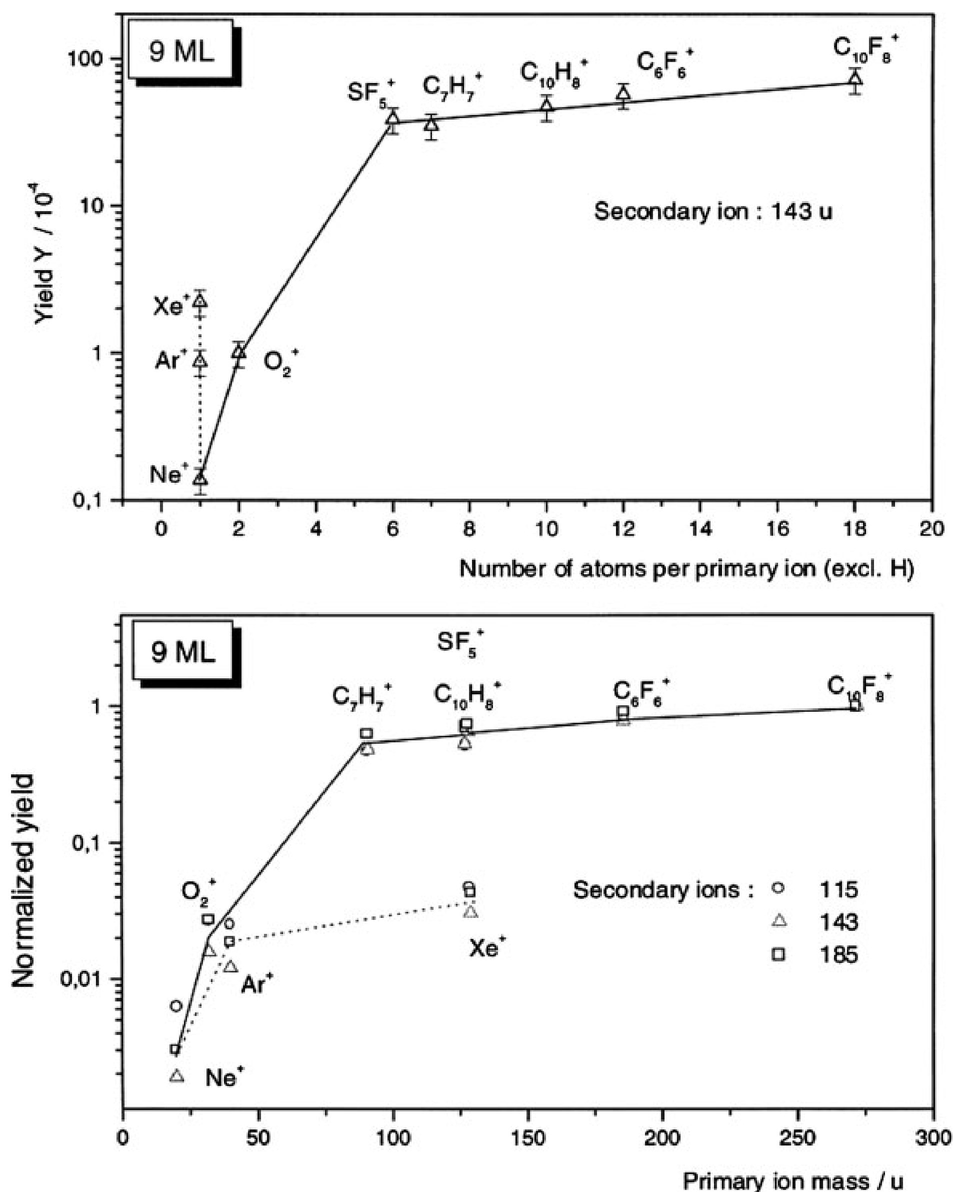

FIGURE 9. Yields and normalized yields of characteristic PMA fragment ions emitted from a multilayer sample under atomic (Ne^+, Ar^+, Xe^+) and molecular (O_2^+, SF_5^+, $C_7H_7^+$, $C_{10}H_8^+$, $C_6F_6^+$, $C_{10}F_8^+$) primary ion bombardment. In the top graph, yields for fragment at $m/z = 143$ are plotted as a function of the number of constituents per primary ion. In the bottom graph, the normalized yields for fragments at $m/z = 115$, 143, and 185 are plotted as a function of primary ion mass. Figure taken from Stapel, Thiemann, and Benninghoven (2000) reprinted with permission from Elsevier, copyright 2000.

the penetration depth and number of displaced atoms was found to be independent of the molecule size in this range.

Stapel and co-workers also noted that there was no observed chemical effect when using fluoronated beams such as SF_5^+ under static SIMS conditions as there was no observed difference when changing from fluorine containing primary ions to hydrocarbon primary ions of comparable mass. All efficiencies were much greater for the molecular beams as compared to the atomic beams, however at extremely low energies (<1 keV), the performance of Xe^+ outweighed the performance of SF_5^+ (secondary ion formation efficiencies were higher for Xe^+ than for low energy SF_5^+). This was attributed to the fact that 1 keV SF_5^+ bombardment corresponds to only 150 eV per atom, an energy close to the sputter threshold (see Appendix for definitions) (Stapel, Thiemann, & Benninghoven, 2000).

Again, it should be noted, that C_{60}^+ and other large cluster ions, such as Au_{400}^+ and massive gas clusters, are not included in Stapel's studies (Stapel, Thiemann, & Benninghoven, 2000). Some of these massive projectiles are known to exhibit abundant multi-ion emission (the emission of multiple ions from a single projectile impact) resulting in even further enhancements in ion yield (Verkjoturov et al., 2006). It is believed that these enhancements result from the different behavior of the massive projectiles when bombarding a surface as compared to smaller cluster projectiles. More specifically, the atoms in these massive projectiles tend to behave as a collective unit when bombarding a surface, as opposed to smaller clusters, where each atom in the cluster forms its own individual collision cascades (Czerwiński et al., 2006).

G. Matrix-Enhanced and Metal-Assisted Cluster SIMS

One way of improving molecular signals prior to the advent of cluster SIMS was to use matrix-enhanced or metal-assisted SIMS. In *metal-assisted* SIMS, the sample is coated with a thin layer of a metal, such as Au or Ag, which can result in significant enhancements in signal (by a factor of 10 or more) and the formation of additional adduct ions (Grade & Cooks, 1978; Linton et al., 1993). In *matrix-enhanced* SIMS, the sample is placed in a signal enhancing matrix (such as sinapic acid) and analyzed in a similar manner as Matrix-Assisted Laser Desorption Ionization (MALDI) (Wu & Odom, 1996; Wittmaack et al., 2000).

One of the questions that some scientists have been trying to answer is whether or not these enhancements will occur with cluster beams as well. Adriaensen et al. attempted to answer this question by depositing Ag and Au layers onto a series of organic dyes and pharmaceuticals and determining the effects on the secondary ion yields when employing Ga^+ and SF_5^+ beams (Adriaensen, Vangaever, & Gijbels, 2004). They found that both ion beams yielded increases in positive secondary ion yields, after deposition of the metal overlayers, though there was a much-reduced effect observed with SF_5^+ as compared to Ga^+.

Later, Delcorte and co-workers characterized the surface of several polymeric-based samples including PS, PE, and PP coated with varying amounts of gold (Delcorte, Poleunis, & Bertrand, 2006b; Delcorte and Garrison, 2007; Delcorte et al., 2007). The samples were analyzed with Ga^+, In^+, and C_{60}^+ probes. In general it was found that gold metallization of the surface did not provide a significant enhancement of the characteristic fragment and parent-like ion yields when employing C_{60}^+. However, it was found that C_{60}^+ lead to an enormous yield enhancement for characteristic gold clusters (three orders of magnitude over what was observed for Ga^+). The general trend observed was that while increasing coverage of the surface by gold leads to increasing organic ion yields when using Ga^+ projectiles, the ion yields decrease with increasing coverage with C_{60}^+ bombardment.

Another example of metal-assisted cluster SIMS was published recently by Guillermier et al. (2006b). In this work, the authors used a Au_{400}^{4+} probe at 136 keV impact energy to characterize a sample of glycine coated with 1 nm of Ag, where the yields of the CN^- ion were doubled with the silver coating. A multitude of CN-based Ag clusters were also formed. However, similar to Delcortes' work, the molecular ion signal was not enhanced by the metal overlayer. In fact, the molecular ion signal dropped dramatically when coated with Ag.

A good example of matrix-enhanced cluster SIMS of organic samples was given by Locklear et al., who used a specialized C_{60}^+ source, in the event-by-event mode (see source section) to investigate the emission of the gramicidin S $(M-H)^-$ ion embedded in a matrix of sinapic acid. There was an observed increase in ion yield by up to 8 times, simply by controlling the ratio of gramicidin S to sinapic acid (Locklear et al., 2006).

Finally, both metal-assisted SIMS and matrix-enhanced SIMS were studied employing Bi^+ polyatomic sources by McDonnell et al. (2006) for biological systems. In this work, the authors characterized Au-coated and matrix-coated (with 2,5-dihydroxybenzoic acid sprayed onto the surface) tissue samples with varying cluster sizes. The authors found a similar enhancement when either employing Bi_1^+ with a gold coating or using Bi_3^+ with no coating (as compared to Bi_1^+ with no Au coating). Characterizing the Au-coated sample with Bi_3^+ primary ions resulted in even further increases in signal. Similar results were obtained from matrix-enhanced SIMS. This effect however, was observed *only* in the positive ion mode, most likely because the mechanisms involve the attachment of protons (which will only be observed in the positive ion mode).

H. 2-D Imaging

The signal enhancements employed for mass spectral analysis can be extremely beneficial for imaging applications, particularly when looking for trace constituents in the mid- to high-mass region, as there can be a dramatic increase in signal in this region. Unfortunately, there is typically an increase in the background signal when employing cluster beams. This can be particularly problematic in the low-mass range, as it may lead to interferences.

The increased signal associated with these cluster sources, particularly liquid metal ion sources such as Au and Bi cluster sources, has led to a large amount of research on biological tissue imaging applications, where these sources have been shown to yield very intense secondary ion images, particularly of phospholipids and cholesterol, in brain tissue (Sjovall, Lausmaa,

& Johansson, 2004; Touboul et al., 2004, 2005b; Nygren et al., 2005), cardiac tissue (Aranyosiova et al., 2006), and other biological cross sections (Touboul et al., 2005a). For an overview of biological tissue imaging with LMIG cluster sources, see references (Brunelle, Touboul, & Laprevote, 2005).

C_{60} sources have also been used for bioimaging and bioanalysis applications (Brunelle et al., 1997; Baker et al., 2006). Although the spot size is much greater for the C_{60}^+ source, than for LMIG sources, the signal enhancement tends to be much greater for C_{60}^+, and it tends to be more surface-sensitive due to the reduced penetration depth of the beam as compared to LMIG clusters (Baker et al., 2006). Jones et al. for example compared Au_3^+ to C_{60}^+ for biological imaging applications, where the authors attempted to image the distribution of a drug, raclopride, in a rat brain section. As expected, the highest efficiencies (E) were found for C_{60}^+ (Jones, Lockyer, & Vickerman, 2007). Although the drug was detected with C_{60}^+, the distribution by SIMS did not corroborate with the known locations of the receptor sites. This was attributed to commonly occurring matrix effects in SIMS. More specifically, the protonated molecular ion of the drug, $(M+H)^+$, was enhanced in regions which contained large amounts of cholesterol, while it was suppressed in regions containing high amounts of phosphatidylcholine. This was attributed to the cholesterol acting as a source of protons for the drug (Jones, Lockyer, & Vickerman, 2006) in that it tends to form deprotonated molecular ions $(M-H)^+$, while the phosphatidlycholine removes a proton from the environment by forming protonated molecular ions $(M+H)^+$ and therefore suppresses the formation of the protonated molecular ion in the drug. This was a very important result, helping to better understand ionization phenomena in complex matrices.

An example of C_{60}^+ imaging in polymeric based materials is given by Xu and co-workers (Xu et al., 2004), who compared Ga^+ and C_{60}^+ primary ion probes for imaging in combinatorial resin particles (Fig. 10). Though the image resolution in the figure is very poor as compared to liquid metal ion sources, the benefits of using C_{60}^+ as a probe are evident in that there are much higher intensities and efficiencies as compared to that observed with the Ga^+ probe (by ~2 orders of magnitude). Also, when C_{60}^+ is used, the signals originating from the polymer are more intense than those measured from the silicon substrate, whereas the opposite is observed in the image obtained with Ga^+. Charge compensation was found to improve dramatically as well when using C_{60}^+, where it was not necessary to use an electron flood gun during analysis.

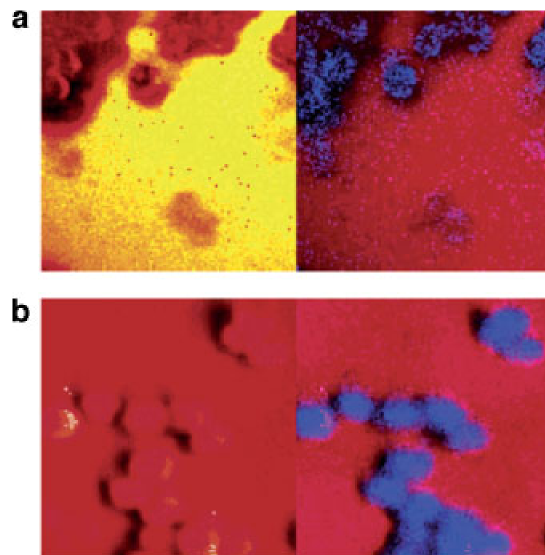

FIGURE 10. SIMS images (400 μm × 400 μm) of Biotin-Sasrin linker—copoly(styrene-1% divinylbenzene) resins acquired with (**a**) Ga^+, and (**b**) C_{60}^+ primary ions. The images on the left in both panels are the total ion images, while the images on the right show an image overlay of the biotin molecular ion (blue), and silicon (red) from the substrate. Figure taken from Xu et al. (2004), reprinted with permission from American Chemical Society, copyright 2006.

V. AN INTRODUCTION TO POLYMER DEPTH PROFILING

The first demonstration of "molecular depth profiling" with cluster ion beams was published in 1994, where authors employed massive glycerol cluster ions to characterize various biological samples (Cornett, Lee, & Mahoney, 1994). The primary results of this work are depicted in Figure 11, which shows secondary ion intensities from a protein sample (pentagetide), plotted as a function of increasing sputter time for both glycerol cluster ions and Xe^+ atomic ions. The investigators were able to demonstrate that when employing glycerol cluster ions, instead of atomic ions, the signal remained constant with increasing sputtering time. In contrast, when similar experiments were performed with Xe^+ ions, there was rapid signal decay with sputtering time. They attributed this behavior to much slower sample damage accumulation when using the low-energy cluster sources as opposed to the intense energetic atomic beams, which cause rapid sample destruction.

The first "molecular depth profile"[3] of a polymeric sample was demonstrated not much later by Gillen and Roberson (1998) using an SF_5^+ cluster source. The results from this work are depicted in Figure 12, which compares depth profiles of a PMMA sample cast onto a silicon substrate. Here, the signal intensity of $m/z = 69$, a fragment characteristic of PMMA, was plotted as a function of increasing sputter time with both Ar^+ (left panel) and SF_5^+ (right panel). While there was rapid signal degradation when using Ar^+, the signal remained relatively constant with increasing sputter time when employing SF_5^+ clusters. The substrate was reached after only 200 sec of sputtering with the SF_5^+ source, while the polymer/Si interface could only be reached after prolonged sputtering of the film at higher primary ion currents when employing the Ar^+ source.

The success of the polymeric depth profile was attributed to both surface-localized damage and increased sputter rates. In other words, there was very little subsurface damage, and the

[3]Note that any depth profile obtained from polymers using this technique is not a true "molecular" depth profile, because one is typically measuring fragment ion intensities that are characteristic of the polymer as a function of depth and not the polymer molecule itself.

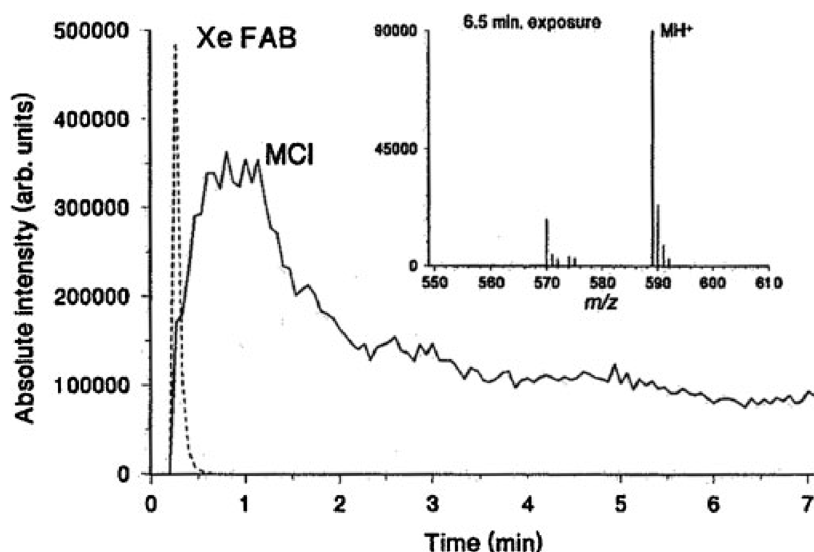

FIGURE 11. Plot of protonated molecular ion intensity versus exposure time for a dry sample of 2 nmol pentagetide using a 15 kV massive glycerol cluster ion beam (solid line) and a 6 kV Xenon beam (dashed line). Data are plotted on the same intensity scale. Inset is the massive glycerol cluster ion mass spectrum acquired after 6.5 min of exposure. Figure from Cornett et al. (1994), reprinted with permission from John Wiley & Sons, Ltd, copyright 1994.

damage that was created was removed rapidly. The authors also attempted to depth profile through polyimide (PI) and polyvinyl pyridine (PVP) samples, without success.

Later, Fuoco and co-workers examined the basic mechanisms of secondary ion yield and sputtering yield enhancement in PMMA, by measuring weight loss (using a quartz crystal microbalance), volume loss (*via* sputter rates) and surface chemical changes (using X-ray Photoelectron Spectroscopy) in PMMA films sputtered by both SF_5^+ and Ar^+ projectiles (Fuoco et al., 2001). The results of this work are summarized in Figure 13.

Figure 13a,b shows the sputter rates (as determined by stylus profilometry) plotted as a function of increasing fluence for Ar^+ and SF_5^+ ions respectively. While there is a decrease in the measured sputter rate with fluence for Ar^+ primary ions, the sputter rate of the PMMA remains constant over the entire thickness of the film (50–60 nm) for SF_5^+ primary ions. These results contradict Norrman et al. who determined that thin

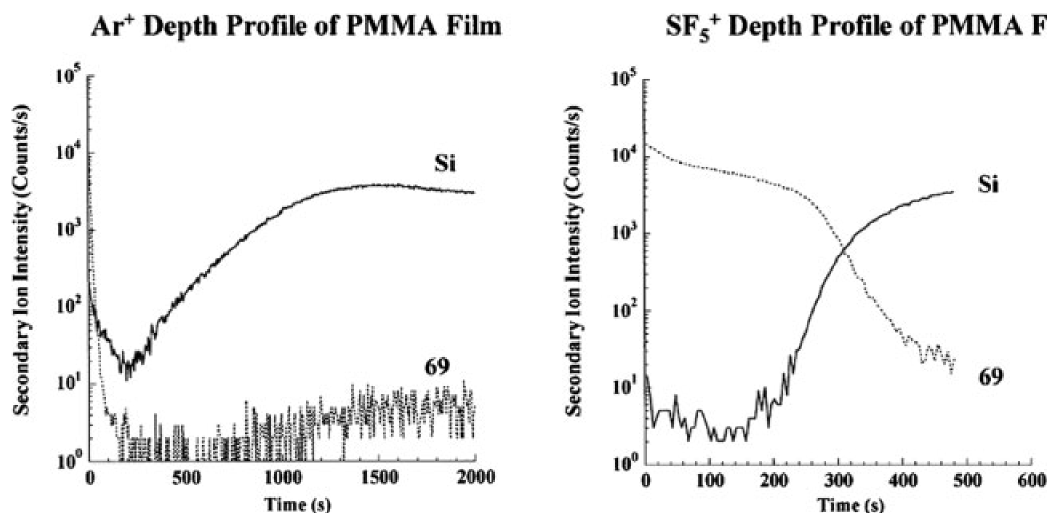

FIGURE 12. Comparison of depth profiles obtained from a 50 nm thick, spun-cast film of PMMA using Ar^+ and SF_5^+ primary ion bombardment under dynamic SIMS conditions. The SF_5^+ primary ion fluence required to reach the interface was approximately 1.7×10^{15} ions/cm^2 (1×10^{16} atoms/cm^2). The characteristic fragment at $m/z = 69$ was monitored. Figure from Gillen and Roberson (1998), reprinted with permission from John Wiley & Sons, Ltd, copyright 1998.

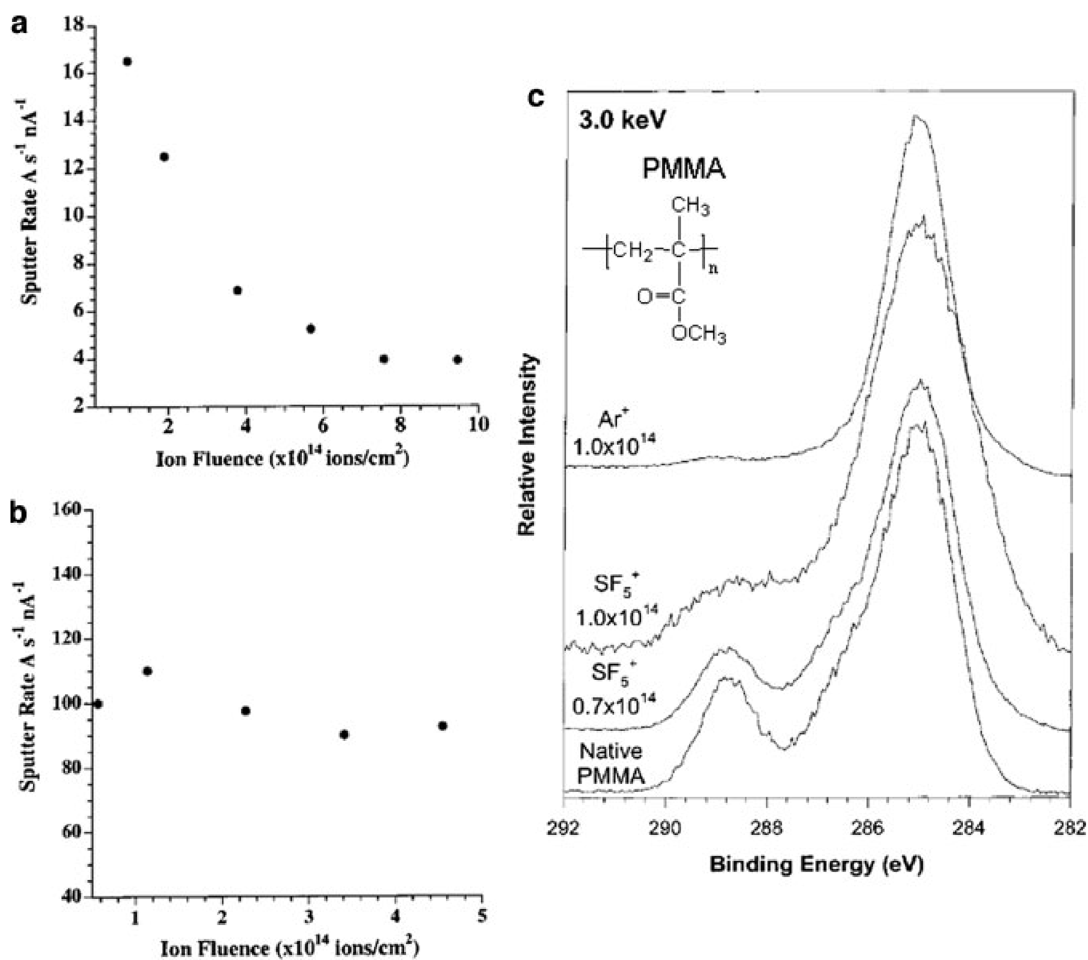

FIGURE 13. (**a**) Sputter rate measurements plotted as a function of increasing ion fluence for PMMA bombarded with 5.5 keV Ar^+ ions, (**b**) Sputter rate measurements plotted as a function of increasing ion fluence for PMMA bombarded with 5.5 keV SF_5^+ ions, and (**c**) Comparison of the C(1s) core level XPS spectra acquired from a PMMA sample bombarded with SF_5^+ and Ar^+ ions. Figure from Fuoco et al. (2001), reprinted with permission from American Chemical Society, copyright 2001.

overlayers of PMMA depth profiled with SF_5^+ yields non-linear increases in sputter rate (Norrman, Haugshoj, & Larsen, 2002). However, this increased sputter rate in this particular study is highly correlated with decreased coverage of the PMMA on the Si substrate at low concentrations. Thus, significant changes in the sputter mechanisms are likely. The finding of constant sputter rate with film thickness has been repeated with other polymeric materials, with similar results (Shard et al., 2007).

XPS studies indicated that there were significantly higher C concentrations and lower O concentrations when sputtering with Ar^+ as compared to SF_5^+ ions under similar conditions (Gillen & Roberson, 1998), consistent with increased chemical damage in the form of side-chain cleavage when employing the atomic source. The high-resolution XPS spectra also illustrate significant differences in the resulting chemistries. Figure 13c depicts the high-resolution C(1s) XPS spectra of the native PMMA surface as compared to SF_5^+ and Ar^+-bombarded regions. In the native PMMA, there are three major components, the largest being the aliphatic carbon peak at a binding energy of 285.0 eV. There is also a methoxylic carbon component, which is shifted to slightly higher binding energies (286.5 eV). Finally, the carboxylic carbon peak occurs at 288.9 eV. As can be seen, the results indicated a significant loss of the carboxylic carbon moiety upon sputtering with Ar^+ as compared to SF_5^+. This is further evidence for decreased chemical damage when employing cluster beams. The overall results for Ar^+ were consistent with what had been observed previously with atomic bombardment of PMMA (Licciardello et al., 1996; Pignataro, Fragalà, & Puglisi, 1997).

XPS of other cluster ion-bombarded polymeric materials have yielded similar results when comparing atomic and polyatomic bombardment, indicating decreased chemical damage when employing polyatomic sources in materials such as PTFE (Sanada et al., 2004), PLA (Yotoriyama et al., 2006; Mahoney et al., 2007b), and polycarbonate (PC) (Zemek et al., 1999).

It should be noted that at energies lower than 1 keV (0.7 keV), the sputter properties (i.e., sputter yields and depth

profile compositions) of SF_5^+ were found to be similar to Ar^+ (Fuoco et al., 2001). More specifically, the sputtering yields of both ions at 0.7 keV were very low, and the depth profiles indicated increased damage accumulation as compared to what was observed for 3 keV SF_5^+. The poor performance of the low energy SF_5^+ ions was attributed to the fact that 0.7 keV SF_5^+ bombardment corresponds to an energy close to or below the sputter threshold for the PMMA, previously defined as 150 eV per atom (Stapel, Thiemann, & Benninghoven, 2000). Though sputtering is often observed subthreshold for many clusters due to the non-linear nature of the sputtering event, SF_5^+ is a relatively small cluster, so the sputtering threshold may play a bigger role in this case.

Brox et al. compared depth profiles of several different polymers using Ar^+, SF_5^+, Cs^+, and Xe^+ (Brox, Hellweg, & Benninghoven, 2000) to explore the capabilities and limitations of cluster beams for polymer depth profiling. While Ar^+ bombardment resulted in rapid signal decay in all cases, Cs^+, Xe^+, and SF_5^+ were able to profile through certain materials without complete loss of characteristic signal. The best results however, were obtained with SF_5^+, yielding constant signals as a function of depth. The sputtering yields measured in this study, were found to increase in the order of $Ar^+ < Xe^+ < SF_5^+$.

The successful depth profiles in this study included thin films of poly(propyleneglycol) (PPG), PEG, and PMMA. In these profiles there was a characteristic decrease in signal intensity at the beginning of the sputtering process, followed by a more or less pronounced stabilization of the signals until the Si interface was reached. At this point, the substrate ion intensities increased rapidly with a commensurate decrease in polymer fragment ion signals. While these polymers did maintain characteristic molecular signals as a function of increasing fluence, there were still many more polymers that did not, including PC, PS, PE, and polyisoprene (PIP). In addition, all bulk polymers except for PTFE showed an immediate and rapid decrease in characteristic secondary ion emission for all applied sputter ions. The authors concluded that polymeric depth profiling was more of an exception than a rule (Brox, Hellweg, & Benninghoven, 2000).

However, starting with the discovery of well-behaved polyesters by Mahoney, Roberson, and Gillen (2004), and followed by the determination and optimization of important experimental parameters, such as temperature (Mahoney et al., 2006a, 2007b; Mahoney, Patwardhan, & McDermott, 2006b; Möllers et al., 2006; Mahoney, Fahey, & Gillen, 2007a), beam chemistry and size (e.g., C_{60}^+ or SF_5^+ or Ar_{2000}), beam angle (Kozole, Wucher, & Winograd, 2008) and beam energy (Fisher et al., 2008; Shard et al., 2008), it is now understood that this is not the case, and that even polymers that were originally thought of as ''impossible to depth profile'' (e.g., PS), can now be depth profiled using certain cluster beams.

In general, attempts to depth profile through polymeric (and other organic) materials will result in one of the following scenarios depicted in Figure 14. In polymers that are more amenable to being depth profiled (such as PLA, PGA, and PCL), the materials will undergo an initial (exponential) signal intensity drop (region 1) (in some cases, there may be an initial increase in intensity). This region has been researched thoroughly and its shape predicted somewhat by the erosion model described earlier for molecular samples (Gillen, Simons, & Williams, 1990; Cheng, Wucher, & Winograd, 2006; Wucher, 2008). Next is a constant signal intensity or steady-state signal region (region 2), and finally, an interfacial region where the signal intensity drops

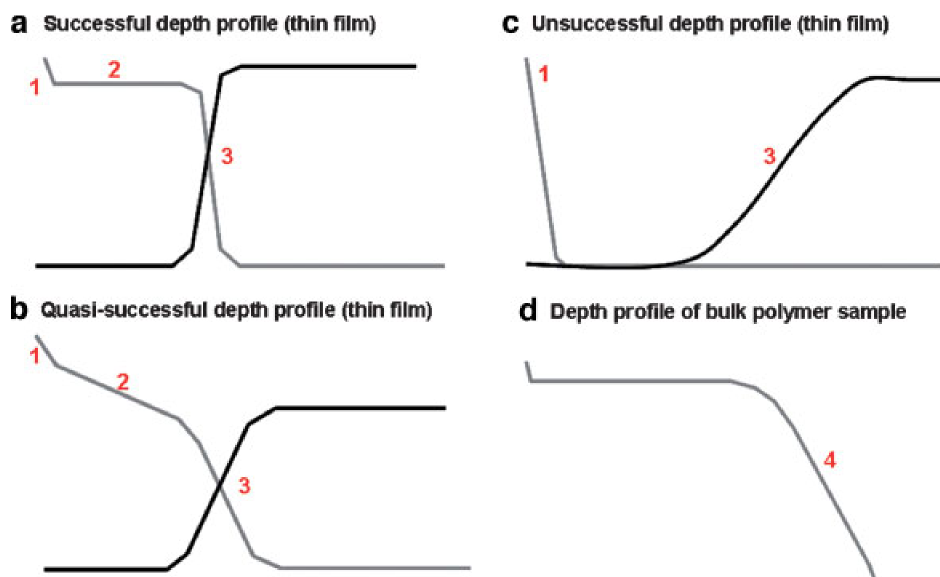

FIGURE 14. Different scenarios (**a–d**) in polymeric depth profiling: In thin films, there are typically 3 regions: (1) Initial drop in signal intensity often defined by disappearance cross section of the material. (2) A steady state region (or pseudo-steady state region in the case of **b**) and interfacial region. In bulk materials there is almost always an eventual loss of signal intensity after a certain critical fluence. This critical fluence varies with source and energy. [Color figure can be viewed in the online issue, which is available at www.interscience.wiley.com.]

with a corresponding increase in substrate signal (region 3). In polymers that are not amenable to depth profiling under polyatomic bombardment, the signal degrades immediately, such as in the case of PS, PE, PP, and PC (Fig. 14c) under C_{60}^{+} or SF_5^{+} bombardment. The substrate will eventually be reached, but the interface width will typically be broad. Some cases exibit intermediate behavior, such as PMMA under SF_5^{+} bombardment (Fig. 14b). Eventually even the materials that are amenable to being depth profiled will lose signal, under higher fluences, typically in a manner as that depicted in Figure 14d. What determines which materials will behave as that shown in Figure 14a or b as opposed to that observed in Figure 13c? What causes the eventual loss of signal shown in Figure 14d? A good portion of the answer has already been determined through well-known degradation chemistries in polymers, which will be described in greater detail in the next section.

VI. RADIATION CHEMISTRY IN POLYMERIC MATERIALS

A. Background

There are generally two groups of polymers, often referred to as Type I and Type II polymers (Chapiro, 1962). Type I polymers typically crosslink when irradiated by various types of radiation (such as electrons, neutrons, alpha particles, accelerated ions, X-rays, gamma rays, and beta rays). These include polymers such as polyethylene, polystyrene, and other polymeric materials that are either aromatic or have very little branching associated with them. Type II polymers however, pre-dominantly degrade under irradiation through a random chain scission process. Type II polymers, include polymers such as PIB, PMMA, and poly(α-methylstyrene) (PAMS) and other polymers with increased branching or ''weakened'' points located on the main-chain backbone (Chapiro, 1962; Calcagno, 1995).

In both types, the mechanisms of degradation are complex and are known to involve free radical intermediates. Tables 1–3 list several polymers and their characteristics under irradiation (Type I and Type II polymers). Also listed in the tables are the gases given off during the irradiation, and the polymers behavior under cluster ion bombardment (i.e., do they depth profile to some degree when employing cluster beams, and if so, which beams are required?). In general, it can be seen that polymers with high concentrations of quaternary carbon atoms along the chain (e.g. CH_2-CR_2) undergo scission, while those with a structure of CH_2-CH_2 or CH_2-CHR tend to crosslink. It is assumed that the presence of a tetrasubstituted carbon in the chain causes strain in the molecule by a steric repulsion effect. This results in the main chain being weakened.

It also appears that the most radiation-resistant (cross-linking) polymers contain aromatic substituents. There is a high radiation resistance of the aromatic nucleus. This effect is said to be related to the deactivation or ''protection'' produced by aromatic compounds. The charge formed is resonance-stabilized and so the molecule does not lose its structure. Also, any activated state is likely to lose its energy through internal conversion (Chapiro, 1962).

Several polymers of group I, which normally cross-link under irradiation, can be degraded if irradiated in a highly divided form (i.e., with a large surface to volume ratio) in the presence of oxygen. It is most likely that when irradiation is carried out in air, some of the polymeric radicals, which would otherwise lead to crosslinking, react with O_2 to form peroxidic structures which eventually decompose and cause oxidative degradation of the main chain. This effect is particularly pronounced in polymers which can be easily oxidized such as for polypropylene. Another good example is PTFE, which undergoes extreme degradation in the presence of O_2. However, when Teflon is irradiated in the absence of oxygen, this polymer also suffers much less radiation damage.

When bulk polymers are subjected to irradiation, these effects are less pronounced, since the oxidation process is then diffusion-controlled and becomes noticeable only at very low fluence rates, when the rate of diffusion of O_2 into the polymer is higher than the rate of consumption of this gas by the chemical reactions. On the other hand, O_2 can inhibit the degradation process in polymers such as PMMA when irradiated in a highly divided form. It is likely that either the deactivation of polymeric free radicals or an energy transfer involving excited polymeric molecules by O_2 is occurring in this case.

Another way to convert a crosslinking polymer into a degrading polymer, is to use specific conditions favoring the formation of a radical polymer-halogen. For PS, for example the reaction is carried out in halogenated solvents (CCl_4, $CHCl_3$) in the presence of O_2.

Even in Type II samples, crosslinking eventually pre-dominates under higher fluences. A good example of this is PMMA, which has been studied extensively. PMMA behaves as a positive resist at low fluences, but behaves as a negative resist at high fluences (Licciardello et al., 1996). Upon ion bombardment, the molecular weight initially decreases with fluence, but at higher fluences the molecular weight actually starts increasing.

The structure of the subsurface region of PMMA bombarded with low energy (250 eV) Ar^+ ions was studied by Koval (2004) who used electron beam lithography and scanning electron microscopy to visualize these layers. In this work, the ion irradiated PMMA was found to contain three distinct layers. The top layer was comprised of an insoluble graphitized material displaying a substantial electrical conductance. Underneath the graphitized PMMA layer, a highly crosslinked stratum was observed, which was found to be insoluble in acetone, like the graphitized region, yet was not conducting. Finally, a low molecular weight layer was located between the crosslinked layer and the bulk PMMA. This layer was observed by selectively dissolving it away using solutions of methyl isobutyl ketone/isopropyl alcohol (MIBK/IPA).

In addition to crosslinking, polymers will tend to form double bonds upon irradiation, increasing the extent of unsaturation in the material. This will often cause a discoloration at higher fluences (Chapiro, 1962). Cyclization also can occur under irradiation *via* intermolecular, and intramolecular cross-linking. It has been suggested that this process is particularly favored by crystallinity (Chapiro, 1962). SIMS results are consistent with this (Mahoney, Patwardhan, & McDermott, 2006b).

TABLE 1. Polymeric structures and their behavior under irradiation

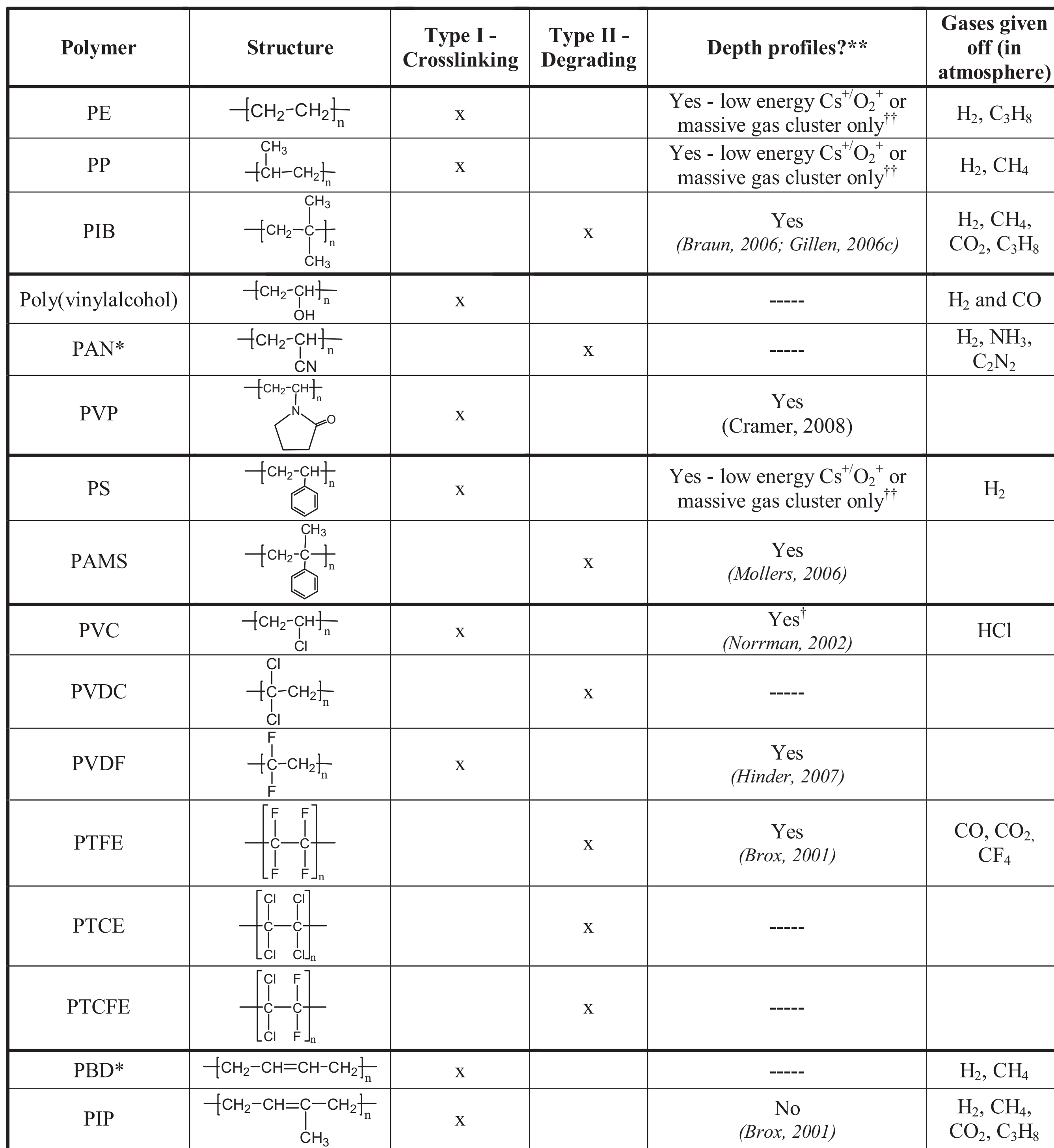

Polymer	Structure	Type I - Crosslinking	Type II - Degrading	Depth profiles?**	Gases given off (in atmosphere)
PE	$-[CH_2-CH_2]_n-$	x		Yes - low energy Cs^{+}/O_2^{+} or massive gas cluster only††	H_2, C_3H_8
PP	$-[CH(CH_3)-CH_2]_n-$	x		Yes - low energy Cs^{+}/O_2^{+} or massive gas cluster only††	H_2, CH_4
PIB	$-[CH_2-C(CH_3)_2]_n-$		x	Yes *(Braun, 2006; Gillen, 2006c)*	H_2, CH_4, CO_2, C_3H_8
Poly(vinylalcohol)	$-[CH_2-CH(OH)]_n-$	x		-----	H_2 and CO
PAN*	$-[CH_2-CH(CN)]_n-$		x	-----	H_2, NH_3, C_2N_2
PVP	$-[CH_2-CH(N\text{-pyrrolidone})]_n-$	x		Yes (Cramer, 2008)	
PS	$-[CH_2-CH(C_6H_5)]_n-$	x		Yes - low energy Cs^{+}/O_2^{+} or massive gas cluster only††	H_2
PAMS	$-[CH_2-C(CH_3)(C_6H_5)]_n-$		x	Yes *(Mollers, 2006)*	
PVC	$-[CH_2-CH(Cl)]_n-$	x		Yes† *(Norrman, 2002)*	HCl
PVDC	$-[CCl_2-CH_2]_n-$		x	-----	
PVDF	$-[CF_2-CH_2]_n-$	x		Yes *(Hinder, 2007)*	
PTFE	$-[CF_2-CF_2]_n-$		x	Yes *(Brox, 2001)*	CO, CO_2, CF_4
PTCE	$-[CCl_2-CCl_2]_n-$		x	-----	
PTCFE	$-[CCl_2-CF_2]_n-$		x	-----	
PBD*	$-[CH_2-CH=CH-CH_2]_n-$	x		-----	H_2, CH_4
PIP	$-[CH_2-CH=C(CH_3)-CH_2]_n-$	x		No *(Brox, 2001)*	H_2, CH_4, CO_2, C_3H_8

Polymers are grouped according to their structural features.
*PAN, polyacrylonitrile; PBD, polybutadiene.
**The answers reported reflect the current state of the literature, under the conditions the literature specifies.
†Rise of Si substrate signal reported only.
††Mine et al. (2007), Cramer et al. (2008), Houssiau, Douhard, and Mine, (2008), Ninomiya et al. (in press).

TABLE 2. Polymeric structures and their behavior under irradiation

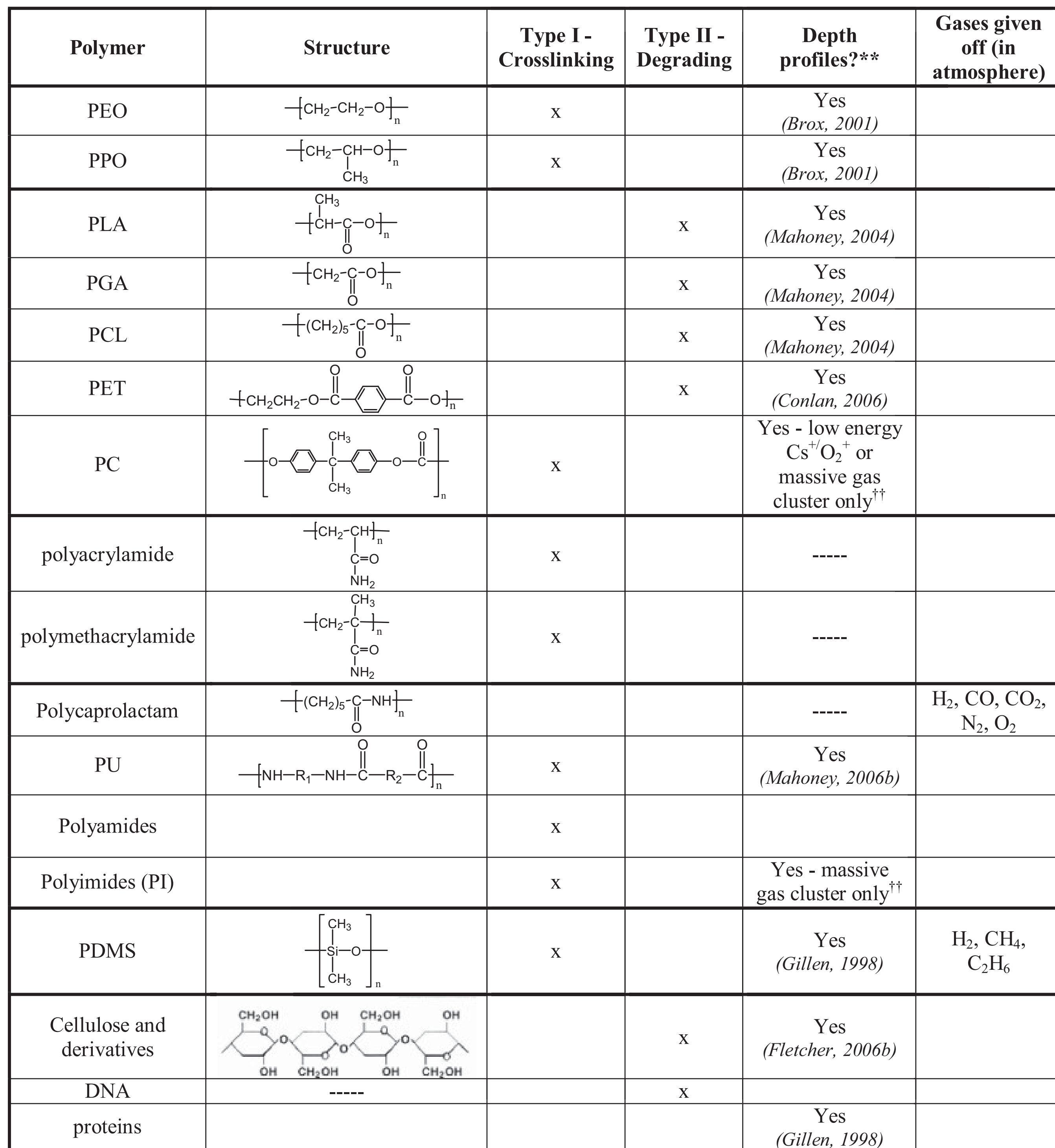

Polymer	Structure	Type I - Crosslinking	Type II - Degrading	Depth profiles?**	Gases given off (in atmosphere)
PEO	$-[CH_2-CH_2-O]_n-$	x		Yes *(Brox, 2001)*	
PPO	$-[CH_2-CH(CH_3)-O]_n-$	x		Yes *(Brox, 2001)*	
PLA	$-[CH(CH_3)-C(=O)-O]_n-$		x	Yes *(Mahoney, 2004)*	
PGA	$-[CH_2-C(=O)-O]_n-$		x	Yes *(Mahoney, 2004)*	
PCL	$-[(CH_2)_5-C(=O)-O]_n-$		x	Yes *(Mahoney, 2004)*	
PET	$-[CH_2CH_2-O-C(=O)-C_6H_4-C(=O)-O]_n-$		x	Yes *(Conlan, 2006)*	
PC	$-[O-C_6H_4-C(CH_3)_2-C_6H_4-O-C(=O)]_n-$	x		Yes - low energy Cs^{+}/O_2^{+} or massive gas cluster only††	
polyacrylamide	$-[CH_2-CH(C(=O)NH_2)]_n-$	x		-----	
polymethacrylamide	$-[CH_2-C(CH_3)(C(=O)NH_2)]_n-$	x		-----	
Polycaprolactam	$-[(CH_2)_5-C(=O)-NH]_n-$			-----	H_2, CO, CO_2, N_2, O_2
PU	$-[NH-R_1-NH-C(=O)-R_2-C(=O)]_n-$	x		Yes *(Mahoney, 2006b)*	
Polyamides		x			
Polyimides (PI)		x		Yes - massive gas cluster only††	
PDMS	$-[Si(CH_3)_2-O]_n-$	x		Yes *(Gillen, 1998)*	H_2, CH_4, C_2H_6
Cellulose and derivatives	CH₂OH OH CH₂OH OH / OH CH₂OH OH CH₂OH (glucose chain)		x	Yes *(Fletcher, 2006b)*	
DNA	-----		x		
proteins				Yes *(Gillen, 1998)*	

Polymers are grouped according to their structural features.
**The answers reported reflect the current state of the literature, under the conditions the literature specifies.
††Mine et al. (2007), Cramer et al. (2008), Houssiau, Douhard, and Mine (2008), Ninomiya et al. (in press).

TABLE 3. Polymeric structures and their behavior under irradiation

Polymer	Structure	Type I - Crosslinking	Type II - Degrading	Depth profiles?**	Gases given off (in atmosphere)
PVA	$-[CH_2-CH(O-C(=O)-CH_3)]_n-$	x		Yes[†] *(Mahoney, 2006b)*	
PAA	$-[CH_2-C(CH_3)(C(=O)OH)]_n-$	x		-----	
PMAA	$-[CH_2-C(CH_3)(C(=O)OH)]_n-$		x	Yes *(Wagner, 2005a)*	
PMA	$-[CH_2-CH(C(=O)OCH_3)]_n-$	x		Yes *(Wagner, 2005a)*	H_2, CO, CO_2, CH_4
PMMA	$-[CH_2-C(CH_3)(C(=O)OCH_3)]_n-$		x	Yes *(Gillen, 1998)*	H_2, CH_4, CO, CO_2, C_3H_8
PBMA	$-[CH_2-C(CH_3)(C(=O)O-(CH_2)_3CH_3)]_n-$		x	Yes *(Wagner, 2005b)*	
POMA	$-[CH_2-C(CH_3)(C(=O)O-(CH_2)_7CH_3)]_n-$	x		Yes *(Wagner, 2005b)*	
PDoMA	$-[CH_2-C(CH_3)(C(=O)O-(CH_2)_{11}CH_3)]_n-$	x		Yes *(Wagner, 2005b)*	
PHEMA	$-[CH_2-C(CH_3)(C(=O)OCH_2CH_2OH)]_n-$			Yes *(Wagner, 2005c)*	
TFAA-PHEMA	$-[CH_2-C(CH_3)(C(=O)OCH_2CH_2O-C(=O)-CF_3)]_n-$			Yes *(Wagner, 2005c)*	

Polymers are grouped according to their structural features.

**The answers reported reflect the current state of the literature, under the conditions the literature specifies.

[†]Data reported in this article (Mahoney, Patwardhan, & McDermott, 2006), are actually obtained from a copolymer of PVA and PE. Since homopolymers of PE are not amenable to being depth profiled, it is assumed that it is the PVA component that allows for the successful profiling in this copolymer system. Therefore it is assumed that PVA homopolymers will be amenable to being depth profiled.

Gel permeation chromatography (GPC) is a tool that can help assess changes in the molecular weight of the soluble fraction of the polymer with increasing irradiation time. This has been done in several polymers, including PS (Calcagno & Foti, 1987; Puglisi et al., 1987), where the molecular weight distribution was determined to first broaden with increasing bombardment characteristic of both chain scission and crosslinking.

When polymers are irradiated, a large amount of gas evolution is typically observed. The compositions of the gases

vary from polymer to polymer and some examples are listed in Tables 1–3. In most cases of gas measurements, the yields are initially higher and decrease with increasing irradiation (Chapiro, 1962). The yield of gas is also much higher when the irradiation is carried out at higher temperatures and particularly if the polymer is irradiated above its glass transition temperature. If a polymer is heated high enough, a chain depolymerization process may be initiated by the free radicals which are trapped in the polymer (Chapiro, 1962).

To summarize, polymeric materials typically demonstrate three distinct chemistries as a function of increasing irradiation fluence: (1) First, degradation mechanisms dominate (particularly in Type II polymers), (2) After a certain fluence, which is dependent upon the polymer and the radiation conditions, crosslinking dominates, and (3) Finally, under higher fluences, graphitization of the surface occurs, resulting in a significant increase in the conductance of the irradiated region. In Type I materials, the crosslinking happens at a much higher rate and at times the degradation is skipped altogether. The following are a list of factors that typically affect the behavior of the polymer during irradiation:

1. Molecular weight: Higher molecular weight polymers crosslink faster than lower molecular weight polymers.
2. Total fluence: Increased fluences result in increased crosslinking.
3. Fluence rate: The extent of crosslinking is not influenced by the rate at which the fluence is delivered to the polymer sample, unless O_2 is present.
4. Crystallinity: the extent of crosslinking is typically lower in highly crystalline materials due to trapped radicals (since the mobility of polymeric segments is much lower in these regions). In general for semicrystalline polymers, the crystalline content tends to decrease with increasing fluence, particularly when the sample is brought above its glass transition temperature. Cyclization tends to increase in these materials.
5. Temperature: The extent of crosslinking decreases with decreasing temperature, in particular below the glass transition temperature. There appears to be decreased degradation or main chain scission occurring at low temperatures as well.
6. O_2: The presence of O_2 during irradiation can cause normally crosslinking polymers to degrade *via* peroxide formation. O_2 can also behave as a free radical inhibitor and prevent degradation in certain cases.

B. Atomic Ion Bombardment of Polymers

There has been a lot of research focused specifically on the chemistry of *atomic ion*-bombarded polymer surfaces, as this information is useful for many applications (photoresists, ion-beam lithography, biomaterials etc.). Specific examples of this include PET (Balik & Said, 1987), PS, PE, and PVDF (Calcagno, 1995). These studies have all indicated major physical and chemical property changes in the surface regions of the polymers, which may or may not be permanent, depending on the fluence. In most cases, there are significant changes in the mechanical (Lee et al., 1991, 1993, 1997; Nishimiya et al., 1991; Lee, Lee, & Mansur, 1992; Ochsner et al., 1993; Rao, Wang, & Lee, 1993; Rao et al., 1995; Tretinnikov & Ikada, 1998), chemical (Puglisi et al., 1986; Nishimiya et al., 1991; Lee et al., 1993, 1997; Švorčík et al., 1998; Tretinnikov & Ikada, 1998), electronic (Forrest et al., 1982; Venkatesan et al., 1983; Liu, Liu, & Zhai, 1989; Lee et al., 1993; Švorčík et al., 1997), diffusion (Calcagno et al., 1993), optical (Calcagno, Compagnini, & Foti, 1992; Rück, Schulz, & Beusch, 1997), and rheological properties (Calcagno, Compagnini, & Foti, 1992) of ion-bombarded polymeric samples.

These changes are obviously a result of the increased crosslinking and unsaturation occurring in these polymers. As with all forms of radiation, ion-bombarded surfaces eventually become graphitic in nature (Davenas et al., 1990), or in rare cases diamond-like (Davenas et al., 1990). While most polymers exhibit an increase in conductivity after irradiation with ion beams (resulting from the formation of the graphitic phase), it is interesting to note that polymers exhibiting aromatic or heterocyclic structures tended to display even higher levels of surface conductivities (Davenas et al., 1989). It is assumed that graphitization is enhanced at polymer surfaces which have benzene ring components (Lee et al., 1997).

There is also a dramatic change in the morphology after sputtering (Yoshida & Iwaki, 1987; Švorčík et al., 1997); with some reporting a smoothing effect (Lee et al., 1991), while others report increased topography (Švorčík et al., 1998; Netcheva & Bertrand, 1999). These significant changes in the surface properties often result in changes in the compatibilities of these polymers with other elements (Zaporojtchenko et al., 2005). For example, ion bombardment of polymeric materials has resulted in increased wettability of PDMS and PS surfaces (Suzuki et al., 1990; Suzuki, Kusakabe, & Iwaki, 1993), and changes in the biocompatibility of PDMS surfaces (Suzuki et al., 1991, 1992; Yotoriyama et al., 2006).

In most polymeric samples, during ion bombardment, there is a critical fluence above which crosslinking rapidly accelerates and the corresponding solubility decreases significantly. This point is considered the gel point of the polymer, and is the point at which a three-dimensional network is formed in the polymer. The process of forming a gel is a slow process, involving the diffusion of mobile radicals into the bulk, where they will eventually crosslink. It is most likely this process of diffusing radicals for which damage accumulation in SIMS depth profiling is based (region II). An example of this is shown in Figure 15, which shows the solubility of PS plotted as a function of increasing fluence of both He^+ and H^+ ions (Calcagno & Foti, 1991; Calcagno, 1995). It is assumed that the corresponding SIMS spectra will have a similar drop in signal intensity at this point as it is well-known that increased crosslinking is correlated to decreased secondary ion yields in SIMS (Chilkoti et al., 1993). Therefore it is likely that the behavior exhibited by polymers, as was discussed in Figure 14d, is actually a result of the approach of the gel point for that particular material.

As can be seen in Figure 15, the gel point is reached earlier for heavier ions. In addition, the efficiency of the damage processes was determined to be lower for high energy ions than for low energy ions. In other words, the gel point was reached much later for higher energy ions. These results were explained in

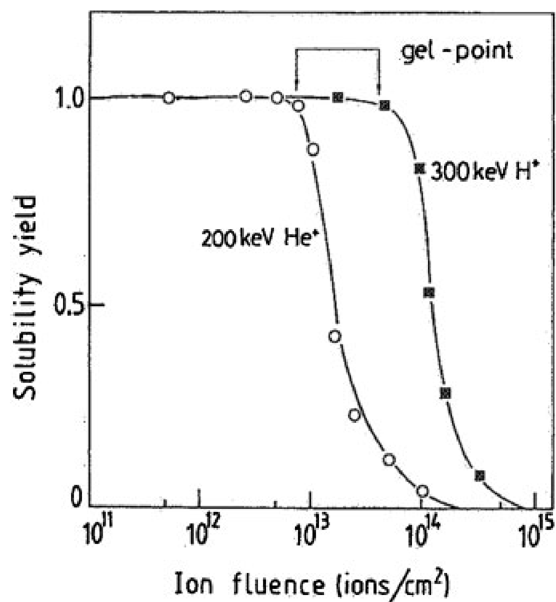

FIGURE 15. Soluble fraction as a function of ion fluence for 9,000 amu polystyrene irradiated with 300 keV H^+ and 200 keV He^+ ions. Figure from Calcagno (1995), reprinted with permission from Elsevier, copyright 1995.

terms of the difference in the spatial energy distribution, which is more localized for a low energy ion. The local energy density is what determines the crosslinking. The chemical yield of crosslinks in PS for example increases with the local energy density.

These decreased damage effects at higher beam energies are consistent with SIMS results, which indicate prolonged signal longevity in samples irradiated at higher energies (see Section VIII-C). Though these energies are much higher than what are typically used for SIMS applications, and therefore different sputtering mechanisms apply, the end result is the same; the formation of a highly crosslinked insoluble material.

This gel point also tends to be reached earlier for higher MW samples, and is highly dependent upon the number average molecular weight in particular (Puglisi et al., 1988). It is assumed that there is a critical number of crosslinks per molecule that needs to be attained, and that number is reached earlier for the larger molecules.

Depth profiling through polymer films can also be performed using atomic beams. However, with the exception of low energy (200 eV) Cs^+ beams (Mine et al., 2007), these profiles typically have significantly increased damage associated with them such that only elemental signals can be monitored as a function of depth (all molecular information is essentially destroyed). In addition, the sputter rate is significantly reduced when employing atomic beams, such that only dynamic SIMS instruments are typically used. There are several examples of polymeric depth profiling with atomic beams including PS (Whitlow & Wool, 1989, 1991; Zhao et al., 1991; Shwarz et al., 1992; Liu et al., 1995; Zheng et al., 1995; Strzhemechny et al., 1997; Rysz et al., 1999; Yokoyama et al., 1999; Shin et al., 2001; Hu et al., 2003; Lin et al., 2003; Harton, Stevie, & Ade, 2006a,b,c; Harton et al., 2006d), PAMA (Valenty et al., 1984), PBMA (Verhoeven et al., 2004), PEVA (Verhoeven et al., 2004), PC (Valenty et al., 1984), PVDF (Chujo, 1991), PEO (Mattsson et al., 2000; Huang et al., 2001), PMMA (Chujo, 1991; Huang et al., 2001; Hu et al., 2003; Harton, Stevie, & Ade, 2006a,b,c; Harton et al., 2006d), polydimethyl phenylene oxide (PDPO) (Lin et al., 2003), PVP (Zheng et al., 1995; Pinto, Novak, & Nicholas, 1999; Yokoyama et al., 1999; Harton, Stevie, & Ade, 2006a,b; c; Harton et al., 2006d), PPV and other polymer based LED materials (Sauer et al., 1995; Bulle-Lieuwma & van de Weijer, 2006), solar cell materials (Bulle-Lieuwma et al., 2003), conducting polymers (Gray et al., 1992), video tapes (Chujo, 1991), silicones (Stein, Leonard, & Smith, 1991), and other polymeric materials (Shwarz et al., 1992; Duan et al., 2001; Reynolds et al., 2005).

Though most atomic beams produce a considerable amount of damage precluding the ability to obtain molecular depth profiles, there are some major breakthroughs occurring in this area as well. Low energy Cs^+ and/or O_2^+ (200 eV) ion beams are generating considerable excitement in the SIMS community for depth profiling in cases where crosslinking is dominant, such as polystyrene, polyethylene, polypropylene and polycarbonate (Mine et al., 2007; Cramer et al., 2008; Houssiau, Douhard, & Mine, 2008). In such cases, using low energy Cs^+ and/or O_2^+ beams will actually outperform conventional cluster sources, such as SF_5^+ and C_{60}^+, for polymeric depth profiling applications. Unlike SF_5^+ or C_{60}^+, these low energy beams yield constant molecular signals characteristic of PS, PE, PP, and PC as a function of increasing fluence in the negative ion mode. It is likely that this effect is in part, a chemical etching effect *via* interaction of the Cs^+ and/or O_2^+ ions with the polymer sample, yielding reactive intermediates, similar to what is observed with irradiation of polymers in the presence of O_2. Either way, this is the one case where atomic beams outperform most cluster beams for in-depth polymeric analysis and should be noted.

VII. POLYMER DEPTH PROFILING APPLICATIONS

A. Surface Cleaning

One of the primary concerns in any TOF–SIMS experiment is contamination of the surface. Cluster SIMS has shown promise for sputter removal of surface contaminants. Szymczak and Wittmaack first showed this in 1994 with SF_n^- clusters (Szymczak & Wittmaak, 1994). Since then, several authors have demonstrated the ability to remove polydimethysiloxane (PDMS) overlayers from contaminated samples (Gillen & Roberson, 1998; Mahoney, Roberson, & Gillen, 2004; Mahoney, Fahey, & Belu, 2008).

This cleaning of contaminants from the surface has many implications for biologically relevant molecules in frozen aqueous matrices, where the surface is often covered in ice and therefore no useful information can be obtained. With cluster sources however, this problem can be alleviated by sputter removal of the ice. Though this can also be done with atomic beams, C_{60} has been shown to remove this overlayer of ice (Wucher et al., 2004) much more rapidly and with very little damage to the underlying structure.

B. Damage Removal

Cluster sources are also able to remove damage previously created by atomic ion beams. This effect was first noticed by McMahon, Dookeran, and Todd (1995). In this work, secondary ion mass spectra and images were obtained from spikes of choline chloride, acetylcholine chloride, and methylphenylpyridinium iodide deposited onto specimens of porcine brain tissue. The samples were subjected to a fluence of 10 keV Cs^+, sufficient to suppress molecular ion emission. However, following ablation of the samples by massive glycerol clusters, the damage was removed. A nice example of this was published more recently by Gillen and co-workers (2006a), where the authors were able to demonstrate the recovery of RDX (explosive) molecular signal when switching back and forth from C_1^- to C_8^- (see Fig. 16). Similar results have been obtained with C_{60}^+ probes (Wucher et al., 2004; Wucher, 2006; Wucher, Chen, & Winograd, 2007).

This removal of previously damaged regions has major implications in possible 3-D Focused Ion Beam SIMS (FIB–SIMS) technology. In FIB milling, a focused Ga beam is used to cross section materials. Characterization of organic FIB cross sections with SIMS however, does not yield any useful information, since Ga beams create large amounts of damage. With cluster beams however, this damaged region can potentially be recovered, enabling 3-D analysis of each section.

C. Drug Delivery

The first demonstration of molecular depth profiling in model drug delivery systems was published by Mahoney, Roberson, and Gillen (2004). In this work PLA as well as PLA drug-doped (acetaminophen, theophylline) films were depth profiled with SF_5^+, and it was demonstrated that both polymer and drug

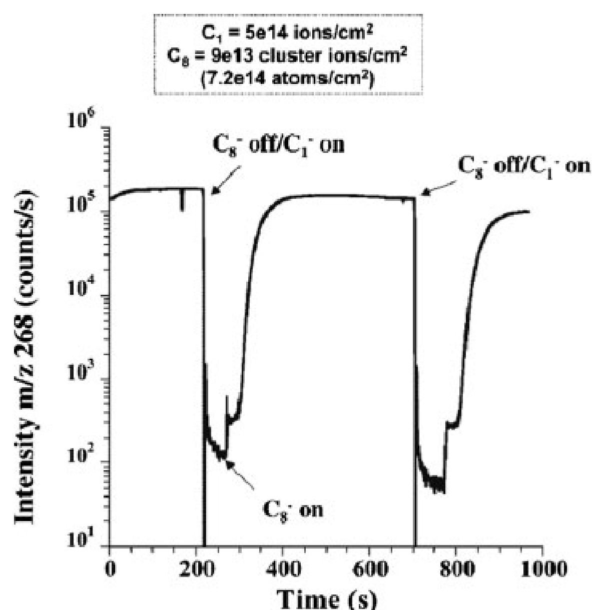

FIGURE 16. Variation of RDX characteristic ion signal at $m/z = 268$ under high primary ion fluence sputtering conditions comparing the effect of C_8^- and C_1^- bombardment. Taken from Gillen et al. (2006a) with permission from John Wiley & Sons, Ltd, copyright 2006.

compositions could be monitored as a function of depth on a nanoscale using this technique. It was also interesting that there was evidence of a drug-depleted surface region with compositional variation in the bulk. The depth profile quality (depth resolution, signal constancy, rapid sputter rates) was found to deteriorate with increasing drug concentration.

Compositional depth profiling was later performed on a series of PLA/Pluronic-P104[4] polymeric blends of varying compositions using SF_5^+ polyatomic primary ion bombardment. The major results from this study are depicted in Figure 17, which shows actual *concentration* depth profiles of three different compositions (Fig. 17a–c). In each profile, there was a surface-enriched Pluronic-P104 region, followed by a depletion layer, and finally a constant bulk composition region. These diffusion profiles were consistent with previous models describing polymer surface segregation. There was also a similar effect occurring in the buried interfacial region (polymer/Si interface).

Also shown in Figure 17d are the images acquired as a function of depth for a three component film containing PLA, P104 and insulin, as a model protein drug. Imaging results showed complete coverage of Pluronic at the surface. This was followed by phase separated domains of the Pluronic (40–50 μm) in the subsurface region. No signals from insulin were detected in the positive ion spectrum, most likely because of matrix effects.

These works resulted in major efforts to further develop cluster SIMS technology for characterization of drug delivery systems and one such application was in the characterization of drug-eluting stent (DES) coatings. One of the earliest works to utilize cluster SIMS for such an effort was published in 2006 (Mahoney, Patwardhan, & McDermott, 2006b). This work describes the efforts to establish feasibility for depth profiling in various materials typically employed for DES applications. These included several polymers currently used or being developed for this application such as poly(ethylene-co-vinyl-acetate) (PEVA), PU and PLGA, as well as drug-loaded films containing paclitaxel or rapamycin (employed in DES). The results indicated that one could depth profile through most of these films when employing cluster primary ion beams.

Braun et al. was able to take this a step further and demonstrate C_{60}^+ depth profiling in Taxus Express 2 stents, comprised of a SIBS coating doped with paclitaxel (Braun et al., 2006). The authors were able to etch through approximately 1.5 μm of material.

Lastly, PLGA-based stents containing varying amounts of rapamycin were characterized in three dimensions using an SF_5^+ sputter source in conjunction with a Bi_3^+ analysis source (Mahoney, Fahey, & Belu, 2008), where the authors were able to demonstrate 3-D compositional imaging in such systems. The results from this latter study are depicted in Figure 18, where Figure 18a is an overlay of the resulting depth profiles of

[4]Pluronic surfactants are non-ionic triblock copolymer surfactants containing alternating PEO and poly(propylene oxide) (PPO) components. When used as drug-releasing matrices, these PLA/Pluronic blends have been proven to extend protein release and minimize the initial protein burst when compared to the pure PLLA homopolymers. These systems are of potential use for protein delivery applications.

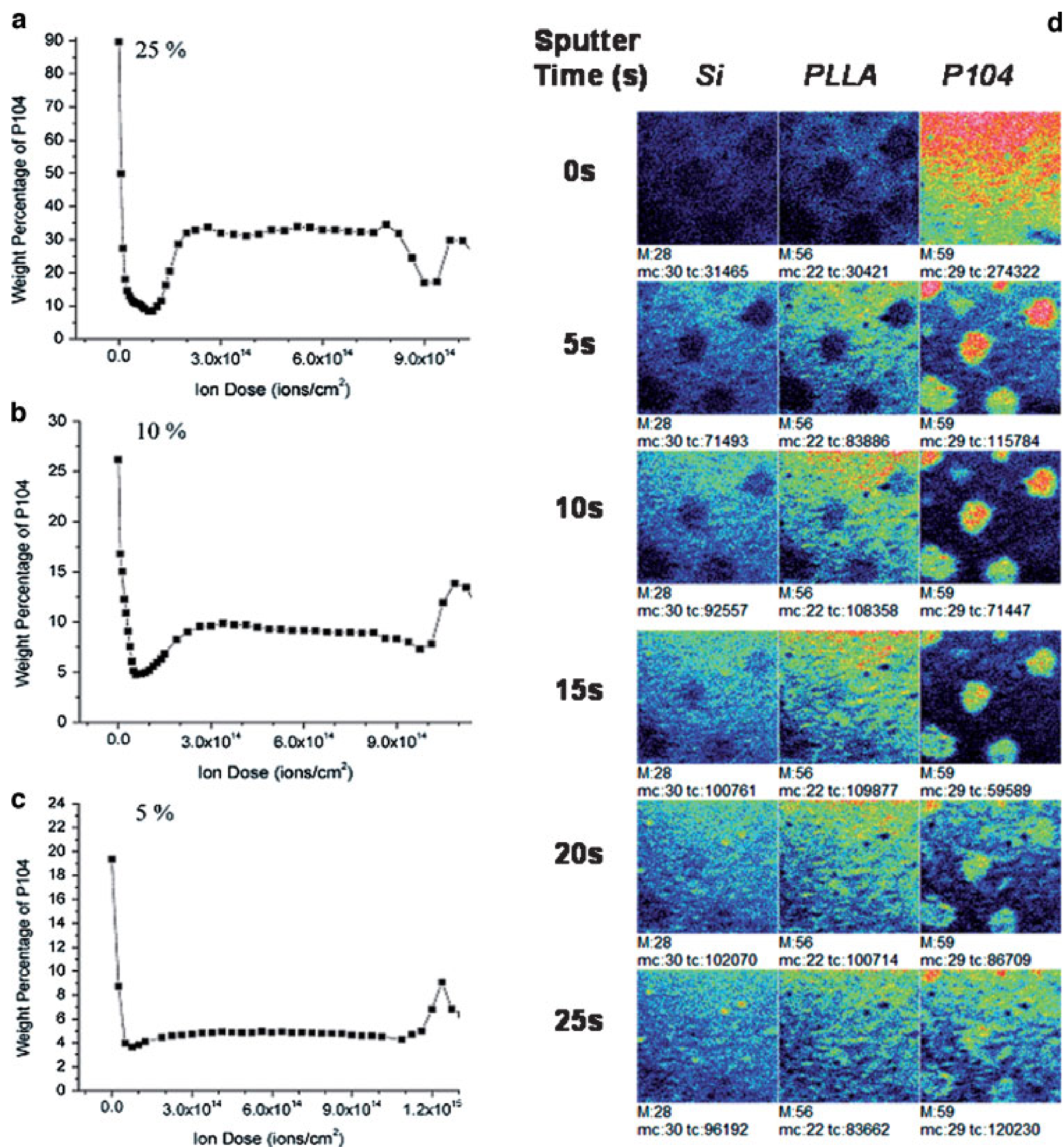

FIGURE 17. Composition depth profiles as measured by SIMS for samples containing: (**a**) 25% (w/w) P104 in PLLA, (**b**) 10% (w/w) P104 in PLLA, and (**c**) 5% (w/w) P104 in PLLA. (**d**) Positive secondary ion images (300 μm × 300 μm) acquired as a function of sputter time for 5% insulin in P104/PLLA blendmatrix (15% w/w P104). Subparts (a–c) taken from Mahoney, Yu, and Gardella (2005), reprinted with permission from American Chemical Society, copyright 2005. Subpart (d) taken from Mahoney et al. (2006c), reprinted with permission from Elsevier, copyright 2006.

samples of varying compositions, and Figure 18b shows the 2-D image overlay as a function of sputter depth in a sample containing 25% rapamycin in PLGA. From these results, it is very clear that one can determine overlayer thicknesses and homogeneities and directly relate this to the release characteristics of the device.

D. Polypeptides

Cheng and Winograd (2005, 2006), Cheng, Wucher, and Winograd (2006), and Cheng et al. (2007) performed a series of studies on depth profiling in polypeptide films. The first article in this series (Cheng & Winograd, 2005) shows the feasibility of

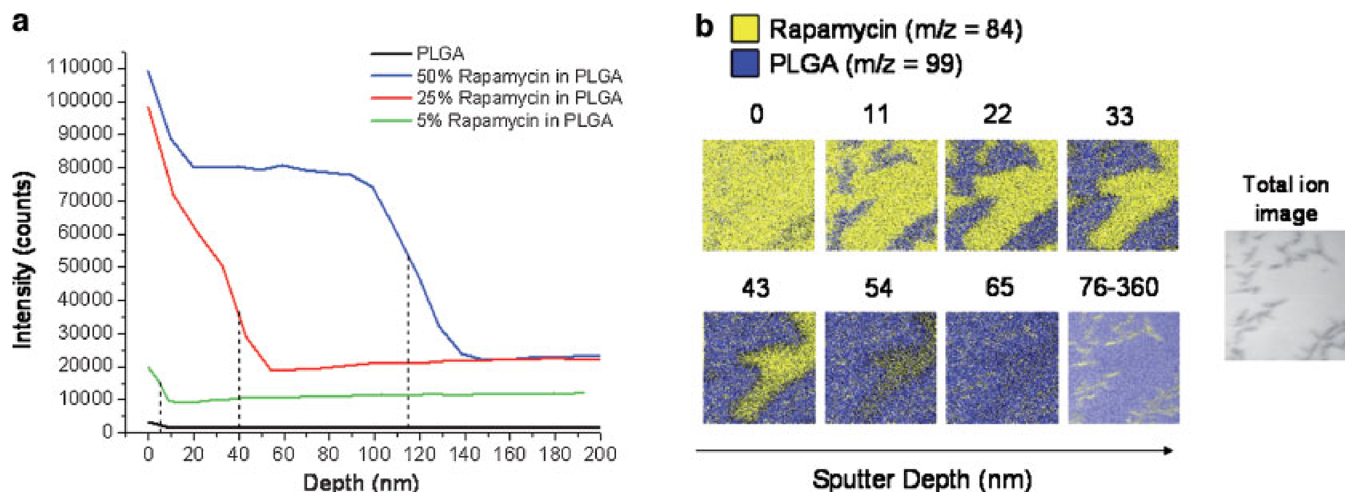

FIGURE 18. (**a**) Depth profile of drug-rich overlayers of rapamycin ($m/z = 84$) in PLGA at various concentrations. These plots were taken from the subsurface region only, with 2 sec sputter intervals, and at low temperatures (-100°C). (**b**) Corresponding 3-D mapping (300 µm × 300 µm) of the distribution of drug and polymer in a DES system containing 25% rapamycin in PLGA. Figure from Mahoney, Fahey, and Belu (2008) reprinted with permission from American Chemical Society, copyright 2008.

using C_{60}^{+} to depth profile through trehalose films (300–1,000 nm) (naturally occurring sugar, which has shown to enhance the stability of biomaterials) containing different polypeptides. This work was followed by a article on depth profiling in protein/trehalose multi-layer films, where the authors found that the best results were obtained when the mass of the overlayer atoms was less than or nearly equal to the mass of the atoms in the buried molecules (Kozole et al., 2006).

Cheng et al. (2007) directly compared the performance of Au_3^{+} and C_{60}^{+} primary ion projectiles for molecular depth profiling in two model films, one being a trehalose film doped with the peptide Gly-Gly-Tyr-Arg (GGYR) and the second doped with dipalmitoylphosphatidylcholine (DPPC). The results indicated increased fragmentation and decreased overall signal intensity with Au_3^{+} clusters as compared to C_{60}^{+}.

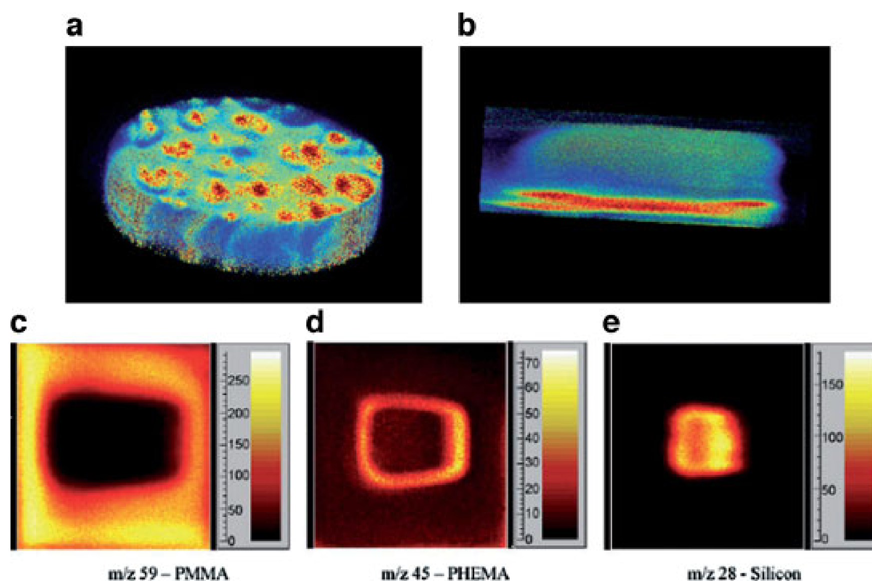

FIGURE 19. Volumetric view of the distribution of $m/z = 152$ in (**a**) homogeneous film, and (**b**) inhomogeneous film of 25% acetaminophen in PLA matrix. This method of 3D images involves the stacking of a series of 74 secondary ion images with a 250 µm field of view and 10 sec image acquisition time. Another form of imaging is displayed in (**c**), which shows the secondary ion images of (**c**) *m/z* 59 (PMMA), (**d**) *m/z* 45 (PHEMA), and (**e**) *m/z* 28 (Si) from a bevel crater cut through a polymer multilayer of PMMA/PHEMA/Si. Field of view is 500 µm × 500 µm for 10 sec acquisition time. All studies were performed with an SF_5^{+} source. Figure from Gillen et al. (2006b), reprinted with permission Elsevier, copyright 2006.

E. 3-D Imaging

Gillen et al. (2006b) first demonstrated the ability to obtain 3-D molecular compositional information from PLA-based drug delivery systems, as well as several other polymeric based systems, employing an SF_5^+ cluster source on a magnetic sector SIMS instrument. The results of this work are depicted in Figure 19. Figure 19a,b shows 3-D representations of a sample containing 25% acetaminophen in a PLA matrix, where Figure 19a,b represents homogeneous and non-homogeneous films respectively. It is likely that these two samples would exhibit very different release characteristics, and thus this result demonstrates the potential role of cluster SIMS for quality control purposes. The authors also presented a unique way of obtaining depth profiles. This method is illustrated in Figure 19c–e, and involves the formation of bevel cross-sections with an SF_5^+ primary ion beam. This allows for laterally magnified cross-sections, which do not contain the beam-induced damage from conventional FIB cross-sectioning. The bevel surface can then be examined using cluster SIMS imaging or other appropriate microanalysis techniques. Figure 19a,c–e depicts the resulting images of the bevel cut in a polymeric multilayer system containing an overlayer of PHEMA on PMMA.

Several attempts have been made to depth profile through biological materials as well, though with limited success. Fletcher et al. obtained 3-D imaging results from a biological system with a C_{60}^+ sputter source (Fletcher et al., 2007). Though there was a significant amount of damage, the authors were able to depth profile through 100 µm of freeze-dried Xenopus laevis oocyte (frog egg).

Later, Debois, Brunelle, and Laprévote (2007) attempted to obtain molecular depth profiles in rat brain tissue using dual beam depth profiling with a C_{60}^+ sputter source and a Bi_3^+ analysis source. The results from this study indicated that the damage induced by the sputter gun was too high for useful 3-D imaging beyond 200–300 nm eroded depth.

Overall, 3-D molecular imaging with cluster beams is a rapidly growing field, and shows much promise. It is therefore necessary to utilize protocols for 3-D molecular imaging, to avoid artifacts created by, for example, differential sputtering rates. These protocols have been developed and described in detail by Wucher, Chen, and Winograd (2007). This work describes a procedure for establishing accurate depth scales in samples with non-uniform compositions in which the sputter rates vary across the sample. This is done with the application of atomic force microscopy (AFM) to measure accurate depth information corresponding to each pixel of the SIMS image. The results show that this type of correction is necessary to obtain an accurate representation of three-dimensional structures.

VIII. PARAMETERS AFFECTING POLYMER DEPTH PROFILES

The parameters that affect polymeric depth profiling and sputtering are very similar to those described in the previous radiation chemistry section and include the polymer structure, temperature during the depth profile process, beam chemistry, beam angle, and beam energy. The following sections describe in detail the studies that have been done to illustrate these important parameters.

A. Polymer Structure

Polymer structure has a profound effect on the mechanism of polymer degradation (crosslinking vs. scission). In general, polymers that undergo main chain scission when irradiated are more amenable to molecular depth profiling (with results similar to the scenarios described in Fig. 14a,b), while those that crosslink will be more likely to fail (similar to scenario in Fig. 14c). This is clearly consistent with Tables 1–3. However, unlike other forms of radiation, including atomic ion bombardment, some of the polymers considered to be crosslinkers, are amenable to being depth profiled under polyatomic ion bombardment indicating that these cluster sources are pushing the damage mechanisms away from crosslinking and more towards degradation mechanisms. A good example of this can be seen in polyethers, such as PEO and PPO. While these materials are considered to be Type I crosslinkers under neutron irradiation, they are amenable to depth profiling when using cluster beams in SIMS. It appears as though materials that have cleavage points in the main chain, such as O or C=O, tend to depth profile with cluster SIMS, as long as there is not a high concentration of aromatic rings, such as is the case with polycarbonate. It is likely that the materials that tend to favor crosslinking under other forms of radiation (i.e. PEO, PDMS etc.), display more competitive mechanisms than do other materials (both cross-linking and degradation occur), and are pushed toward degrading mechanisms *only* when employing cluster ion beams. Other examples of this phenomena can be seen in polyurethanes (PU), poly(dimethylsiloxane) (PDMS), poly(vinylchloride) (PVC), poly(vinylidenedifluoride) (PVDF), polyvinylacetate (PVA), and poly(methylacrylate) (PMA) (see Tables 1–3). Certain type I polymers, such as PS and PE, can only be depth profiled when employing massive gas cluster sources or low energy Cs^+/O_2^+ sources, and do not work under C_{60}^+ and SF_5^+ bombardment.

A lot of work has been published in particular, on the bombardment of PMMA with both atomic and cluster beams and the mechanisms of its structural degradation. Wagner et al. for example performed several important investigations into PMMA depth profiling with SF_5^+ at variable energies, where it was shown that 5 keV SF_5^+ resulted in decreased disappearance cross sections, and relatively constant C/O ratios (associated with methyl ester pendent scission) and C–H/C–C ratios (associated with cross-linking and increased unsaturation) in contrast to what was observed under 5 keV Cs^+ bombardment (Wagner, 2004). The results confirmed that there are significant decreases in crosslinking when employing the cluster source and corresponding increases in polymer degradation. No fluorocarbon species were observed in the mass spectra, though there was a slight amount of F implanted into the sample. Cs^+ on the other hand resulted in significant implantation.

There were also significant increases in peaks characteristic of polycyclic aromatic hydrocarbons (PAH's) after bombardment with Cs^+ as compared to SF_5^+. The existence of such peaks is consistent with what has been observed previously with atomic ion bombardment under higher ion fluences (Briggs & Hearn, 1986; Hearn & Briggs, 1988; Van Ooij & Brinkhuis, 1988; Leggett & Vickerman, 1992) and is associated with increased beam damage to the sample. Essentially, the material becomes increasingly unsaturated, until cyclic structures are formed and ultimately aromatic units such as the cyclic tropylium ion at $m/z = 91$ ($C_7H_7^+$) (Briggs & Hearn, 1986) are observed. This cyclization is known to occur under other forms of irradiation as well (Chapiro, 1962) and is consistent with the graphitic nature of highly damaged surfaces.

Temperature also plays a very important role in the mechanisms of degradation in PMMA, where at high temperatures, ion-induced depolymerization mechanisms dominate. Conversely, at low temperatures, the data is consistent with a significant decrease in crosslinking (Mahoney et al., 2006a; Mahoney, Patwardhan, & McDermott, 2006b; Mahoney, Fahey, & Gillen, 2007a; Mahoney et al., 2007b; Mahoney, Fahey, & Belu, 2008). These temperature effects will be described in greater detail later.

The overall degradation mechanism of PMMA when irradiated by cluster ion beams is illustrated in Scheme 1, which shows the possible degradation routes under variable conditions. The degradation pathways shown in Scheme 1 represents a summary from several references (Hearn & Briggs, 1988; Leggett & Vickerman, 1992; Van Ooij & Brinkhuis, 1988; Briggs & Hearn, 1986; Bermudez, 1999; Wagner, 2004; Mahoney, Fahey, & Gillen, 2007a; Mahoney et al., 2007b). The route of degradation is best described as a two-step degradation process, starting first with the loss of the methyl ester pendent group. This is immediately followed by main chain scission occurring at low fluences, and eventual crosslinking and unsaturation at higher fluences. The fluence at which this crosslinking occurs varies with the type of source used, and the conditions under which the source is operated (e.g., temperature, beam energy). While atomic sources will tend to cause crosslinking of the sample almost immediately, polyatomic sources, such as SF_5^+ and C_{60}^+ exhibit delayed crosslinking of the sample, making depth profiling feasible. C_{60}^+, particularly at higher energies, tends to be a better performer in terms of preventing crosslinking, where signal can be maintained for much higher primary ion fluences as compared to SF_5^+ (Fisher et al., 2008).

Wagner performed several investigations into the effect of polymer structure on sputtering mechanisms in a series of publications that further demonstrates the importance of chemical structure on damage accumulation during depth profiling of methacrylics (Wagner, 2005a,b,c). As can be seen from Table 3, all of these profiles are considered to be "successful" to some degree. However, when we say that a material is "successful", we mean that we can to some degree, maintain molecular signal characteristic of the polymer as a function of depth. Whether or not there is a more gradual degradation of signal or a limitation in depth is not included in this table, as it most likely varies with cluster source selection and/or other experimental conditions. The first article in this series was a systematic study of the effect of exchanging main chain and side-chain methyl groups on the resulting SF_5^+ depth profiles, by comparing PMMA, PMA, and PMAA (Wagner, 2005a). The structures of the three different polymers differ only in their placement of a methyl group (see Table 3), where the PMA has the methyl group on the side chain only, the PMAA, has it on the main chain only and the PMMA has the methyl groups in both places. Overall the highest sputter rates and signal constancies were obtained from PMMA, though all were successfully profiled with SF_5^+ to some degree. The sputter rates for PMMA were reported to be approximately twice as high as that obtained for PMA and PMAA under identical sputtering conditions.

The theory behind this change in sputter properties was discussed in reference to the known degradation pathways of the different materials. In particular, PMA is more likely to crosslink

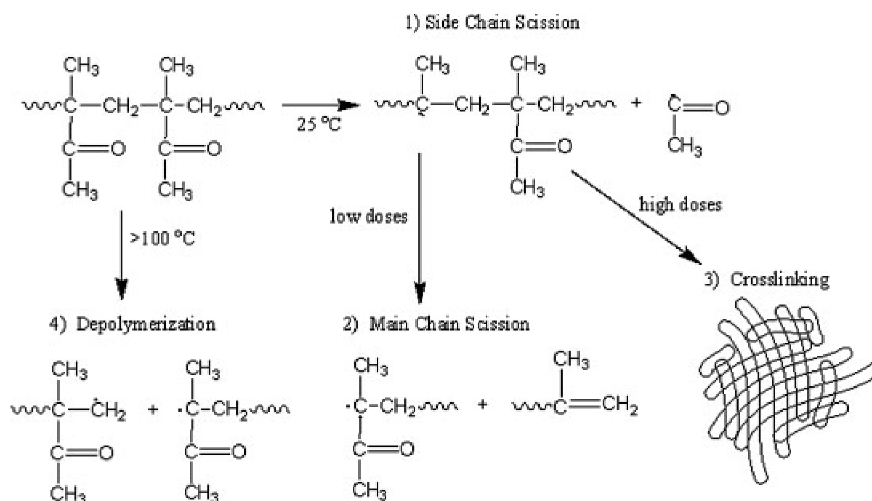

SCHEME 1. Mechanism of PMMA degradation under ion bombardment.

due to the lack of the methyl group on the main chain as discussed earlier (Note, in Table 3, that PMA is listed as a type I polymer that prefers to undergo crosslinking when irradiated). PMAA is also more likely to crosslink however, as it is known to undergo decarboxylation and subsequent intermolecular crosslinking. It was theorized that the polymers that undergo thermal or radiation-induced decomposition primarily by depolymerization, as is the case with PMMA, maintain strong characteristic secondary ion intensities as a function of increasing SF_5^+ fluence, whereas those that can potentially form intra- and intermolecular cross-links have lower sputter rates and higher signal degradation rates.

In the second article in this series, Wagner studied the effects of side-chain length in a series of poly(methacrylates), where poly(*n*-butyl methacrylate) (PBMA), Poly(*n*-octyl methacrylate) (POMA) and Poly(*n*-dodecyl methacrylate) (PDoDMA) were characterized and compared to PMMA (Wagner, 2005b). These materials have 4, 8, and 12 carbons on the side-chain respectively (see Table 3 for structures). Examples from this work are depicted in Figure 20 below which compares PBMA (Fig. 20a) and PDoMA (Fig. 20b) depth profiles (4 and 10 carbons respectively) and plots the sputter rates of all these materials as a function of the number of carbons in the alkyl side-chain. It is evident that the depth profile characteristics (e.g., signal constancy, interface widths, sputter rates) are significantly improved for the shorter side chain materials. The results were attributed once again to increases in cross-linking in the polymers containing longer side-chain lengths, and a change in probability of ion-induced depolymerization (lower probability for longer side-chain lengths). It is already known that the degradation yields are much lower in the radiolysis of polymethacrylates with longer side chains (Chapiro, 1962). More specifically, there is a decrease in degradation from methyl to ethyl to *n*-butyl ester, while the dodecyl and the octadecyl methacrylate polymers are found to crosslink (Chapiro, 1962).

The last article in this series characterizes a trifluoro acetic acid-derivatized PMMA (TFAA-PMMA) and compares this with underivatized PMMA (Wagner, 2005c). The results indicate that the derivatized PMMA has a much higher sputtering yield and undergoes a significant decrease in damage accumulation. This was attributed to the presence of the electron-withdrawing fluorine atoms on the pendant group, which has been shown to

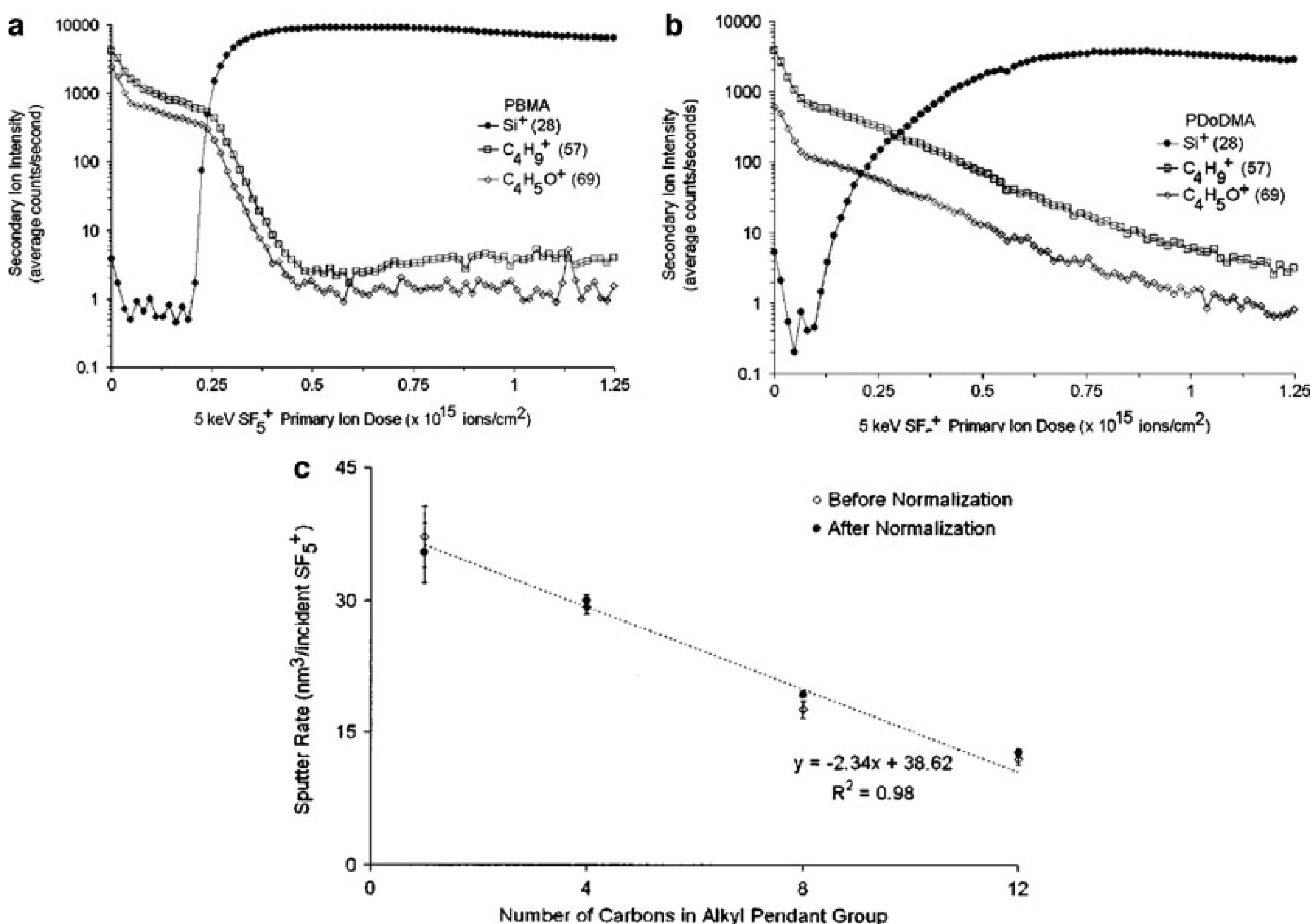

FIGURE 20. Positive ion depth profiles of spin-cast PBMA (**a**), and PDoMA (**b**) on Si wafer substrates. Sputter beam = 5 keV SF_5^+ analysis beam = 10 keV Ar^+. (**c**) Sputter rates for the positive ion depth profiles of the various poly(alkyl methacrylates) as a function of alkyl chain length. Figure from Wagner (2005b), reprinted with permission from John Wiley & Sons, Ltd, copyright 2005.

weaken the polymer backbone in radiation studies, increasing the probability of main-chain scission or depolymerization under SF_5^+ bombardment.

Wagner was also able to demonstrate molecular depth profiling in polymer multilayer thin films of various methacrylics (Wagner, 2005d). The multilayer samples characterized consisted of bilayers and trilayers of PMMA, PHEMA, and TFAA-PHEMA. The overall results of this study indicated that the ordering of the layers was important and affected the damage accumulation in the profile, similar to what was observed by Kozole et al. (2006). In particular, when PHEMA was the outermost layer, there was a reduction in sputter rates for the underlying polymer layer. This was attributed to increased ion-induced damage accumulation rates in PHEMA, which carries through to the next layer.

The effect of increased crosslinking on depth profilability is also consistent with results obtained later on, by Wagner et al. (2006), displayed in Figures 21 and 22. In this work, Wagner was able to demonstrate that when increasing the amount of crosslinking in PMMA (by adding increased amounts of the crosslinker EGDMA during the polymerization) there is a corresponding decrease in sputter rate and increased damage accumulation. This work stems from early experiments involving surface analysis of such materials, where changes in the peak intensities of atomic versus molecular secondary ions were observed as a function of cross-linker concentration (Chilkoti et al., 1993), indicating a loss in signal with increasing crosslinker content.

To summarize, one can predict the success of polymeric depth profiling based on its structure. The following rules apply:

Rule 1: Type I (crosslinking) polymers are less likely to retain molecular information as a function of depth, even with cluster sources.

Rule 2: All or most Type II (degrading) polymers are likely to retain molecular information as a function of depth.

Rule 3: Polymers that have increased strain on the main chain backbone, due to the existence of quaternary C structures and/or stereochemistry changes (discussed later) are more likely to retain molecular information as a function of depth.

Rule 4: Any sample with a cleavage point in the main chain, whether or not it is type I or type II, is more likely to retain molecular information as a function of depth (e.g., –O–, –COO–, –NH-CO–).

Rule 5: Halogen-containing polymers are more likely to retain molecular information as a function of depth due to an enhanced chemical etching.

Rule 6: Polymers that are particularly susceptible to depolymerization mechanisms are more likely to retain molecular information as a function of depth. Polyesters are particularly successful because of this.

Rule 7: Increased aromaticity results in a decreased ability to retain molecular information as a function of depth, due to the protection of the resonance stabilized structures.

Rule 8: Many of the difficulties with Type I crosslinking polymers, such as PS, PE, PC, and PP can be alleviated by using low energy Cs^+ and/or O_2^+ atomic and diatomic ions, which have shown to outperform SF_5^+ and C_{60}^+ cluster sources for these particular cases (Mine et al., 2007). Moreover, gas cluster sources have recently been shown to outperform all beams (clusters and atomics) for depth profiling of type I polymers.

Rule 9: Even though a polymer retains molecular information as a function of depth to some degree, the maximum achievable erosion depths and signal constancy will vary with chemical structure, cluster source used, temperature, beam angle, and other experimental variables defined herein.

B. Polyatomic Ion

After SF_5^+ and C_8^- were shown to be feasible for molecular depth profiling applications (Gillen & Roberson, 1998; Gillen et al., 2001), several other probes were investigated as tools as well. C_{60}^+ was demonstrated to be useful for polymeric depth profiling in 2004, when depth profiling in PMMA was performed with a C_{60}^+ probe (Szakal et al., 2004), and since then has been used repeatedly. Another source demonstrated to be useful for depth profiling in polymeric materials is $Ir_4(CO)_7^+$ which has recently been proven to profile through thin PMMA overlayers (Fujiwara et al., 2006). More recently, gas cluster sources (e.g., Ar_{3000}) have been shown to be useful for depth profiling in polymers as well (55th American Vaccum Society International Symposium and Exhibition, October 19th–24th, 2008). The question one needs to ask therefore is obvious. Are all sources equal in terms of depth profiling?

1. Interface Width Measurements

Before discussing this issue, it is important to point out, that one has to be careful when making comparisons between results reported in the literature, because there is a lack of common terminology and standardized methods. A good example of literature inconsistencies can be seen in definitions of interface widths and sputter rates. Definitions for interface widths for example, range from that defined by ASTM standard method E1438,[5] to those which take into account the different sputter rates of the materials at the interface, similar to what is done in semiconductor metrology (Wagner, 2004). Some of the more recently published works do not even define how their interface widths are measured. This can be a huge problem when comparing sources and needs to be standardized. A good example of the differences can be illustrated by comparing values reported by Wagner (2004), who reports an interface width for PMMA on Si to be approximately 28 nm when accounting for differential sputter rates in the interfacial region, and Mahoney, Roberson, and Gillen (2004), who reports the interface width of the same sample, under the same conditions to be 60.9 ± 3.4 nm when employing only polymer sputter rates to describe interface features.

[5]ASTM Standard Guide for Measuring Widths of Interfaces in Sputter Depth Profiling Using SIMS: Designation E 1438-91.

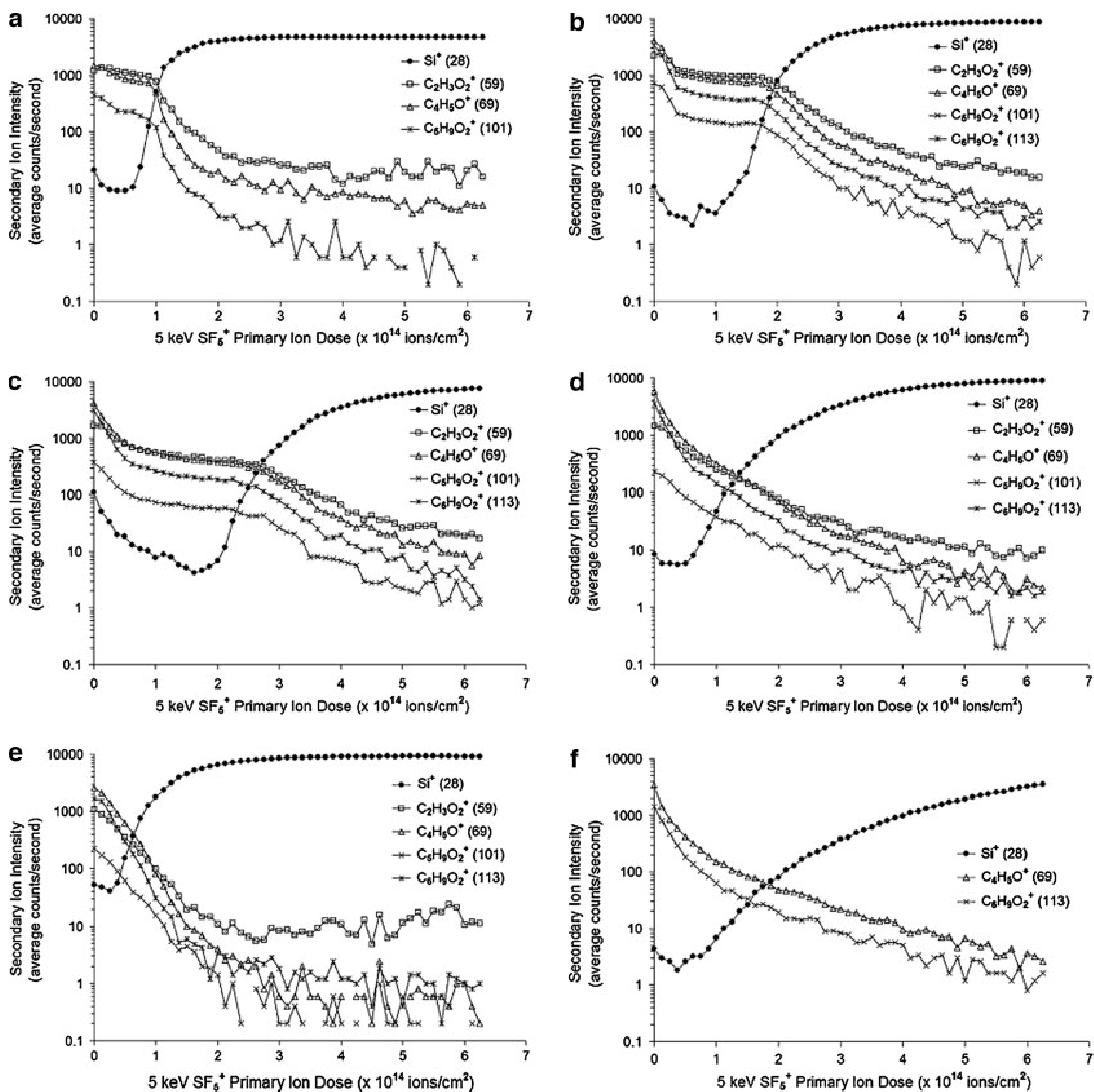

FIGURE 21. Positive ion damage profiles of the MMA-co-EGDMA SIP films prepared in this study. Analysis ion = 10 keV Ar^{+}, sputter ion = 5 keV SF_5^{+}. (**a**) 100% MMA; (**b**) 5% EGDMA; (**c**) 10% EGDMA; (**d**) 20% EGDMA; (**e**) 33% EGDMA; (**f**) 100% EGDMA. Figure taken from Wagner et al. (2006) reprinted with permission from Elsevier, copyright 2006.

Measurements of interface widths from organic materials cast onto Si is a particularly difficult scenario for multiple reasons. First, there are expected to be numerous artifacts resulting from the dramatic changes in density that occur at this interface. There is expected to be a significant enhancement in the sputter and/or damage mechanisms that occur at the interface due in part to the recoiling of Si atoms occurring at the polymer/Si interface. It is also possible that there could be rebound scattering of the primary ions and other factors such as T_g changes at the interface, making it difficult to obtain an accurate value for interface widths in these types of samples. Despite all these difficulties, it is still very important to have some means of

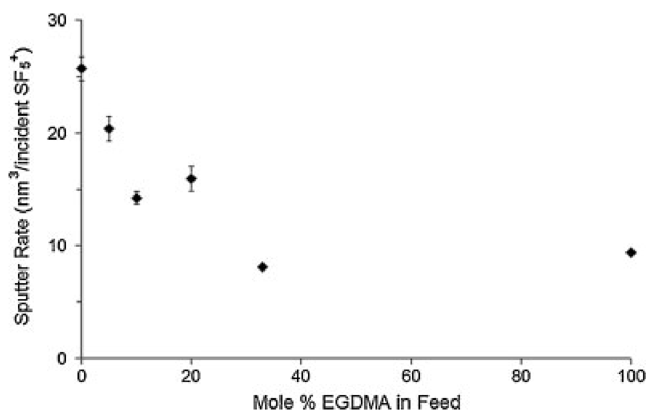

FIGURE 22. Sputter rates of the EGDMA-co-MMA SIP films under 5 keV SF_5^+ bombardment. Figure taken from Wagner et al. (2006) reprinted with permission from Elsevier, copyright 2006.

measuring and comparing relative interfacial widths in these systems, as it is a means of optimizing the source and experimental conditions. The following explains, from the authors' perspective, when one should employ each method of measuring interface widths.

1. Standard method ASTM E1428-91 uses the following equation; $\Delta Z = [\Delta t/t]*Z$, where ΔZ is the interface width, Δt is the sputtering time required for a decrease in the signal intensity of the overlayer from 84% to 16% of the signal intensity (or an increase in the substrate from 16% to 84%), t is the time required to sputter through the overlayer as defined by the time at which the overlayer (or substrate) signal intensity reaches 50% of its maximum value, and Z is the measured thickness of the overlayer. *This method is should only be used as a relative measure of interface widths and only for; (a) polymeric samples that have constant sputter rates throughout the depth of the overlayer, and (b) minimal interlayer mixing occurring, such as certain "well-behaved" polymers cast on Si substrates. Even in these cases, this method should only be used as an approximation of interfacial widths*. So for a PLA sample deposited on Si for example, this is an ideal method for interface width approximation, as PLA has rapid sputter rates that tend to be constant with increasing fluence (Mahoney, Roberson, & Gillen, 2004; Shard et al., 2008). However, it is not quite as useful for samples which crosslink quicker, such as is the case with thicker films of PMMA sputtered with SF_5^+ in which the sputter rate decreases significantly prior to the interface (Mahoney et al., 2006a). In the latter case, the result reported by ASTM will tend to result in an overestimated interface width. The width in this case should be measured after conversion of the profile to a depth scale using measured polymer sputter rates in the interfacial region. This method should also not be used for materials in which there will be considerable interfacial mixing, as would be the case in polymeric multilayers.

2. The method that is used to account for interlayer mixing uses a weighted average sputter rate between the substrate and the overlayer signal. The equation is shown below:

$$SR_{overall} = \left[\frac{I_{sub}}{I_{submax}}\right] SR_{sub} + \left[1 - \frac{I_{sub}}{I_{submax}}\right] SR_{polymer} \quad (4)$$

where $SR_{overall}$ is the weighted average sputter rate, I_{sub} is the intensity of the signal characteristic of the substrate at a given time, I_{submax}, is the substrate maximum, after the overlayer has been removed, SR_{sub} is the sputter rate of the substrate material, and $SR_{polymer}$ is the sputter rate of the polymer. This weighted average sputter rate is then used to convert the profile to a depth scale, and the interlayer thickness is measured based on the interface width guidelines described above (84%/16% maximum substrate intensity). In cases where there are multilayers of soft materials, this is the preferred method. However, *this equation is not accurate in cases where there is negligible interlayer mixing, and where the densities and sputter rates of the substrate are strikingly different than that of the coating by 2 or more orders of magnitude, such as is the case of thin polymer films on Si.* The sputtering yield of Si, for example is extremely low as compared to most polymers. Under similar sputtering conditions (SF_5^+ at 5 keV), the following sputtering yields have been reported (Mahoney, Roberson, & Gillen, 2004; Wagner, 2004): Si sputtering yield = 0.1 nm^3/ion, PMMA sputtering yield = 20 nm^3/ion and PLA sputtering yield = 60 nm^3/ion. This is over a factor of 200 decrease in sputtering yield from the organic to the Si interface! Therefore, any sputtering of Si is negligible during the removal of the polymer overlayers. In such cases, the result reported by this method, will result in an underestimated interface width. The width therefore in these cases should be measured after conversion of the profile to a depth scale using known polymer sputter rates at the interface. A good example of this underestimation is the interface widths calculated in Mahoney's work for PLA. The interface widths were calculated to be approximately 11 nm as calculated by conversion to a depth scale with known PLA sputter rates (Mahoney, Roberson, & Gillen, 2004). However, when the weighted sputter rate method was applied to these same systems, one achieves a depth resolution of only 3 nm!

It is not likely that a significant amount of interlayer mixing is occurring in thin "well-behaved" films on Si due to the huge differences in their densities, although it is certainly expected that some Si will rebound back into the polymer. However, this will cause either enhanced sputtering yields (in "well-behaved" systems) or significant chemical damage at the interface (in polymers exhibiting moderate to extreme crosslinking). In the second case, the sputter rate at the interface is expected to be reduced because the material being removed from the interface is a highly damaged overlayer with significantly reduced sputter rates as compared to the original polymer. In such cases, there is a slightly increased probability of

interfacial mixing, but the interface width measurements should be based on the actual sputtering rates observed at the interface.

More recent work has been published on the preparation of model multilayer films, which can serve as organic ‘‘delta-layers’’ (commonly used reference samples for dynamic SIMS in the semiconductor industry), thus allowing for more direct comparisons (Shard et al., 2008; Zheng, Wucher, & Winograd, 2008). In these films, the sputter rates and densities of the materials are very similar such that accurate depth resolutions can be obtained and compared.

3. There are still arguments as to whether the rise of the substrate signal or the fall of the organic signal should be used to define the interface widths. For now, this decision may need to be made on a case by case basis. In most works, the properties of the Si substrate signal have been used to define interface locations and widths. However, more recently, it is being discovered that this may not be the best way to make these measurements, as there is likely to be an interfacial damage layer (graphitic in nature) existing between the organic film and the Si substrate (Mahoney, 2009). The influence of this layer is dependent upon the sample and experimental conditions. In samples that do not accumulate damage before the interface is reached (PLA, for example) this may not contribute much to the interface measurements. However, in samples where damage starts accumulating prior to the interface (e.g., thicker films, or samples exhibiting increased crosslinking), this damage layer causes a reduced sputter rate at the interface which in turn results in significant broadening of the Si width, and a shift in the location of the interface towards higher ion fluences with respect to the location as defined by the organic signal decay. These interface effects can not be accounted for by employing differential sputtering rates.

Similar shifts in interface locations have been found by Green et al. (2009) in depth profiles of Irganox on Si. In this case, the authors found that the choice of ion (i.e., Si_x^-, Si_H^-, or SiO_2^-) used to define the organic/Si interface plays a very important role. More specifically, the authors illustrated that the presence of the SiO_2 layer was particularly problematic and resulted in artificial broadening of the interface when employing the Si_x^- signals as a means to characterize the interface (Green et al., 2009). It is possible that the same sorts of effects are observed when employing Si^+ ions in the positive mode as well.

Another potential problem with using the Si side for characterization of interface properties is that some sources, such as SF_5^+, may cause non-linear Si^+ ion yield enhancements, making for unreliable interface property measurements. Alternatively, the decline of the polymer signal can also be a source of error, as it is difficult to decide where the maximum polymer signal is located, especially in a case where there is a steady decline in signal.

Either method requires direct measurements of the sputter rates at the interface, to obtain more accurate sputter rate information. The sputtering yields at the interface can be measured *via* a quartz crystal microbalance (QCM) for example. In addition, film preparations have to be optimized, such that there are no ripples in the polymer films, and/or the raw data manipulated such that the depth profile is obtained only in common areas of the film where the thickness is consistent (Wucher, 2008; Mahoney, 2009).

2. C_{60} Versus SF_5^+

Taking the above notions into consideration, it can be stated that C_{60}^+ is an ideal source for depth profiling through *thicker* polymeric layers (Fisher et al., in press), as the signal tends to remain stable for much higher fluences, and has comparably higher sputtering yields. The following approximate sputtering yields were reported for PLA under varying conditions for both SF_5^+ and C_{60}^+:

- $250\,nm^3/C_{60}^+$ at 30 keV (500 eV per atom) (Shard et al., 2007).
- $75\,nm^3/C_{60}^+$ at 20 keV (333 eV per atom) (Shard et al., 2007).
- $40\,nm^3/C_{60}^+$ at 10 keV (167 eV per atom) (Shard et al., 2007).
- $40 - 59\,nm^3/SF_5^+$ at 5 keV (833 eV average energy per atom) (Mahoney, Roberson, & Gillen, 2004; Mahoney, Yu, & Gardella, 2005).

Similarly for PMMA, the sputtering yields are reported as follows:

- $38\,nm^3/C_{60}^+$ at 10 keV (167 eV per atom) (Möllers et al., 2006).
- $20\,nm^3/SF_5^+$ at 5 keV (833 eV average energy per atom) (Wagner, 2004; Mahoney et al., 2007a).
- $65\,nm^3/SF_5^+$ at 8.75 keV (1,460 eV average energy per atom) (Wagner, 2004).
- $8\,nm^3/SF_5^+$ at 2.5 keV (417 eV average energy per atom) (Wagner, 2004).

As can be seen in both cases, the sputtering yields are much higher for C_{60}^+, even at lower energies per atom.

Despite the obvious successes of C_{60}^+ bombardment of polymeric materials, deposition of carbon and large topography features can be associated with C_{60}^+ beams at lower energies (Fahey et al., 2006; Gillen et al., 2006a; Green et al., 2009). This is a particular problem with Si substrates, which is often used as a support for polymer thin films. These factors may result in degradation of the depth resolution. SF_5^+ tends to exhibit excellent depth resolution, and also tends to be well-rounded in its uses for both organic and inorganic applications, but cannot attain the depths that C_{60}^+ has achieved, even when low temperatures are applied. From comparison of PLA depth profiles and other comparisons obtained in the literature thus far, it appears to be that SF_5^+ may have slightly improved depth resolutions as compared to C_{60}^+ (Mahoney, Roberson, & Gillen, 2004; Shard et al., 2007) although it is too early to confirm at this juncture.

3. Massive Gas Clusters

Even more recently, data has been presented which indicates that massive gas clusters can achieve even greater sampling depths than C_{60}^{+}. In addition, unlike C_{60}^{n+} and SF_{5}^{+}, these gas cluster sources have been shown to work well for *both* type I and type II polymers.

4. LMIG Clusters

LMIG clusters have been demonstrated to profile through thin organic layers, but do so very poorly as compared to SF_{5}^{+} or C_{60}^{+}. For example, the damage characteristics of PET under Au_{3}^{+} and C_{60}^{+} ion bombardment were studied in detail by Conlan et al. (2006). In this study, the authors plotted the relative intensity of selected PET secondary ions as a function of increasing primary ion fluence. It was found that damage accumulated under Au cluster bombardment (signal decreased with fluence), but not under C_{60}^{+} bombardment, which maintained relatively constant signals with increasing fluence. Similar results were found in other kinds of molecular samples, such as trehalose (Cheng et al., 2007). Finally, the sputter rates were found to be enhanced significantly for PS 2000 when employing C_{60}^{+} ion beams as opposed to Au_{3}^{+} beams (Hill & Blenkinsopp, 2004).

C. Beam Energy

It has been repeatedly demonstrated, that increasing cluster beam energies generally results in increases in sputter and secondary ion yields in organic and polymeric samples (Wagner, 2004; Bolotin, Tetzler, & Hanley, 2006; Fletcher et al., 2006a; Shard et al., 2007). A nice example is shown below in a plot taken from Shard et al. (2007), which shows the sputtering yield volumes for PLA, Irganox 1010 and Alq_3 samples as a function of C_{60}^{+} beam energy (see Fig. 23).

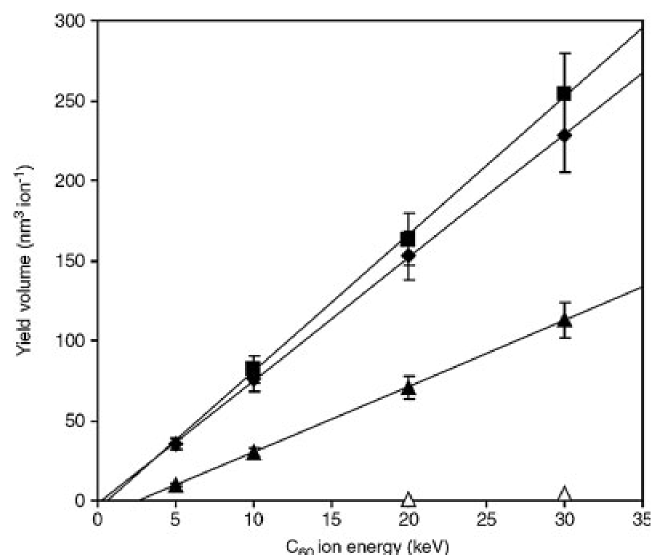

FIGURE 23. Yield volumes for PLA (◆), Irganox 1010 (■), and Alq_3 as a function of primary ion energy. The initial (▲), and final (△) yield volumes for Alq_3 are provided. Figure taken from Shard et al. (2007) reprinted with permission from John Wiley & Sons, Ltd, copyright 2007.

More recently it has been determined (Fisher et al., 2008) that as the C_{60} beam energy increases, one can maintain molecular secondary ions for longer sputter times, or increased sputtered depths into the sample. Figure 24, displays the normalized intensities of $m/z = 85$ and $m/z = 185$ (peaks characteristic of PMMA) as a function of increasing depth for 10, 20, and 40 keV C_{60}^{n+} ion bombardment of bulk PMMA. The results indicate that signal loss occurs much later with the higher energy beams. These results are consistent with previous work with atomic bombardment which showed that the efficiencies of the damage processes (e.g., crosslinking, etc) are lower for high-energy ions than for low energy ions (Calcagno, 1995). However, it is also likely that the onset of damage accumulation at lower energies with C_{60} is actually brought about by deposition of carbon, rather than crosslinking. Therefore it is not clear at this point whether the same effects would be observed for other beams as well.

The topography, modulus and chemistry of the crater bottoms were subsequently measured using nanoindentation and XPS. Roughness was found to increase with beam energy,

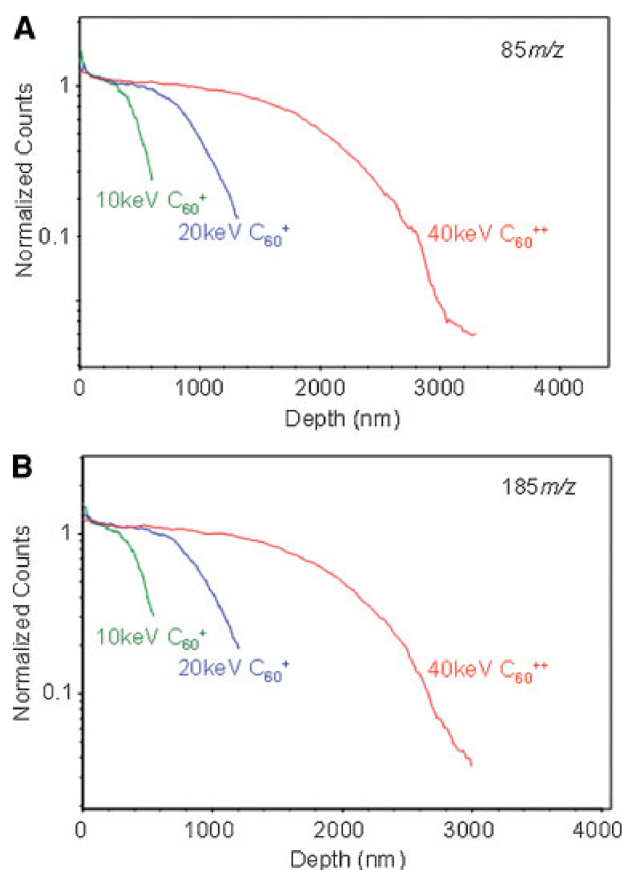

FIGURE 24. Negative TOF–SIMS depth profiles of bulk PMMA generated using 10 keV C_{60}^{+} (green), 20 keV C_{60}^{+} (blue) and 40 keV C_{60}^{++} (red) primary ions for both sputtering and acquisition. (**A**) Normalized counts at 85 m/z plotted against sputter depth. (**B**) Normalized counts at 185 m/z plotted against sputter depth. Figure taken from Fisher et al. (Fisher et al., 2008) reprinted with permission from Elsevier, copyright 2008. [Color figure can be viewed in the online issue, which is available at www.interscience.wiley.com.]

with peak to peak roughness values of 6 nm for the surface, 57 nm for the 10 keV C_{60}^{+} crater bottom, 183 nm for 20 keV C_{60}^{+} crater bottom, and 309 nm for 40 keV C_{60}^{++} crater bottom. This increased roughness was attributed to defects in the PMMA film. These are fairly high values for topography formation, and hence there should be a corresponding decrease in depth resolution at higher energies. The hardness and modulus were found to decrease with increasing beam energy. The XPS spectra also indicated decreased O concentrations and decreased C=O content with increasing energy. Although these changes could be attributed to increased damage accumulation at higher energies resulting from the longer sputtering times, it could also be attributed to C deposition.

More recently, alternating layers of two different Irganox samples were prepared as a means to create model organic ''delta-layers'' (Shard et al., 2008). The results from this work are similar to that observed by Fisher et al. (2008) in that there is evidence of decreased erosion depths for lower energy beams, and increased roughness at higher energies. The corresponding depth resolutions however were determined to be greater at lower energies.

D. Beam Angle

It has recently been demonstrated that glancing ion beam angles are most ideal for organic and polymeric depth profiling with C_{60}^{+} beams due to a reduction in penetration depths (Kozole, Wucher, & Winograd, 2008; Miyayama et al., 2008). Kozole et al. show that there is a reduction in molecular damage at more glancing angles, even though the total sputtering yield is reduced. Figure 25 illustrates this important result in a thin film of cholesterol on Si. These results suggest reduced damage is not necessarily dependent upon enhanced sputtering yields and that depositing the incident energy nearer the surface by using glancing angles is most important. It is unclear at this point if carbon deposition plays a role as well.

E. Charge

Szymczak and Wittmaack (Szymczak & Wittmaak, 1994) acquired positive and negative TOF mass spectra of Si sputter-cleaned with SF_6^-, SF_5^-, SF_5^+, and Xe^+. Charge was found to play little, if any, role in the ion yields. Several investigations use C_{60}^{+}, C_{60}^{2+}, and C_{60}^{3+} interchangeably for depth profiling applications (Shard et al., 2007; Wucher, Chen, & Wingorad, 2008; Fisher et al., 2008) with very little difference in the results. Therefore it is assumed that charge does not play a significant role in depth profiling.

F. Oxygen Flooding

Recent studies have indicated that oxygen flooding during polymeric depth profiling can enhance secondary ion yields during depth profiling, but only slightly. To the author's knowledge, there has not yet been a publication in regards to the maximum erosion depths achievable with and without oxygen flooding. Though the presence of oxygen during irradiation has been shown to enhance degradation mechanisms in some polymers (Chapiro, 1962), the pressures are most likely too low during a typical SIMS experiment to have any appreciable affect. In either case, more work needs to be done in this area before the issue can be discussed further.

G. Temperature

Because most crosslinking and degradation mechanisms rely heavily on the formation of free radical intermediates, temperature and crystallinity typically play a very important role in the

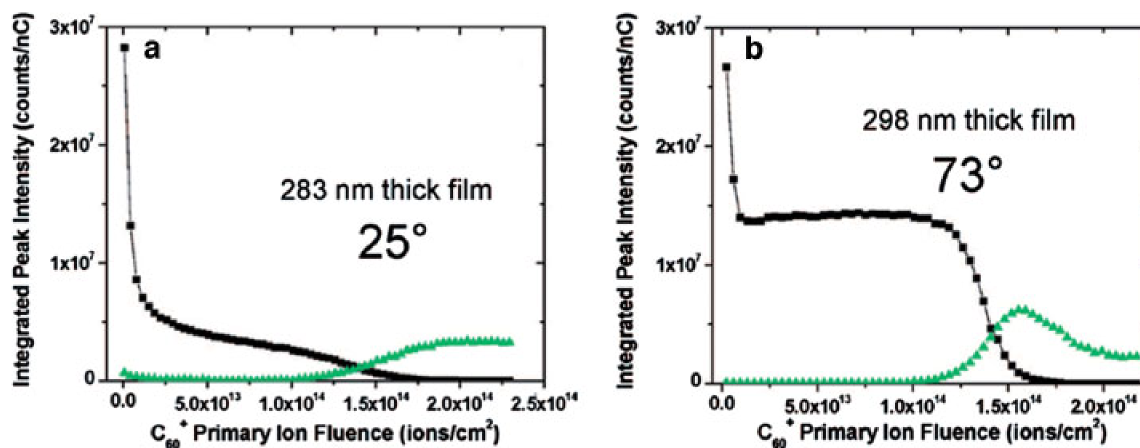

FIGURE 25. Depth profile plots of cholesterol quasi-molecular ion (*m/z* 369, $[M-H_2O]^+$; squares) and silicon (*m/z* 28, Si^+; triangles) ion intensities as a function of C_{60}^{+} fluence. The depth profiles were acquired using 40 keV C_{60}^{+} at 5°, (**a**) 25° and (**b**) 73° incidence. The Si intensity is multiplied by a factor of 10 in each depth profile plot. Figure taken from Kozole, Wucher, and Winograd (2008) reprinted with permission from American Chemical Society, copyright 2008. [Color figure can be viewed in the online issue, which is available at www.interscience.wiley.com.]

degradation and crosslinking processes in polymers (Chapiro, 1962). This is because free radicals will lose their reactivity if they are embedded in a solid medium as they become "trapped" or "frozen." This tends to be the case when polymers are below their glass transition temperature or have crystalline regions where there is decreased mobility of the polymer chains. Therefore, at low temperatures (−100°C range), it may take a lot longer before a critical fluence is reached, where the polymer starts forming a gel. When the sample is later "unfrozen" again, for example, by an increase in temperature beyond its glass transition temperature or by addition of a solvent, the radical is again free to react. On the other hand, increased temperatures allow for increased availability of these radicals, and therefore crosslinking and/or degradation mechanisms can be sped up. In addition, ion-induced depolymerization mechanisms will start playing a role at high temperatures resulting in more rapid removal of material.

A series of studies at NIST recently demonstrated that temperature indeed plays a significant role in polymeric depth profiling, as well as for polymeric surface analysis in SIMS (Mahoney et al., 2006a; Mahoney, Patwardhan, & McDermott, 2006b; Mahoney, Fahey, & Gillen, 2007a; Mahoney et al., 2007b; Mahoney, Fahey, & Belu, 2008). It was demonstrated that depth profiling in PMMA is optimized at low temperatures with an SF_5^+ source (Mahoney et al., 2006a). Figure 26 depicts the main results from this work, with depth profiles obtained from PMMA films (160 nm) on Si at three different temperatures (−75°C, 25°C, and 125°C), along with the corresponding AFM topography maps of the crater bottoms. As can be seen, the best overall depth profiles were acquired at −75°C, as evidenced by the increased signal constancy, interfacial widths and corresponding decrease in topography formation. The worst overall depth profiles were obtained at room temperature, where there was significant signal degradation prior to the interface location, and much more accumulation of topography shown in the AFM. It should be noted that this extensive signal degradation observed in the PMMA film is not typically observed with thinner films (<80 nm) (Gillen & Roberson, 1998). The premature decay observed at 25°C, is therefore considered to be of a type similar to that displayed in Figure 14d. It is likely that at room temperature, the critical crosslinking fluence of the PMMA was reached earlier than at low temperatures.

The corresponding AFM micrographs indicated an increase in topography formation at room temperature as compared to the other temperatures, and particularly smooth crater bottoms were obtained at −75°C. Corresponding XPS analysis of PMMA crater bottoms also showed a higher C/Si ratio (C/Si = 5) in crater bottoms created at 25°C as compared to the other temperatures (C/Si ratios measured in crater bottoms at 125°C and −75°C were 1.58 and 0.47 respectively), even though all corresponding molecular signal in the SIMS depth profiles were absent. This indicates that there is still highly damaged PMMA material remaining at the 25°C crater bottom. The lowest C/Si ratio was observed in the −75°C crater bottom indicating that the PMMA was successfully removed from the wafer by the SF_5^+ beam. Intermediate topography and C/Si ratios were obtained at 125°C, similar to what was observed in the depth profiles.

Along with the improvements observed in the depth profiles at high temperatures, there was a measured increase in sputter rate at higher temperatures. The reported sputter rates at room temperature were approximately 25 nm^3/SF_5, while at 125°C the sputter rates increase to approximately 49 nm^3/SF_5. This increase in sputter rate was attributed to ion beam-induced depolymerization, a well-known phenomenon that occurs during atomic bombardment (Fragalà et al., 1998). Residual gas analysis (RGA) was utilized to confirm that high temperature depth profiling mechanisms in PMMA do indeed involve a depolymerization or "unzipping" process, as evidenced by the existence of the methyl methacrylate monomer at $m/z = 120$ above 50°C (Mahoney et al., 2007b). The results from this analysis are depicted in Figure 27, which displays the pressure of the gaseous monomer released as a function of temperature. As can be seen, there is an increase with temperature and the point at which the monomer concentration started to increase was around 50°C. This is the same point at which the measured sputter rate of the material increased (Mahoney, Fahey, & Gillen, 2007a). Also consistent with

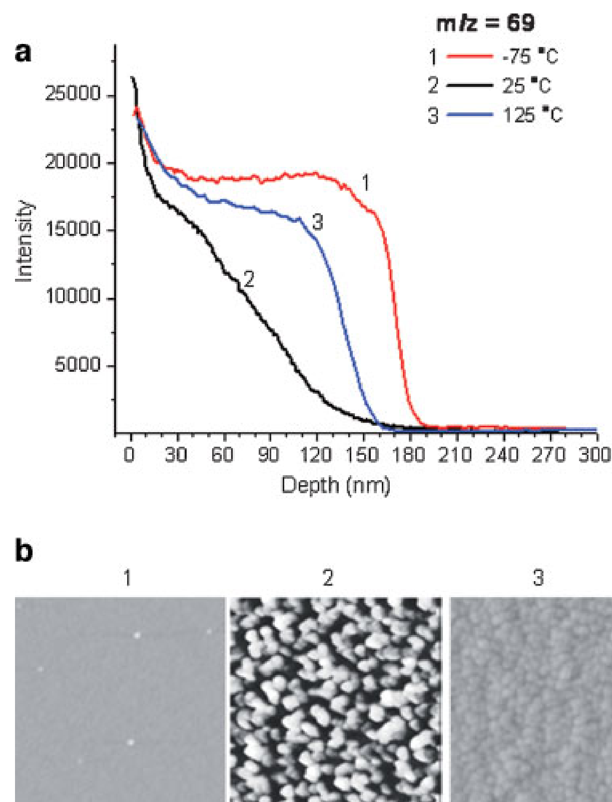

FIGURE 26. (**a**) Positive secondary ion intensities of $m/z = 69$ plotted as a function of depth for a PMMA film (~160 nm) on Si measured at: (1) −75°C, (2) 25°C, and (3) 125°C. All depth profiles were acquired using dual beam depth profiling (10 keV Ar^+ analysis source, and 5 keV SF_5^+ sputter source). (**b**) Atomic force microscopy (AFM) topography images of crater bottoms formed at different temperatures (1 μm × 1 μm area): (1) −75°C, $R_{rms} \sim 0.27$ nm; (2) 25°C, $R_{rms} = \sim 11.37$ nm; (3) 125°C, $R_{rms} = \sim 1.00$ nm. Note: control sample of PMMA surface before sputtering had an R_{rms} of ~0.85 nm, while that of pure Si is around 0.2 nm. Figure from Mahoney et al. (2006a) reprinted with permission from Elsevier, copyright 2006. [Color figure can be viewed in the online issue, which is available at www.interscience.wiley.com.]

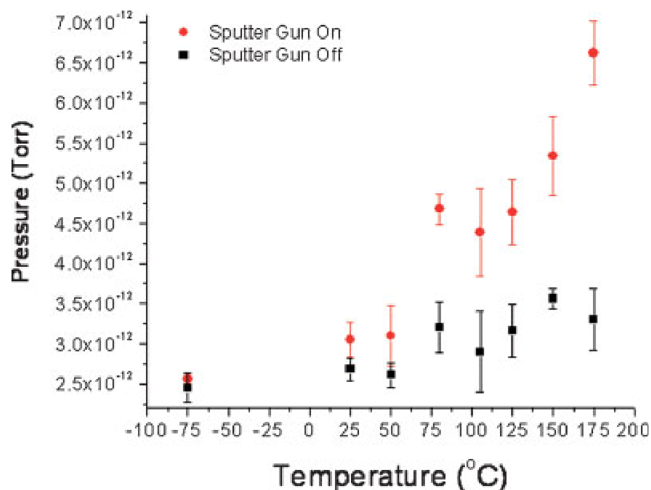

FIGURE 27. Pressure of PMMA monomer as a function of increasing temperature, with (●) and without (■) SF_5^+ sputtering. Each point represents an average of at least 3 measurements on the same sample, where the error bars represent 1 standard deviation. Figure from Mahoney et al. (2007b) reprinted with permission from American Chemical Society, copyright 2007. [Color figure can be viewed in the online issue, which is available at www.interscience.wiley.com.]

depolymerization was the XPS C1s spectra, which indicated a decreased content of the C=O moiety in the samples bombarded at −75°C and 25°C, as compared to the control, but very little difference between ion-bombarded and pristine PMMA at 125°C (Mahoney et al., 2007b).

Temperature studies were also performed with C_{60}^+ ion beams on PMMA (Möllers et al., 2006). The results were similar to Mahoney's work in regards to high temperatures, where there was a significant increase in erosion rates of the PMMA at high temperatures. More specifically, the erosion rates were reported to be 20 nm^3/C_{60}^+ at −140°C, 38 nm^3/ion at 20°C and 60 nm^3/C_{60}^+ at 180°C. However, no improvements in the profile quality were observed at low temperatures with the C_{60}^+. It should be noted that the depth profile obtained with C_{60}^+ at room temperature looks much better than the same achieved with the SF_5^+, meaning there is no degradation in signal at room temperature. It is assumed that there is still some form of ion-induced polymerization effect occurring even at room temperature with the C_{60}^+, since there are still decreases in the sputter rate below room temperature. It could also be that there is a significantly higher critical fluence required to reach the gel point of the PMMA in the case of C_{60}^+ as compared to SF_5^+.

It was this work (Möllers et al., 2006) that first suggested that at high temperatures, there was a change in the chemical sputtering mechanism to that of ion-induced depolymerization. This idea was corroborated by the fact that at these high temperatures, depth profiling of PMMA could even be achieved using Ga beams. In addition to PMMA samples, the authors of this work also investigated the effect of temperature on depth profling in poly(α-methyl-styrene) (PAMS) and PS samples. PAMS could not be profiled at room temperature. However, when the temperature was increased to above 160°C, the material was depth profiled successfully because of depolymerization (see Fig. 28). PS depth profiling was unsuccessful at all temperatures, similar to what was observed with SF_5^+ (Mahoney et al., 2006a). Though low temperatures did not appear to help with the PMMA

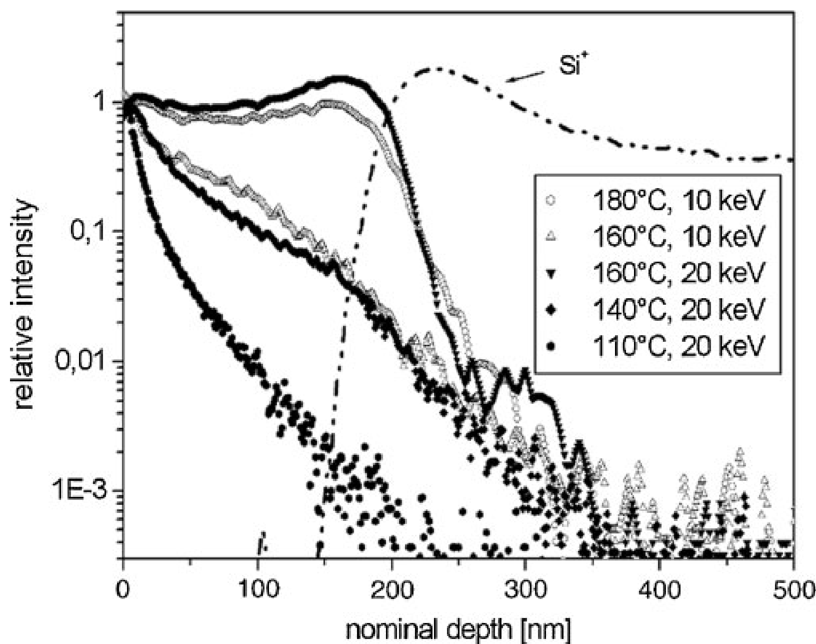

FIGURE 28. Normalized intensity of $m/z = 105$ yield versus depth in PAMS films measured at various sample temperatures. Erosion beam: C_{60}, 10 keV (open symbols) or 20 keV (solid symbols). Depth scale is calibrated with the silicon substrate signal, shown as dash-dotted line only for the 180° experiment. Figure taken from Möllers et al. (2006) reprinted with permission from Elsevier, copyright 2006.

samples when employing C_{60}^{+}, low temperatures are still turning out to be ideal in some organic systems (Zheng, Wucher, & Winograd, 2008).

The relaxation of the craters at different temperatures plays a very critical role as well, and helps to describe the resulting topography formation shown in the AFM images. In studies by Papaléo et al. (2001, 2006), PMMA films were bombarded with 20 MeV Au^{+} ions at low fluences and at variable temperatures from −196°C to 150°C. Scanning force microscopy (SFM) was then used to image the bombarded regions after cooling. The SFM images revealed nm-sized craters and/or raised regions (hillocks) around the point of each ion impact, where the size of the craters and hillocks was independent of the temperature up to 80°C, but at higher temperatures, the crater dimensions increased steeply and no hillock was observed. The effects of local temperature were prominent as well. When the sample was rapidly cooled, therefore quenching the relaxation of the crater, the hillocks disappeared closer to the glass transition temperature of the polymer (105°C). The presence of the hillocks at room temperature, under slow cooling conditions, therefore indicates that the transient local heating induced by the incoming ion itself cannot be higher than 100°C at the hillock position, during a time interval greater than several seconds. In other words, *if* after the bombardment of the surface (at 25°C), the local temperature then increases above the glass transition, it remains at this temperature for a *shorter time scale than is required for large scale movement of macromolecules,* otherwise the hillocks would not be observed. This is true, given that the relaxation times for large-scale chain movements of PMMA after mechanical deformation is on the order of seconds to hours depending on the temperature, while the increased temperature at the site of the bombardment is increased for approximately 300 psec as predicted by thermal spike models (Papaléo et al., 2001; Papaléo et al., 2006). These results are consistent with the topography observed during SF_5^{+} bombardment, where the initial topography features in the PMMA were shown to be broader at higher temperatures (Mahoney et al., 2007b).

Even more information was obtained from the mass spectra of the PMMA acquired before and after sputtering with SF_5^{+} at variable temperatures (Mahoney et al., 2007b). Figure 29 shows the results from principal components analysis of the PMMA positive and negative ion SIMS spectra acquired before and after sputtering in a PMMA film, at variable temperatures. Figure 29a,b represents the scores and loadings from principal component 1 (80.5% of total variance) of the positive ion spectra, and Figure 29c,d shows the scores and loadings for principal component 1 (74.6% of total variance) of the negative ion spectra. As can be seen, there is a large difference in the mass spectra acquired before and after sputtering. In general, after sputtering there are more peaks indicative of the formation of polycyclic aromatic hydrocarbons and a decrease in the peaks associated with PMMA in the positive spectra. In the negative spectra, there are larger amounts of C and F signals present after sputtering, and a large decrease in the O signals. Note that in both positive and negative ion mass spectra, the smallest differences before and after sputtering are observed at 125°C, indicating that the least amount of structural damage is occurring at high temperatures, consistent with depolymerization.

Although the XPS, AFM, SIMS, and RGA results were consistent with increased depolymerization at high temperatures, it was unclear at the time, what caused the improvement at low temperatures. Though the morphology changed significantly, there was very little to no difference in the C=O moiety at −75°C versus 25°C. If anything, there was evidence of increased damage in the SIMS spectra, where there were more peaks indicative of damage in the form of unsaturation and crosslinking (PAH's) at −75°C, than at 25°C (after sputtering). These results were initially quite surprising, based on the dramatic improvement in SIMS depth profiles obtained at low temperatures. It was therefore suggested, that the primary reason for the excellent depth profile results in PMMA at low temperatures was not because of decreased chemical damage to the material, but a result of the variation in sputter properties at low temperatures. It was argued that at these low temperatures, the polymers had much better inter- and intra-chain coupling, leading to more uniform sputtering. This therefore leads to a reduction in sputter induced topography formation (as indicated in the AFM) and improvements in the depth profile characteristics.

However, while the change in sputter-induced topography formation may affect the interface widths, this does not fully describe the loss of signal that occurs in a manner as that shown in Figure 14d. It is the authors belief, that even though the mass spectra show evidence of increased damage at low temperatures, there is actually a significant decrease in crosslinking occurring at low temperatures, due to a combination of trapped radicals and decreased chain mobility, and that increases in PAH signal are only associated with decreased depolymerization mechanisms. It could also be that the decreased chain mobilities are the result of increased PAH signal. For example, cyclization (formation of PAH) is known to occur more frequently in crystalline regions (Chapiro, 1962) under irradiation as compared to non-crystalline regions. This increased cyclization in crystalline samples could result from increased intramolecular versus intermolecular interactions in the crystalline regions (intramolecular interactions are more likely to result in cyclization and formation of PAH's). Similarly, low temperature materials exhibit decreased chain mobility and therefore may show increased cyclization mechanisms as well.

Temperature effects of several other polymeric materials with SF_5^{+} were investigated by Mahoney et al. as well, including PLA, PS, polyurethanes (PU), poly(ethylene-co-vinyl acetate) (PEVA) and poly(styrene-co-isobutylene) (Mahoney et al., 2006a; Mahoney, Patwardhan, & McDermott, 2006b; Mahoney, Fahey, & Gillen, 2007a; Mahoney, Fahey, & Belu, 2008). Most polymers tended to have increased PAH peaks when characterized at low temperatures, similar to that observed with PMMA. These differences are observed, even in the static SIMS spectra acquired. A good example is shown in Figure 30, which shows the static mass spectra (acquired with 10 keV Ar^{+}) of the surface of a polyurethane sample acquired at two different temperatures. This particular PU contains methylene diisocyanate (MDI), poly ethylene-glycol adipate (PEGA), and butanediol (BD) monomers, where the hard segment is comprised of MDI-BD segments, and the soft segment is comprised of MDI-PEGA segments ($[\text{MDI-BD}]_m$-$[\text{MDI-PEGA}]_n$). Note in the mass spectra that peaks characteristic of MDI are more intense in the spectra acquired at low temperatures, and are not even seen at room

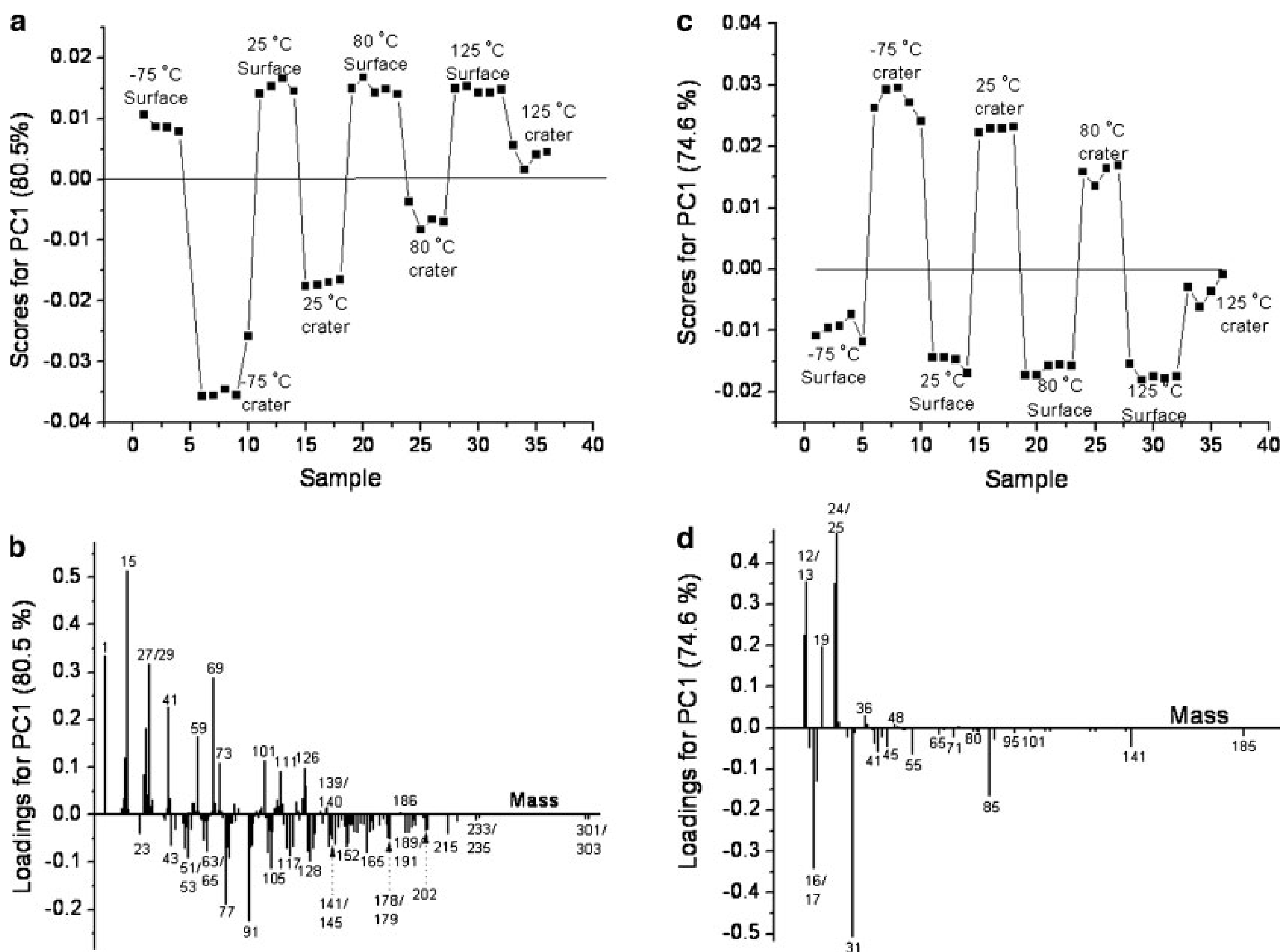

FIGURE 29. Results from principle components analysis (PCA) of both positive and negative TOF–SIMS spectra acquired from both the PMMA surface and sputtered PMMA crater bottoms at varying temperatures: (**a**) scores from positive-ion mass spectra, (**b**) loadings from positive-ion mass spectra, (**c**) scores from negative-ion mass spectra, and (**d**) loadings from negative-ion mass spectra. All PCA results shown here are from principle component 1 (PC1) describing the majority of the variance in the spectra (80.5% of variance in positive spectra and 74.6% variance in negative spectra.) Figure from Mahoney et al. (2007b), reprinted with permission from American Chemical Society, copyright 2007.

temperature. Conversely, peaks characteristic of the PEGA are diminished at low temperatures and are much more intense at room temperature. It appears as though in all of the analysis performed thus far, aromatic-type structures are preferred at low temperatures.

In some materials, the effect of low temperatures was particularly extreme (Mahoney, Patwardhan, & McDermott, 2006b). A good example is illustrated in Figure 31, which shows polyurethane depth profiles at −100°C and 25°C. While at 25°C, there is essentially no useful information, as indicated by the nearly complete loss of signal in the profile, at −100°C there are relatively constant secondary ion signals with depth, and a more "well-defined" interface. This difference can be seen in the optical images of the crater bottoms.

It has also been found that when applying low temperatures, one can potentially depth profile through much thicker polymeric layers before any loss of signal occurs. For example, the depth profiles acquired from the drug-eluting stent coatings displayed in Figure 18 were acquired at −100°C (Mahoney, Fahey, & Belu, 2008). It was shown that the signal was lost after only around 1–2 μm of material was removed at room temperature. However, at low temperatures, the entire 6 μm thick film was removed with maintenance of characteristic signal. It is assumed that the gel point is delayed at low temperatures and the signal can be maintained for much longer periods of time.

H. Crystallinity and Stereochemistry

Similar to what is observed at low temperatures, it can be expected that the crystalline regions in polymers will have trapped radicals, therefore preventing crosslinking in these

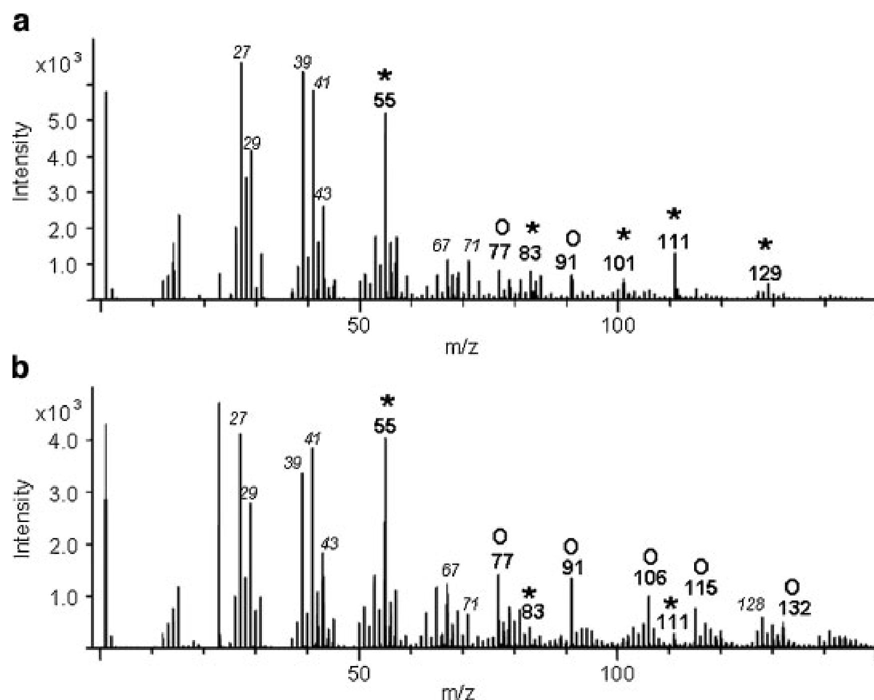

FIGURE 30. Positive ion mass spectra of polyurethane (Estane 5767) measured at: (**a**) 25°C, and (**b**) −100°C. Peaks labeled with [O] are characteristic of the polyurethane hard segment, while peaks labeled with [*] are characteristic of the polyurethane soft segment. Figure from Mahoney, Patwardhan, and McDermott (2006b) reprinted with permission from Elsevier, copyright 2006.

regions. Although not much work has been done to confirm this observation, there have been preliminary studies on the effects of stereochemistry on depth profiling. The results have indicated that the polymer tacticity may play a significant role in depth profiling of polymers. More specifically, isotactic PMMA was found to have decreased damage accumulation effects then syndiotactic and atactic PMMA's (Mahoney, 2009). The improvements were not attributed to changes in their crystallinity however, but rather from increases in strain along the backbone in the isotactic structure (Soldera, 2002).

I. Co-Sputtering

Recent evidence suggests that co-sputtering with C_{60}^{+} and other ion beams, such as Ar^{+} can prevent the accumulation of damage associated with carbon deposition in the source (Yu et al., 2008), where it has been shown that C_{60}^{+}/Ar^{+} co-sputtering can be used to extend the depth profile range and maintain a more constant sputter rate in polymer depth profiles. The theory is that the Ar^{+} gun prevents the deposition of carbon and therefore can both improve the quality of the depth profile and increase the achievable erosion depth.

J. Other Considerations

Electron flood gun fluence should be limited due to the sensitivity of certain polymers to electron bombardment. The use of a flood gun could accelerate the damage mechanisms occurring during depth profiling. Gilmore and Seah (2002) defined a useful electron fluence limit of 6×10^{18} electrons/m^2 for organic and polymer samples. When using an LMIG source for analysis during depth profiling in thicker films, care should be taken to use the most minimal fluence because this has also been shown to accumulate damage. Sample rotation may or may not play an important role as well.

IX. SUMMARY AND CONCLUSIONS

Cluster secondary ion mass spectrometry (cluster SIMS) has played a critical role in the characterization of organic and polymeric materials over the last decade, allowing for significant enhancements in molecular sensitivities and the ability to obtain compositional information as a function of depth from several organic and polymeric systems. This has lead to active research in many areas, including bioimaging and drug delivery applications. Though it was initially thought that this technology would have too many limitations for organic depth profiling, it is very clear from the resulting literature, that these limitations are rapidly disappearing.

It has been repeatedly demonstrated that parameters such as temperature, beam energy, and beam type can play a crucial role in polymeric depth profiling, and needs to be considered in any SIMS experiment. Although both SF_5^{+} and C_{60}^{+} beams perform well in depth profiling of thin polymer overlayers (<1 μm), C_{60}^{+} is

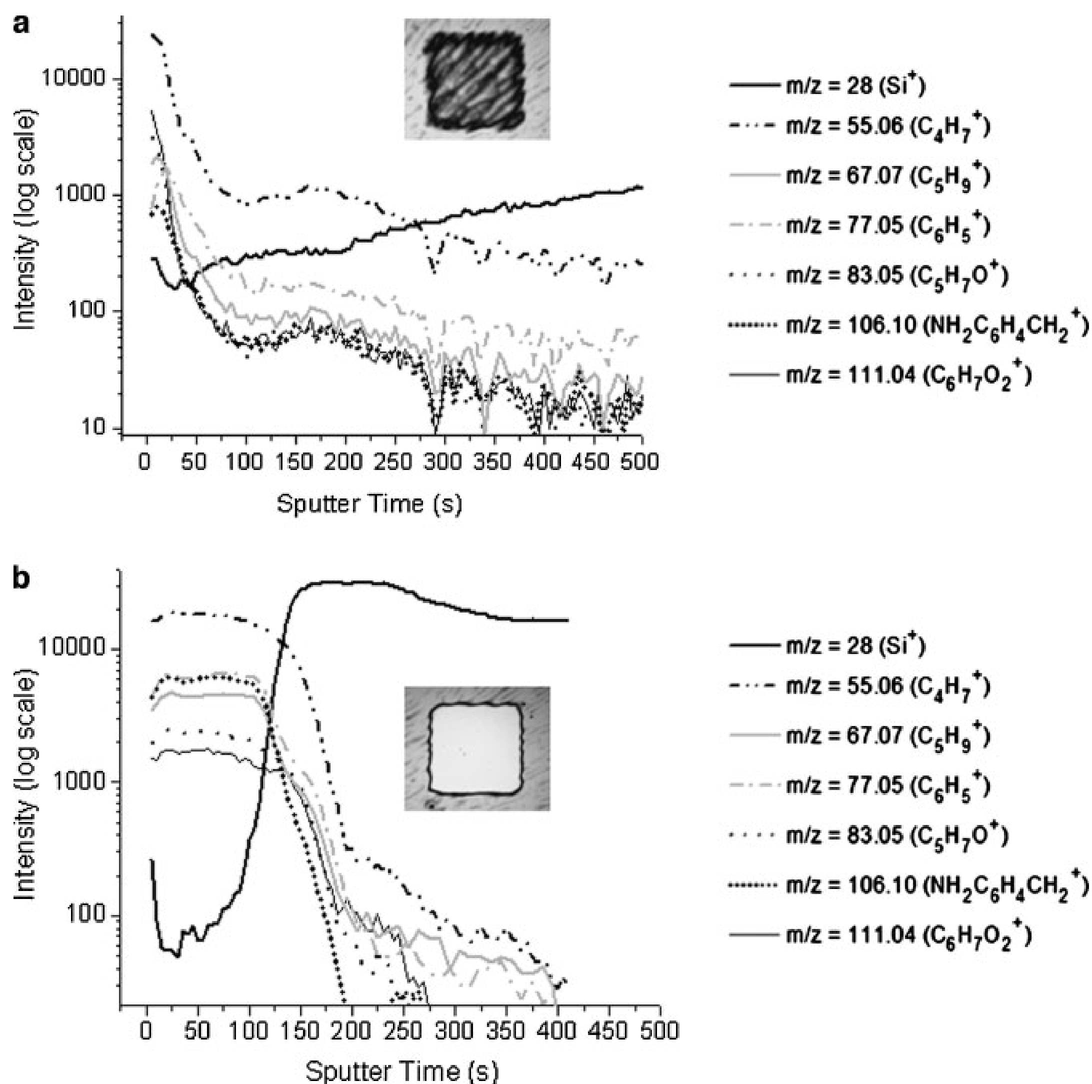

FIGURE 31. Characteristic positive secondary ion intensities plotted as a function of increasing SF_5^+ sputter time (2 nA continuous current and 500 μm × 500 μm raster) for a spin-cast film of Estane 5767 measured at: (**a**) 25°C and (**b**) −100°C. Optical images of the sputtered crater bottoms (500 μm × 500 μm) are displayed as insets. Figure from Mahoney, Patwardhan, and McDermott (2006b) reprinted with permission from Elsevier, copyright 2006.

ideal for thicker overlayers as it has been shown to maintain constant secondary ion signals for much higher fluences and therefore increased erosion depths as compared to SF_5^+. Although these sources are ideal for depth profiling in most polymeric materials, many Type I polymers still present a problem for these sources, a problem that is currently being eliminated with the advent of the gas cluster ion beam.

It should be noted that the polymers that are particularly amenable to depth profiling with cluster beams have contained either quaternary C carbon atoms along the chain or have cleavage points in the main chain, such as –O–, –NH– or –(C=O)–. It is assumed that the presence of a tetrasubstituted carbon in the chain causes strain in the molecule, resulting in a weakening of the main chain. It also appears that the most radiation-resistant (crosslinking) polymers have decreased branching and/or contain aromatic substituents. For these types of materials, it may be best to use either low energy Cs^+/O_2^+ or massive gas clusters (such as Ar_{2000}), which work much better than the more conventional cluster sources for these crosslinking polymers.

For static SIMS analysis of surfaces, Au_{400}^{4+}, Bi_n^+ ($n = 3, 5$, or 7) and C_{60}^+ beams have been determined to have the highest efficiencies. Bi_n^+, in particular, has been useful for imaging applications due to its high spatial resolution. In general, all cluster sources result in significant benefits over atomic sources in static SIMS analysis of thick polymer films. Besides the increased signal intensities, there are often decreased charging effects and decreased damage accumulation associated with these sources, which allows for much longer signal averaging times.

Cluster beams exhibit significant enhancements in sensitivity (as compared to atomic beams), with nanoscale depth resolution (5–10 nm) and sub-micron lateral resolution, making cluster SIMS a promising characterization tool enabling high-resolution three-dimensional imaging for organic and polymeric-based materials.

REFERENCES

Adriaensen L, Vangaever F, Gijbels R. 2004. Metal-assisted secondary ion mass spectrometry: Influence of Ag and Au deposition on molecular ion yields. Anal Chem 76:6777–6785.

Aimoto K, Aoyagi S, Kato N, Iida N, Yamamoto A, Kudo M. 2006. Evaluation of secondary ion yield enhancement from polymer material by using TOF-SIMS equipped with a gold cluster ion source. Appl Surf Sci 252:6547–6549.

Andersen HH, Bay HL. 1974. Nonlinear effects in heavy-ion sputtering. J Appl Phys 45(2):953–954.

Andersen HH, Bay HL. 1975. Heavy-ion sputtering yields of gold: Further evidence of nonlinear effects. J Appl Phys 46(6):2416–2422.

Andersen HH, Brunelle A, Della-Negra S, Depauw J, Jacquet D, Le Beyec Y. 1998. Giant metal sputtering yields induced by 20-5000 keV/atom gold clusters. Phys Rev Lett 80(24):5433–5436.

Appelhans AD, Delmore JE. 1987. Focused, rasterable, high-energy neutral molecular beam probe for secondary ion mass spectrometry. Anal Chem 59:1685–1691.

Appelhans AD, Delmore JE. 1989. Comparison of polyatomic and atomic primary beams for secondary ion mass spectrometry of organics. Anal Chem 61:1087–1093.

Aranyosiova M, Chorvatova A, Chorvat D, Jr., Biro CS, Velic D. 2006. Analysis of cardiac tissue by gold cluster ion bombardment. Appl Surf Sci 252:6782–6785.

Baker MJ, Fletcher JS, Jungnickel H, Lockyer NP, Vickerman JC. 2006. A comparative study of secondary ion yield from model biological membranes using Au_n^+ and C_{60}^+ primary ion sources. Appl Surf Sci 252:6731–6733.

Balik CM, Said MA. 1987. High-energy ion implantation of polymers: Poly(ethylene terephtalate). J Polym Sci B 25:817–827.

Benguerba M, Brunelle A, Della-Negra S, Depauw J, Joret H, Le Beyec Y, Blain MG, Schweikert EA, Assayag GB, Sudraud P. 1991. Impact of slow gold clusters on various solids: Nonlinear effects in secondary ion emission. Nucl Instr Meth Phys Res B 62(1):8–22.

Bermudez VM. 1999. Low-energy electron-beam effects on poly(methyl methacrylate) resist films. J Vac Sci Technol B 17(6):2512–2518.

Biddulph GX, Piwowar AM, Fletcher JS, Lockyer NP, Vickerman JC. 2007. Properties of C_{84} and $C_{24}H_{12}$ molecular ion sources for routine TOF-SIMS analysis. Anal Chem 79:7259–7266.

Blain MG, Della-Negra S, Joret H, Le Beyec Y, Schweikert EA. 1989. Secondary-ion yields from surfaces bombarded with keV molecular and cluster ions. Phys Rev Lett 63(15):1625–1628.

Bolotin IL, Tetzler SH, Hanley L. 2006. Sputtering yields of PMMA films bombarded by keV C_{60}^+ ions. Appl Surf Sci 252:6533–6536.

Boschmans B, Van Royan P, Van Vaeck L. 2005. Use of monoatomic and polyatomic projectiles for the characterization of polylactic acid by static secondary ion mass spectrometry. Rapid Commun Mass Spectrom 19:2517–2527.

Boussofiane-Baudin K, Bobach G, Burnelle A, Della-Negra S, Hakansson P, Lebeyec Y. 1994. Secondary-ion emission under cluster-impact at low energies (5–60 keV)—Influence of the number of atoms in the projectile. Nucl Instr Meth Phys Res B 88(1–2):160–163.

Braun RM, Cheng J, Parsonage EE, Moeller J, Winograd N. 2006. Surface and depth profiling investiagion of a drug-loaded copolymer utilized to coat Taxus Express(2) stents. Anal Chem 78(24):8347–8353.

Briggs D, Hearn MJ. 1986. Interaction of ion beams with polymers, with particular reference to SIMS. Vacuum 36(11–12):1005–1010.

Brox O, Hellweg S, Benninghoven A. 2000. Dynamic SIMS of polymer films? Proc 12th Int Conf Secondary Ion Mass Spectrom 12:777–780.

Brunelle A, Della-Negra S, Deprun C, Depauw J, Hakansson P, Jacquet D, Le Beyec Y, Pautrat M. 1997. High desorption-ionization yields of large biomolecules induced by fast C_{60} particles. Int J Mass Spectrom Ion Proc 164:193–200.

Brunelle A, Touboul D, Laprevote O. 2005. Biological tissue imaging with time-of-flight secondary ion mass spectrometry and cluster ion sources. J Mass Spectrom 40:985–999.

Bryan SR, Belu AM, Hoshi T, Oiwa R. 2004. Evaluation of a gold LMIG for detecting small molecules in a polymer matrix by TOF-SIMS. Appl Surf Sci 231–232:201–206.

Bulle-Lieuwma CWT, van de Weijer P. 2006. 3D TOFSIMS characterization of black spots in polymer light emitting diodes. Appl Surf Sci 252:6597–6600.

Bulle-Lieuwma CWT, van Gennip WJH, van Duren JKJ, Jonkheijm P, Janssen RAJ, Niemantsverdriet JW. 2003. Characterization of polymer solar cells by TOF-SIMS depth profiling. Appl Surf Sci 203–204:547–550.

Calcagno L. 1995. Ion-chains interaction in polymers. Nucl Instr Meth Phys Res B 105:63–70.

Calcagno L, Foti G. 1987. Ion-chain interaction in keV ion-beam-irradiated polystyrene. Appl Phys Lett 51(12):907–909.

Calcagno L, Foti G. 1991. Ion irradiation of polymers. Nucl Instr Meth Phys Res B B59/60:1153–1158.

Calcagno L, Compagnini G, Foti G. 1992. Ion-beam effects on optical and theological properties of polystyrene. Phys Rev B 46(17):10573–10578.

Calcagno L, Percolla R, Masciarelli D, Foti G. 1993. Chain diffusion in ion crosslinked polystyrene gel. J Appl Phys 74(12):7572–7576.

Chapiro A. 1962. Radiation chemistry of polymeric systems. New York & London: John Wiley & Sons. p. 712.

Cheng J, Winograd N. 2005. Depth profiling of peptide films with TOF-SIMS and a C_{60} probe. Anal Chem 77:3651–3659.

Cheng J, Winograd N. 2006. Molecular depth profing of multi-layer systems with cluster ion sources. Appl Surf Sci 252:6498–6501.

Cheng J, Wucher A, Winograd N. 2006. Molecular depth profiling with cluster ion beams. J Phys Chem B 110:8329–8336.

Cheng J, Kozole J, Hengstebeck R, Winograd N. 2007. Direct comparison of Au_3^+ and C_{60}^+ cluster projectiles in SIMS molecular depth profiling. J Am Soc Mass Spectrom 18:406–412.

Chilkoti A, Lopez GP, Ratner BD, Hearn MJ, Briggs D. 1993. Analysis of polymer surfaces by SIMS. 16. Investigation of surface cross-linking in polymer gels of 2-hydroxyethyl methacrylate. Macromolecules 26:4825–4832.

Chujo R. 1991. SIMS depth profiling of polymer surfaces. Polym J 23(5): 367–377.

Conlan XA, Gilmore IS, Henderson A, Lockyer NP, Vickerman JC. 2006. Polyethylene terepthalate (PET) bulk film analysis using C_{60}^+, Au_3^+ and Au^+ primary ion beams. Appl Surf Sci 252:6562–6565.

Cornett DS, Lee TD, Mahoney JF. 1994. Matrix-free desorption of biomolecules using massive cluster-impact. Rapid Commun Mass Spectrom 8(12):996–1000.

Cramer H-G, Grehl T, Kollmer F, Moellers R, Niehuis E, Rading D. 2008. Depth profiling of organic materials using improved ion beam conditions. Appl Surf Sci.

Czerwiński B, Delcorte A, Garrison BJ, Samson R, Winograd N, Postawa Z. 2006. Sputtering of thin benzene and polystyrene overlayers by keV Ga and C_{60} bombardment. Appl Surf Sci 252:6419–6422.

Davenas J, Xu XL, Boiteux G, Sage D. 1989. Relation between structure and electronic properties of ion irradiated polymers. Nucl Instr Meth Phys Res B 39:754–763.

Davenas J, Thevenard P, Boiteux G, Gallavier M, Lu XL. 1990. Hydrogenated carbon layers produced by ion beam irradiation of PMMA and Polystyrene films. Nucl Instr Meth Phys Res B 46:317–323.

Davies N, Weibel P, Blenkinsopp N, Lockyer N, Hill R, Vickerman JC. 2003. Development and experimental application of a gold liquid metal ion source. Appl Surf Sci 203–204:223–227.

Debois D, Brunelle A, Laprévote O. 2007. Attempt for molecular depth profiling directly on a rat brain tissue section using fullerene and bismuth cluster ion beams. Int J Mass Spectrom 260:115–120.

Delcorte A. 2005. Modeling keV particle interactions with molecular and polymeric samples. Nucl Instr Meth Phys Res B 236:1–10.

Delcorte A, Garrison BJ. 2000. High yield events of molecular emission induced by kiloelectronvolt particle bombardment. J Phys Chem B 104:6785–6800.

Delcorte A, Garrison BJ. 2007. keV fullerene interaction with hydrocarbon targets: Projectile penetration, damage creation and removal. Nucl Instr Meth Phys Res B 255(1):223–228.

Delcorte A, Eynde XV, Bertrand P, Reich DF. 1999. Influence of the primary ion beam parameters (nature, energy, and angle) on the kinetic energy distribution of molecular fragments sputtered from poly(ethylene terephthalate) by kiloelectron volt ions. Int J Mass Spectrom 189: 133–146.

Delcorte A, Poleunis C, Bertrand P. 2006a. Energy distributions of atomic and molecular ions sputtered by C_{60}^+ projectiles. Appl Surf Sci 252:6542–6546.

Delcorte A, Poleunis C, Bertrand P. 2006b. Stretching the limits of static SIMS with C_{60}^+. Appl Surf Sci 252:6494–6497.

Delcorte A, Yunis S, Wehbe N, Nieuwjaer N, Poleunis C, Felten A, Houssiau L, Pireaux JJ, Bertrand P. 2007. Metal-assisted secondary ion mass spectrometry using atomic (Ga^+, In^+) and fullerene projectiles. Anal Chem 79:3673–3689.

Della-Negra S, Brunelle A, Le Beyec Y, Curaudeau JM, Mouffron JP, Waast B, Hakansson P, Sundqvist BUR, Parilis E. 1993. Acceleration of C_{60}^{n+} molecules to high energy. Nucl Instr Meth Phys Res B 74:453–456.

Delmore JE, Appelhans AD, Peterson ES. 1995. A rare earth oxide matrix for emitting perrhenate anions. Int J Mass Spectrom Ion Process 146/ 147:15–20.

Diehnelt CW, Van Stipdonk MJ, Schweikert A. 2001. Effectiveness of atomic and polyatomic primary ions for organic secondary ion mass spectrometry. Int J Mass Spectrom 207:111–122.

Duan Y, Pearce EM, Kwei TK, Xuesong H, Rafailovich M, Sokolov J, Zhou K, Schwarz S. 2001. Surface enrichment in polymer blends involving hydrogen bonding. Macromolecules 34:6761–6767.

Fahey A, Gillen G, Chi P, Mahoney C. 2006. Performance of a C_{60}^+ ion source on a dynamic SIMS instrument. Appl Surf Sci 252:7312–7314.

Fisher GL, Dickinson M, Bryan SR, Moulder J. 2008. C_{60} sputtering of organics: A study using TOF-SIMS, XPS and nanoindentation. Appl Surf Sci.

Fletcher JS, Conlan XA, Jones EA, Biddulph G, Lockyer NP, Vickerman JC. 2006a. TOF-SIMS analysis using C60. Effect of impact energy on yield and damage. Anal Chem 78:1827–1831.

Fletcher JS, Conlan XA, Lockyer NP, Vickerman JC. 2006b. Molecular depth profiling of organic and biological materials. Appl Surf Sci 252:6513–6516.

Fletcher JS, Lockyer NP, Vaidyanathan S, Vickerman JC. 2007. TOF-SIMS 3D biomolecular imaging of Xenopus laevis oocytes using buckminsterfullerene (C-60) primary ions. Anal Chem 79(6):2199–2206.

Forrest SR, Kaplan ML, Schmidt PH, Venkatesan T, Lovinger AJ. 1982. Large conductivity changes in ion beam irradiated organic thin films. Appl Phys Lett 41(8):708–710.

Fragalà ME, Compagnini G, Torrisi L, Puglisi O. 1998. Ion beam assisted unzipping of PMMA. Nucl Instr Meth Phys Res B 141:169–173.

Fujiwara Y, Kondou K, Nonaka H, Saito N, Itoh H, Fujimoto T, Kurokawa A, Ichimura S, Tomita M. 2006. Secondary ion mass spectrometry of organic thin films using metal-cluster-complex ion source. Jpn J Appl Phys 45(36):L987–L990.

Fuoco ER, Gillen G, Wijesundara BJ, Wallace WE, Hanley L. 2001. Surface analysis studies of yield enhancements in secondary ion mass spectrometry by polyatomic projectiles. J Phys Chem B 105:3950–3956.

Garrison BJ, Postawa Z. 2008. Computational view of surface based organic mass spectrometry. Mass Spectrom Rev 27:289–315.

Gillen G, Roberson S. 1998. Preliminary evaluation of an SF_5^+ polyatomic primary ion beam for analysis of organic thin films by secondary ion mass spectrometry. Rapid Commun Mass Spectrom 12:1303–1312.

Gillen G, Simons DS, Williams P. 1990. Molecular ion imaging and dynamic secondary ion mass spectrometry of organic compounds. Anal Chem 62:2122–2130.

Gillen G, King RL, Chmara F. 1999. Development of a triplasmatron ion source for the generation of SF_5^+ and F^- primary ion beams on an ion microscope secondary ion mass spectrometry instrument. J Vac Sci Technol A 17:845–852.

Gillen G, King L, Freibaum B, Lareau R, Bennett J, Chmara F. 2001. Negative cesium sputter ion source for generating cluster primary ion beams for secondary ion mass spectrometry analysis. J Vac Sci Technol A 19:568–575.

Gillen G, Batteas J, Michaels CA, Chi P, Small J, Windsor E, Fahey A, Verkouteren J, Kim KJ. 2006a. Depth profiling using C_{60}^+ SIMS—Deposition and topography development during bombardment of silicon. Appl Surf Sci 252:6521–6525.

Gillen G, Fahey A, Wagner M, Mahoney C. 2006b. 3D molecular imaging SIMS. Appl Surf Sci 252:6537–6541.

Gillen G, Mahoney C, Wight S, Lareau R. 2006c. Characterization of high explosive particles using cluster secondary ion mass spectrometry. Rapid Commun Mass Spectrom 20:1949–1953.

Gilmore IS, Seah MP. 2002. Electron flood gun damage in the analysis of polymers and organics in time-of-flight SIMS. Appl Surf Sci 187:89–100.

Grade H, Cooks RG. 1978. Secondary ion mass spectrometry—Cationization of organic molecule with metals. J Am Chem Soc 100(18):5615–5621.

Gray KH, Gould S, Leasure RM, Musselman IH, Lee JJ, Meyer TJ, Linton RW. 1992. Three-dimensional characterization of conducting polymer arrays using secondary ion mass spectrometry. J Vac Sci Technol A 10(4):2679–2683.

Green FM, Shard AG, Gilmore IS, Seah MP. 2009. Analysis of the interface and its position in C_{60}^{n+} secondary ion mass spectrometry depth profiling. Anal Chem 81:75–79.

Gresham GL, Groenewold GS, Appelhans AD, Olson JE, Benson MT, Jeffery MT, Rowland B, Weibel MA. 2001. Static secondary ionization mass spectrometry and mass spectrometry/mass spectrometry (MS2) characterization of the chemical warfare agent HD on soil particle surfaces. Int J Mass Spectrom 208:135–145.

Groenewold GS, Delmore JE, Olson JE, Appelhans AD, Ingram JC, Dahl DA. 1997. Secondary ion mass spectrometry of sodium nitrate: Comparison of ReO_4^- and Cs^+ primary ions. Int J Mass Spectrom Ion Process 163(3):185–195.

Groenewold GS, Appelhans AD, Gresham GL, Olson JE, Jeffery M, Wright JB. 1999. Analysis of VX on soil particles using ion trap secondary ion mass spectrometry. Anal Chem 71:2318–2323.

Groenewold GS, Appelhans AD, Gresham GL, Olson JE, Jeffery M, Weibel M. 2000. Characterization of VX on concrete using ion trap secondary ion mass spectrometry. J Am Soc Mass Spectrom 11:69–77.

Gronlund F, Moore WJ. 1960. Sputtering of silver by light ions with energies from 2 to 12 keV. J Chem Phys 32:1540.

Guillermier C, Della-Negra S, Rickman RD, Pinnick V, Schweikert EA. 2006a. Influence of massive projectile size and energy on secondary ion yields from organic surfaces. Appl Surf Sci 252:6529–6532.

Guillermier C, Pinnick V, Verkhoturov SV, Schweikert EA. 2006b. Organic SIMS with single massive gold projectile: Ion yield enhancement by silver metallization. Appl Surf Sci 252:6644–6647.

Hager GJ, Guillermier C, Verkhoturov SV, Schweikert EA. 2006. Au-analyte adducts resulting from single massive gold cluster impacts. Appl Surf Sci 252:6558–6561.

Hand OW, Majumdar TK, Cooks RG. 1990. Effects of primary ion polyatomicity and kinetic energy on secondary ion yield and internal energy in SIMS. Int J Mass Spectrom 97:35–45.

Harper S, Krantzman KD. 2004. Molecular dynamics simulations to explore the role of mass matching in the keV bombardment of organic films with polyatomic projectiles. Appl Surf Sci 231–232:44–47.

Harris RD, Baker WS, Van Stipdonk MJ, Crooks RM, Schweikert EA. 1999. Secondary ion yields produced by keV atomic and polyatomic ion impacts on a self-assembled monolayer surface. Rapid Commun Mass Spectrom 13:1374–1380.

Harton SE, Stevie FA, Ade H. 2006a. Carbon-13 labeling for improved tracer depth profiling of organic materials using secondary ion mass spectrometry. J Am Soc Mass Spectrom 17(8):1142–1145.

Harton SE, Stevie FA, Ade H. 2006b. Investigation of the effects of isotopic labeling at a PS/PMMA interface using SIMS and mean-field theory. Macromolecules 39:1639–1645.

Harton SE, Stevie FA, Ade H. 2006c. Secondary ion mass spectrometry depth profiling of amorphous polymer multilayers using O_2^+ and Cs^+ ion bombardment with a magnetic sector instrument. J Vac Sci Technol A 24(2):362–368.

Harton SE, Stevie FA, Griffis DP, Ade H. 2006d. SIMS depth profiling of deuterium labeled polymers in polymer multilayers. Appl Surf Sci 252(19):7224–7227.

Hearn MJ, Briggs D. 1988. Analysis of polymer surfaces by SIMS: 12. On the fragmentation of acrylic and methacrylic homopolymers and the interpretation of their positive and negative ion spectra. Surf Interface Anal 11:198–213.

Hill R, Blenkinsopp PWM. 2004. The development of C_{60} and gold cluster ion guns for static SIMS analysis. Appl Surf Sci 231–232:936–939.

Hill R, Blenkinsopp P, Barber A, Everest C. 2006. The development of a range of C_{60} ion beam systems. Appl Surf Sci 252:7304–7307.

Hinder SJ, Lowe C, Watts JF. 2007. ToF-SIMS depth profiling of a complex polymeric coating employing a C_{60} sputter source. Surf Interface Anal 39:467–475.

Hirata K, Saitoh Y, Narumi K, Kobayashi Y. 2002. Prevention of electric breakdown during ion bombardment of organic insulators using a cluster ion beam. Appl Phys Lett 81(19):3669–3671.

Hirata K, Saitoh Y, Chiba A, Narumi K, Kobayashi Y, Arakawa K. 2003. Time-of-flight secondary ion mass spectrometry for surface analysis of insulators using a cluster ion beam. Appl Phys Lett 813(23):4872–4874.

Houssiau AL, Douhard B, Mine N. 2008. Molecular depth profiling of polymers with very low energy ions. Appl Surf Sci 255(4):970–972.

Hu X, Zhang W, Si M, Gelfer M, Hsia B, Rafailovich M, Sokolov J, Zaitsev V, Schwarz S. 2003. Dynamics of polymers in organosilicate nano-composites. Macromolecules 36:823–829.

Huang WY, Matsuaoka S, Kwei TK, Okamoto Y, Hu X, Rafailovich MH, Sokolov J. 2001. Organization and orientation of a triblock copolymer poly(ethylene glychol)-b-poly(p-phenylene ethynylene)-b-poly(ethylene glycol) and its blends in thin films. Macromolecules 34:7809–7816.

Ichiki K, Ninomiya S, Nakata Y, Honda Y, Seki T, Aoki T, Matsuo J. 2008. High sputtering yields of organic compounds by large gas cluster ions. Appl Surf Sci 255(4):1148–1150.

Jones EA, Lockyer NP, Vickerman JC. 2006. Suppression and enhancement of non-native molecules within biological systems. Appl Surf Sci 252:6727–6730.

Jones EA, Lockyer NP, Vickerman JC. 2007. Mass spectral analysis and imaging of tissue by ToF-SIMS—The role of buckminsterfullerene, C_{60}^+, primary ions. Int J Mass Spectrom 260:146–157.

Kim KW, Hong CE, Choi SC, Cho SJ, Whang CN, Shim TE, Lee DH. 1994. Characteristics of polyimide films deposited by ionized cluster beam. J Vac Sci Technol A 12(6):3180–3184.

Kollmer F. 2004. Cluster primary ion bombardment of organic materials. Appl Surf Sci 231–232:153–158.

Kötter F, Benninghoven A. 1998. Secondary ion emission from polymer surfaces under Ar^+, Xe^+ and SF_5^+ ion bombardment. Appl Surf Sci 133:47–57.

Koval Y. 2004. Mechanism of etching and surface relief development of PMMA under low-energy ion bombardment. J Vac Sci Technol B 22(2):843–851.

Kozole J, Szakal C, Kurczy M, Winograd N. 2006. Model multilayer structures for three-dimensional cell imaging. Appl Surf Sci 252:6789–6792.

Kozole J, Wucher A, Winograd N. 2008. Energy deposition during molecular depth profiling experiments with cluster ion beams. Anal Chem 80:5293–5301.

Le Beyec Y. 1998. Cluster impacts at keV and MeV energies: Secondary emission phenomena. Int J Mass Spectrom 174:101–117.

Lee EH, Lewis MB, Blau PJ, Mansur LK. 1991. Improved surface properties of polymer materials by multiple ion beam treatment. J Mater Res 6(3):610–628.

Lee Y, Lee EH, Mansur LK. 1992. Hardness and wear properties of boron-implanted poly(ether-ether-ketone) and poly-ether-imide. Surf Coatings Technol 57:267–272.

Lee EH, Rao GR, Lewish MB, Mansur LK. 1993. Ion beam application for improved polymer surface properties. Nucl Instr Meth Phys Res B 74:326–330.

Lee JW, Kim TH, Kim SH, Kim CY, Yoon YH, Lee JS, Han JG. 1997. Investigation of ion bombarded polymer surfaces using SIMS, XPS and AFM. Nucl Instr Meth Phys Res B 121:474–479.

Leggett GL, Vickerman JC. 1992. Effects of damage during the SIMS analysis of poly(vinyl chloride) and poly(methyl methacrylate). Appl Surf Sci 55:105–115.

Licciardello A, Fragalà ME, Foti G, Compagnini G, Puglisi O. 1996. Ion beam effects on the surface and on the bulk of thin films of polymethylmethacrylate. Nucl Instr Meth Phys Res B 116:168–172.

Lin HC, Tsai IF, Yang ACM, Hsu MS, Ling YC. 2003. Chain diffusion and microstructure at a glassy-rubbery polymer interface by SIMS. Macromolecules 36:2464–2474.

Linton RW, Mawn MP, Belu AM, Desimone JM, Hunt MO, Menceloglu YZ, Cramer HG, Benninghoven A. 1993. Time-of-flight secondary-ion mass-spectrometric analysis of polymer surfaces and additives. Surf Interface Anal 20(12):991–999.

Liu Y, Schwarz SA, Zhao W, Quinn J, Sokolov J, Rafailovich M, Iyengar D, Kramer EJ, Dozier W, Fetters LJ, Dickman R. 1995. Concentration profiles of end-grafted, diblock and triblock polymers in the melt: Near-wall structure and effects of segment-wall interaction. Europhys Lett 32:211–216.

Locklear JE, Guillermier C, Verkhoturov SV, Schweikert EA. 2006. Matrix-enhanced cluster-SIMS. Appl Surf Sci 252:6624–6627.

Mahoney CM, 2009. (Submitted). Cluster SIMS depth profiling of stereospecific PMMA thin films on Si: Damage accumulation and interfacial properties. Surface and Interface Analysis.

Mahoney CM, Roberson SV, Gillen G. 2004. Depth profiling of 4-acetaminophenol-doped poly(lactic acid) films using cluster secondary ion mass spectrometry. Anal Chem 76:3199–3207.

Mahoney CM, Yu J-X, Gardella JA, Jr. 2005. Depth profiling of poly(L-lactic acid)/triblock copolymer blends with time-of-flight secondary ion mass spectrometry. Anal Chem 77:3570–3578.

Mahoney CM, Fahey AJ, Gillen G, Xu C, Batteas JD. 2006a. Temperature-controlled depth profiling in polymeric materials using cluster secondary ion mass spectrometry (SIMS). Appl Surf Sci 252:6502–6505.

Mahoney CM, Patwardhan DV, McDermott MK. 2006b. Characterization of drug-eluting stent (DES) materials with cluster secondary ion mass spectrometry (SIMS). Appl Surf Sci 252:6554–6557.

Mahoney CM, Yu J-X, Fahey AJ, Gardella JA, Jr. 2006c. SIMS depth profiling of polymer blends with protein based drugs. Appl Surf Sci 252:6609–6614.

Mahoney CM, Fahey AJ, Gillen G. 2007a. Temperature-controlled depth profiling of poly(methyl methacrylate) using cluster secondary ion mass spectrometry. 1. Investigation of depth profile characteristics. Anal Chem 79:828–836.

Mahoney CM, Fahey AJ, Gillen G, Xu C, Batteas JD. 2007b. Temperature-controlled depth profiling of poly(methylmethrylate) using cluster secondary ion mass spectrometry. 2. Investigation of sputter-induced topography, chemical damage, and depolymerization effects. Anal Chem 79:837–845.

Mahoney CM, Fahey AJ, Belu AM. 2008. Three-dimensional compositional analysis of drug eluting stent (DES) coatings using cluster secondary ion mass spectrometry. Anal Chem 80:624–632.

Mahoney JF, Perel J, Ruatta SA, Martino PA, Husain S, Lee TD. 1991. Massive cluster impact mass spectrometry: A new desorption method for the analysis of large biomolecules. Rapid Commun Mass Spectrom 5:441–445.

Matsuo J, Okubo C, Seki T, Aoki T, Toyoda N, Yamada I. 2004. A new secondary ion mass spectrometry (SIMS) system with high-intensity cluster ion source. Nucl Instr Meth Phys Res B 219–220:463–467.

Matsuo J, Ninomiya S, Nakata Y, Honda Y, Ichiki K, Seki T, Aoki T. 2008. What size of cluster is most appropriate for SIMS? Appl Surf Sci 255(4):1235–1238.

Mattsson J, Forrest JA, Krozer A, Södervall U, Wennerberg A, Torell LM. 2000. Characterization of sub micron salt-doped polymer electrolyte films. Electrochim Acta 45:1453–1461.

McDonnell LA, Heeren MA, de Lange RPJ, Fletcher IW. 2006. Higher sensitivity secondary ion mass spectrometry of biological molecules for high resolution, chemically specific imaging. J Am Soc Mass Spectrom 17:1195–1202.

McMahon JM, Dookeran NN, Todd PJ. 1995. Organic ion imaging beyond the limit of static secondary ion mass spectrometry. J Am Soc Mass Spectrom 6:1047–1058.

Mine N, Douhard B, Brison J, Houssiau L. 2007. Molecular depth-profiling of polycarbonate with low-energy Cs^+ ions. Rapid Commun Mass Spectrom 21:2680–2684.

Miyayama T, Sanada N, Iida S-I, Hammond JS, Suzuki M. 2008. The effect of angle of incidence to low damage sputtering of organic polymers using a C_{60} ion beam. Appl Surf Sci 255(4):951–953.

Mizota T, Nonaka H, Fujimoto T, Kurokawa A, Ichimura S. 2007. Development of compact cluster ion sources using metal cluster complexes—Ionization properties of metal cluster complexes. Appl Surf Sci 231:945–948.

Möllers R, Tuccitto N, Torrisi V, Niehuis E, Licciardello A. 2006. Chemical effects in C_{60} irradiation of polymers. Appl Surf Sci 252:6509–6512.

Nagy G, Walker AV. 2007. Enhanced secondary ion emission with a bismuth cluster ion source. Int J Mass Spectrom 262:144–153.

Nagy G, Gelb LD, Walker AV. 2005. An investigation of enhanced secondary ion emission under Au_n^+ ($n = 1$–7) bombardment. J Am Soc Mass Spectrom 16:733–742.

Nakata Y, Honda Y, Ninomiya S, Seki T, Aoki T, Matsuo J. 2008. A fragment-free ionization technique for organic mass spectrometry with large Ar cluster ions. Appl Surf Sci 255(4):1588–1590.

Netcheva S, Bertrand P. 1999. Surface topography development of thin polystyrene films under low energy ion irradiation. Nucl Instr Meth Phys Res B 151:129–134.

Ninomiya S, Aoki T, Seki T, Matsuo J. 2006. High-intensity Si cluster ion emission from a silicon target bombarded with large Ar cluster ions. Appl Surf Sci 252:6550–6553.

Ninomiya S, Ichiki K, Yamada H, Nakata Y, Seki T, Aoki T, Matsuo J. (in press). Precise and fast SIMS depth profiling of polymer materials with large Ar cluster ion beams. Rapid Com Mass Spectrom.

Nishimiya N, Ueno K, Noshiro M, Satou M. 1991. Chemical processes and surface hardening in ion-implanted polyester films. Nucl Instr Meth Phys Res B 59/60:1276–1280.

Norrman K, Haugshoj KB, Larsen NB. 2002. Lateral and vertical quantification of spin-coated polymer films on silicon by TOF-SIMS, XPS, and AFM. J Phys Chem B 106:13114–13121.

Nygren H, Borner K, Hagenhoff B, Malmberg P, Mansson JE. 2005. Localization of cholesterol, phosphocholine and galactosylceramide in rat cerebellar cortex with imaging TOF-SIMS equipped with a bismuth cluster ion source. Biochim Biophys Acta 1737:102–110.

Ochsner R, Kluge A, Zechel-Malonn S, Gong L, Ryssel H. 1993. Improvement of surface properties of polymers by ion implantation. Nucl Instr Meth Phys Res B 80/81:1050–1054.

Papaléo RM, de Oliveira LD, Farenzena LS, Livi RP. 2001. Probing glass transition of PMMA thin films at the nanometer scale with single ion bombardment and scanning force microscopy. Nucl Instr Meth Phys Res B 185:55–60.

Papaléo RM, Hasenkamp W, Barbosa LG, Leal R. 2006. Relaxation of craters produced by ion bombardment on PMMA as a function of temperature. Nucl Instr Meth Phys Res B 242:190–193.

Pignataro B, Fragalà ME, Puglisi O. 1997. AFM and XPS study of ion bombarded poly(methyl methacrylate). Nucl Instr Meth Phys Res B 131:141–148.

Pinto JR, Novak SW, Nicholas M. 1999. Aqueous dye diffusion in thin films of water-soluble poly(vinyl pyrrolidone) copolymers: A dynamic secondary ion mass spectrometry study. J Phys Chem B 103:8026–8032.

Postawa Z, Czerwinski B, Szewczyk M, Smiley EJ, Winograd N, Garrison BJ. 2003. Enhancement of sputtering yields due to C60 bombardment of Ag{1 1 1} as explored by molecular dynamics simulations. Anal Chem 75:4402–4407.

Postawa Z, Czerwinski B, Szewczyk M, Smiley EJ, Winograd N, Garrison BJ. 2004. Microscopic insights into the sputtering of Ag{1 1 1} induced by C_{60} and Ga bombardment. J Phys Chem B 108:7831–7838.

Postawa Z, Czerwinski B, Winograd N, Garrison BJ. 2005. Microscopic insights into the sputtering of thin organic films on Ag{1 1 1} induced by C_{60} and Ga bombardment. J Phys Chem B 109:11973–11979.

Puglisi O, Licciardello A, Pignataro S, Calcagno L, Foti G. 1986. Primary chemical events ion bombarded polystyrene films: An infrared study. Radiat Eff 98:161–170.

Puglisi O, Licciardello A, Calcagno L, Foti G. 1987. Molecular weight distribution and solubility changes in ion-bombarded polystyrene. Nucl Instr Meth Phys Res B 19/20:865–871.

Puglisi O, Licciardello A, Calcagno L, Foti G. 1988. Ion beam induced aggregation in polystyrene: The influence of the molecular parameters. J Mater Res 3(6):1247–1252.

Rao GR, Wang ZL, Lee EH. 1993. Microstructural effects on surface mechanical properties of ion-implanted polymers. J Mater Res 8(4): 927–933.

Rao GR, Lee EH, Bhattacharya R, McCormick AW. 1995. Improved wear properties of high energy ion-implanted polycarbonate. J Mater Res 10(1):190–201.

Reuter W. 1987. Secondary ion emission from metal targets under CF_3^+ and O_2^+ bombardment. Anal Chem 59:2081–2087.

Reuter W, Clabes JG. 1988. Secondary ion emission and sputter yields from metal targets under F_2^+ bombardment. Analytical Chemistry 60:1405–1408.

Reuter W, Scilla GJ. 1988. Application of a CF_3^+ primary ion source for depth profiling in secondary ion mass spectrometry. Anal Chem 60:1401–1404.

Reynolds BJ, Ruegg ML, Mates TE, Radke CJ, Balsara NP. 2005. Experimental and theoretical study of the adsorption of a diblock copolymer to interfaces between two homopolymers. Macromolecules 38:3872–3882.

Rück DM, Schulz J, Beusch N. 1997. Ion irradiation induced chemical changes of polymers used for optical applications. Nucl Instr Meth Phys Res B 131:149–158.

Rysz J, Ermer H, Budkowski A, Lekka M, Bernasik A, Wrobel S, Brenn R, Lekki J, Jedlinski J. 1999. Depth profiling studies of the surface directed phase decomposition in thin polymer films. Vacuum 54(1–4):303–307.

Salehpour M, Fishel DL, Hunt JE. 1988a. Collective effects in electronic sputtering of organic molecular ions by fast incident cluster ions. J Appl Phys 64(2):831–834.

Salehpour M, Fishel DL, Hunt JE. 1988b. Nonlinear effects in desorption of valine with fast incident molecular ions. Phys Rev B 38(17):12320–12328.

Sanada N, Yamamoto A, Oiwa R, Ohashi Y. 2004. Extremely low sputtering degradation of polytetrafluoroethylene by C_{60} ion beam applied in XPS analysis. Surf Interface Anal 36:280–282.

Sauer G, Kilo M, Hund M, Wokaun A, Karg S, Meier M, Riess W, Schwoerer M, Suzuki H, Simmerer J, Meyer H, Haarer D. 1995. Characterization of polymeric light-emitting-diodes by SIMS depth profiling analysis. Fresenius J Anal Chem 353(5–8):642–656.

Seah MP. 2007. Cluster ion sputtering: Molecular ion yield relationships for different cluster primary ions in static SIMS of organic materials. Surf Interfac Anal 39:890–897.

Liu SH, Liu ZC, Zhai BX. 1989. Modification of polyvinyl chloride surface electrostatic properties by an ion beam. Vacuum 39(2–4):271–272.

Shard AG, Brewer PJ, Green FM, Gilmore IS. 2007. Measurement of sputtering yields and damage in C_{60} SIMS depth profiling of model organic materials. Surf Interface Anal 39:294–298.

Shard AG, Green FM, Brewer PJ, Seah MP, Gilmore IS. 2008. Quantitative molecular depth profiling of organic delta-layers by C_{60} ion sputtering and SIMS. J Phys Chem B 112:2596–2605.

Shin K, Hu X, Zhen X, Rafailovich MH, Sokolov J, Zaitsev V, Schwarz SA. 2001. Silicon oxide surface as a substrate of polymer thin films. Macromolecules 34:4993–4998.

Shwarz SA, Wilkens BJ, Pudensi MAA, Rafailovich MH, Sokolov J, Zhao X, Zheng X, Russell TP, Jones RAL. 1992. Studies of surface and interface segregation in polymer blends by secondary ion mass spectrometry. Mol Phys 76(4):937–950.

Sigmund P, Claussen C. 1981. Sputtering from elastic-collision spikes in heavy-ion-bombarded metals. J Appl Phys 52:990.

Sjovall P, Lausmaa J, Johansson B. 2004. Mass spectrometric imaging of lipids in brain tissue. Anal Chem 76:4271–4278.

Soldera A. 2002. Energetic analysis of the two PMMA chain tacticities and PMA through molecular dynamics simulations. Polymer 43:4269–4275.

Stapel D, Benninghoven A. 2001. Application of atomic and molecular primary ions for TOF-SIMS analysis of additive containing polymer surfaces. Appl Surf Sci 174:261–270.

Stapel D, Brox A, Benninghoven A. 1999. Secondary ion emission from arachidic acid LB-layers under Ar^+, Xe^+, Ga^+ and SF_5^+ primary ion bombardment. Appl Surf Sci 140:156–167.

Stapel D, Thiemann M, Benninghoven A. 2000. Secondary ion emission from polymethacrylate LB-layers under 0.5–0.11 keV atomic and molecular primary ion bombardment. Appl Surf Sci 158:362–374.

Stein J, Leonard TM, Smith GA. 1991. Application of the dynamic SIMS technique to the study of silicone release coatings. J Appl Polym Sci 42(8):2355–2360.

Strzhemechny YM, Schwarz SA, Schachter J, Rafailovich MH, Sokolov J. 1997. Secondary ion mass spectrometry study of silicon surface preparation and the polystyrene/silicon interface. J Vac Sci Technol A 15(3):894–898.

Suzuki Y, Swapp C, Kusakabe M, Iwaki M. 1990. Aging effects on wettability and structure of ion implanted silicone. Nucl Instr Meth Phys Res B 46:354–357.

Suzuki Y, Kuskabe M, Akiba H, Kusakabe K, Iwaki M. 1991. In vivo evaluation of antithrombogenicity for ion implanted silicone rubber using indium-111-tropolone platelets. Nucl Instr Meth Phys Res B 59/60:698–704.

Suzuki Y, Kusakabe M, Lee JS, Kaibara M, Iwaki M, Sasabe H. 1992. Endothelial cell adhesion to ion implanted polymers. Nucl Instr Meth Phys Res B 65:142–147.

Suzuki Y, Kusakabe M, Iwaki M. 1993. Surface modification of polystyrene for improving wettability by ion implantation. Nucl Instr Meth Phys Res B 80/81:1067–1071.

Švorčík V, Areholz E, Rybka V, Hnatowicz V. 1997. AFM surface morphology investigation of ion beam modified polyimide. Nucl Instr Meth Phys Res B 122:663–667.

Švorčík V, Areholz E, Hnatowicz V, Rybka V, Öchsner R, Ryssel H. 1998. AFM surface investigation of polyethylene modified by ion bombardment. Nucl Instr Meth Phys Res B 142:349–354.

Szakal C, Sun S, Wucher A, Winograd N. 2004. C_{60} molecular depth profiling of a model polymer. Appl Surf Sci 231–232:183–185.

Szymczak W, Wittmaak K. 1994. Evidence for strongly enhanced yield of negative molecular secondary ions due to bombardment with SF_n ions. Nucl Instr Meth Phys Res B 88:149–153.

Tempez A, Schultz JA, Della-Negra S, Depauw J, Jacquet D, Novikov A, Le Beyec Y, Pautrat M, Caroff M, Ugarov M, Bensaoula H, Gonin M, Fuhrer K, Woods A. 2004. Orthogonal time-of-flight secondary ion mass spectrometric analysis of peptides using large gold clusters as primary ions. Rapid Commun Mass Spectrom 18:371–376.

Thompson DA, Johar SS. 1979. Nonlinear sputtering effects in thin metal films. Appl Phys Lett 34:342–345.

Touboul D, Halgand F, Brunelle A, Kersting R, Tallarek E, Hagenhoff B, Laprévote O. 2004. Tissue molecular ion imaging by gold cluster ion bombardment. Anal Chem 76:1550–1559.

Touboul D, Brunelle A, Halgand F, De La Porte S, Laprevote O. 2005a. Lipid imaging by gold cluster time-of-flight secondary ion mass spectrometry: Application to duchenne muscular dystrophy. J Lipid Res 46:1388–1395.

Touboul D, Kollmer F, Niehuis E, Brunelle A, Leprévote O. 2005b. Improvement of biological time-of-flight secondary ion mass spectrometry imaging with a bismuth cluster ion source. J Am Soc Mass Spectrom 16:1608–1618.

Townes JA, White AK, Wiggins EN, Krantzman KD, Garrison BJ, Winograd N. 1999. Mechanism for increased yield with SF_5^+ projectiles in organic SIMS: The substrate effect. J Phys Chem A 103(24):4587–4589.

Tretinnikov ON, Ikada Y. 1998. Surface characterization of ion-implanted polyethylene. J Polym Sci B 36:715–725.

Valenty SJ, Chera JJ, Olson DR, Webb KK, Smith GA, Katz W. 1984. Multitechnique depth profiling of small molecules in polymeric matrices. J Am Chem Soc 106:6155–6161.

Van Ooij WJ, Brinkhuis RHG. 1988. Interpretation of the fragmentation patterns in static SIMS analysis of polymers. Part I. Simple aliphatic hydrocarbons. Surf Interface Anal 11:430–440.

Van Royen P, Taranu A, Van Vaeck L. 2005. Comparison of primary monoatomic with primary polyatomic ions for the characterization of polyesters with static secondary ion mass spectrometry. Rapid Commun Mass Spectrom 19:552–560.

Van Stipdonk MJ, Harris RD, Schweikert EA. 1996. A comparison of desorption yields from C_{60}^+ to atomic and polyatomic projectiles at keV energies. Rap Commun Mass Spectrom 10:1987–1991.

Venkatesan T, Forrest SR, Kaplan ML, Murray CA, Schmidt PH, Wilkens BJ. 1983. Ion beam-induced conductivity in polymer films. J Appl Phys 54(6):3150–3153.

Verhoeven MLPM, Driessen AAG, Paul AJ, Brown A, Canry J-C, Hendriks M. 2004. DSIMS characterization of a drug-containing polymer-coated cardiovascular stent. J Control Release 96:113–121.

Verkjoturov SV, Rickman RD, Guillermier C, Hager GJ, Locklear JE, Schweikert EA. 2006. Molecular ion emission from single large cluster impacts. Appl Surf Sci 252:6490–6493.

Wagner MS. 2004. Impact energy dependence of SF_5^+-induced damage in poly(methyl methacrylate) studied using time-of-flight secondary ion mass spectrometry. Anal Chem 76:1264–1272.

Wagner MS. 2005a. Degradation of poly(acrylates) under SF_5^+ primary ion bombardment studied using time-of-flight secondary ion mass spectrometry. 1. Effect of main chain and pendant methyl groups. Surf Interface Anal 36:42–52.

Wagner MS. 2005b. Degradation of poly(acrylates) under SF_5^+ primary ion bombardment studied using time-of-flight secondary ion mass spectrometry. 2. Poly(n-alkyl methacrylates). Surf Interface Anal 36: 53–61.

Wagner MS. 2005c. Degradation of poly(acrylates) under SF_5^+ primary ion bombardment studied using time-of-flight secondary ion mass spectrometry. 3. Poly(hydroxyethylmethacrylate) with chemical derivatization. Surface Interface Anal 36:62–70.

Wagner MS. 2005d. Molecular depth profiling of multilayer polymer films using time-of-flight secondary ion mass spectrometry. Anal Chem 77:911–922.

Wagner MS, Lenghaus K, Gillen G, Tarlov MJ. 2006. Characterization and ion-induced degragdation of cross-linked poly(methyl methacrylate) studied using time of flight secondary ion mass spectrometry. Appl Surf Sci 253:2603–2610.

Webb RP, Kerford M, Kappes M, Brauchle G. 1997. A comparison between fullerene and single atom impacts on graphite. Nucl Instr Meth Phys Res B 122:318–321.

Weibel D, Wong S, Lockyer N, Blenkinsopp P, Hill R, Vickerman JC. 2003. A C_{60} primary ion beam system for time of flight secondary ion mass spectrometry: its development and secondary ion yield characteristics. Anal Chem 75:1754–1764.

Whitlow SJ, Wool RP. 1989. Investigation of diffusion in polystyrene using secondary ion mass spectroscopy. Macromolecules 22:2648–2652.

Whitlow SJ, Wool RP. 1991. Diffusion of polymers at interfaces: A secondary ion mass spectroscopy study. Macromolecules 24:2938–5926.

Winograd N. 2005. The magic of cluster SIMS. Anal Chem 77:143A–149A.

Wittmaack K, Szymczak W, Hoheisel G, Tuszynski W. 2000. Time-of-flight secondary ion mass spectrometry of matrix-diluted oligo- and polypeptides bombarded with slow and fast projectiles: Positive and negative matrix and analyte ion yields, background signals, and sample aging. J Am Chem Soc 11(6):553–563.

Wong SS, Stoll R, Röllgen FW. 1982. Ionization of organic molecules by fast molecular ion bombardment. Z Naturforsch 37a:718–719.

Wong SCC, Hill R, Blenkinsopp P, Lockyer NP, Weibel DE, Vickerman JC. 2003. Development of a C_{60}^+ ion gun for static SIMS and chemical imaging. Appl Surf Sci 203–204:219–222.

Wu KJ, Odom RW. 1996. Matrix-enhanced secondary ion mass spectrometry: A method for molecular analysis of solid surfaces. Anal Chem 68(5): 873–882.

Wucher A. 2006. Molecular secondary ion formation under cluster bombardment: A fundamental review. Appl Surf Sci 252:6482–6489.

Wucher A. 2008. A simple erosion dynamics model of molecular sputter depth profiling. Surf Interface Anal 40:1545–1551.

Wucher A, Sun S, Szakal C, Winograd N. 2004. Molecular depth profiling of histamine in ice using a buckminsterfullerene probe. Anal Chem 86:7234–7242.

Wucher A, Chen J, Winograd N. 2007. Protocols for three-dimensional molecular imaging using mass spectrometry. Anal Chem 79:5529–5539.

Wucher A, Chen J, Wingorad N. 2008. Molecular depth profiling using a C cluster beam: the role of impact energy. J Phys Chem C 112(42):16550–16555.

Xu J, Szakal CW, Martin SE, Peterson BR, Wucher A, Winograd N. 2004. Molecule-specific imaging with mass spectrometry and a buckminsterfullerene probe: Application to characterizing solid-phase synthesized combinatorial libraries. J Am Chem Soc 126:3902–3909.

Yamada I, Matsuo J, Toyoda N, Kirkpatrick A. 2001. Materials processing by gas cluster ion beams. Mat Sci Eng R 34:231–295.

Yamazaki H, Mitani Y. 1997. O_3^+ cluster primary ion bombardment for secondary ion mass spectrometry. Nucl Instr Meth Phys Res B 124:91–94.

Yokoyama H, Kramer EJ, Hajduk DA, Bates FS. 1999. Diffusion in mixtures of asymmetric diblock copolymers with homopolymers. Macromolecules 32:3353–3359.

Yoshida K, Iwaki M. 1987. Structure and morphology of ion-implanted polyimide films. Nucl Instr Meth Phys Res B 19/20:878–881.

Yotoriyama T, Nakao A, Suzuki Y, Tsukamota T, Iwaki M. 2006. Analysis of cell-adhesion surface induced by ion-beam irradiation into biodegradable polymer. Nucl Instr Meth Phys Res B 242:51–54.

Yu B-Y, Chen Y-Y, Wang W-B, Hsu M-F, Tsai S-P, Lin W-C, Lin Y-C, Jou J-H, Chu C-W, Shyue J-J. 2008. Depth profiling of organic films with X-ray Photoelectron Spectroscopy using C_{60}^+ and Ar^+ co-sputtering. Anal Chem 80(9):3412–3415.

Zaporojtchenko B, Zekonyte J, Wille S, Schuermann U, Faupel F. 2005. Tailoring of the PS surface with low energy ions: Relevance to growth and adhesion of noble metals. Nucl Instr Meth Phys Res B 236:95–102.

Zemek J, Yamada I, Takaoka G, Matsua J. 1999. Polycarbonate surface modified by argon cluster ion beams. J Vac Sci Technol B 17(6):2653–2655.

Zhao X, Zhao W, Sokolov J, Rafailovich MH, Schwarz SA, Wilkens BJ, Jones RAL, Kramer EJ. 1991. Determination of the concentration profile at the surface of d-PS/h-PS blends using high-resolution ion scattering techniques. Macromolecules 24:5991–5996.

Zheng X, Sauer BB, Van Alsten JG, Schwarz SA, Rafailovich MH, Sokolov J, Rubinstein M. 1995. Reptation dynamics of a polymer melt near an attractive solid interface. Phys Rev Lett 74(3):407–410.

Zheng L, Wucher A, Winograd N. 2008. Chemically alternating langmuir-blodgett thin films as a model for molecular depth profiling by mass spectrometry. J Am Soc Mass Spectrom 19:96–102.

Zhu Z, Kelley MJ. 2006. ToF-SIMS analysis of a fluorocarbon-grafted PET with a gold cluster ion source. Appl Surf Sci 252:6619–6623.

X. APPENDIX

Several terms are utilized throughout this work to describe the performance of cluster beams and are defined here as follows. Please see ISO 18815 for more detailed terminology definitions.[6] The secondary ion yield (Y) is defined as the number of detected secondary ion species (N) divided by the total number of applied primary ions (N_p) (Kötter & Benninghoven, 1998). The molecular ion yield is therefore the number of molecules detected per primary ion impact. This is not to be confused with the total ion yield, which is defined as the total number of positive and negative secondary ions sputtered from a specimen per incident primary particle. The sputtering yield or sputter volume is defined as the number of molecules, fragments, atoms or volume equivalents removed per incident primary ion. This is different from the term, sputter rate, which is defined as the eroded depth per unit time.

The disappearance cross section is a term describing the damage and/or disappearance of molecules from a surface, defined here as $\sigma = N_{des}/N_0$, where N_{des} is the average number of molecular surface species being destroyed and/or disappearing from a surface as a result of a single primary ion impact and N_0 is the total number of molecular species M in the unit area of 1 cm^2 (Kötter & Benninghoven, 1998). The disappearance cross section is measured *via* the following equation:

$$I = I_0 e^{-\sigma f t} \tag{5}$$

where I_0 is the initial signal intensity, I is the signal intensity of a selected ion at a time, t, and f is the primary ion flux (Stapel, Brox, & Benninghoven, 1999). The secondary ion efficiency (E) is defined as the secondary ion yield (Y), divided by the corresponding disappearance cross section (σ) and is a very useful term to help describe the performance of a particular ion source (Kötter & Benninghoven, 1998).

The disappearance cross section is not to be confused with the damage cross section, which is related to the disappearance cross section in the following manner (Cheng, Wucher, & Winograd, 2006; Wucher, 2008):

$$\sigma = \frac{Y}{nd} + \sigma_d \tag{6}$$

where n is the density of molecules, d is the thickness of the altered layer and Y is the secondary ion yield.

Sputter threshold: physical sputtering has a well-defined minimum energy threshold which is equal to or larger than the ion energy at which the maximum energy transfer of the ion to a sample atom equals the binding energy of a surface atom.

Christine M. Mahoney received her bachelors in chemistry at the State University of New York at Potsdam in 1997. She later received her Ph.D. in chemistry in 2003, under the direction of Prof. Joseph A. Gardella Jr. at the State University of New York at Buffalo, where she studied polymer surfaces using Secondary Ion Mass Spectrometry (SIMS) and X-ray Photoelectron Spectroscopy (XPS). She was then awarded a post-doctoral fellowship at the National Institute of Standards and Technology (NIST), in the Surface and Microanalysis Division, where she went on to study cluster SIMS of polymers and related materials. She is currently employed at NIST as a senior staff member.

[6]ISO standards from TC201/SC1 for terminology relating to surface analysis and TC201/SC6 for SIMS standards.